SPATIAL INTERPOLATION AND MAPPING OF RAINFALL (SIMAR)

VOLUME 2. RADAR AND SATELLITE PRODUCTS

I.T.H. DEYZEL[1], G.G.S. PEGRAM[2] , P.J.M. VISSER[1]
and
D. DICKS[1]

[1]METSYS, South African Weather Service, Bethlehem
[2]University of Natal, Durban

Final Report to the Water Research Commission

by the

South African Weather Service

WRC Report No 1152/1/04
ISBN 1-77005-160-0

Executive Summary

The programme ***Spatial Interpolation and Mapping of Rainfall (SIMAR)*** was a three-year initiative encompassing three component projects, viz:

- Maintenance and upgrading of radar and raingauge infrastructure
- Radar and satellite products
- Optimal integration of raingauge, radar and satellite derived data in the production of daily rainfall maps

The final report on this programme, which was undertaken by scientists, researchers and engineers of the METSYS group of the South African Weather Service (SAWS) and the School of Civil Engineering of the University of Natal, in collaboration with the Department of Water Affairs (DWAF) and ESKOM, is contained in three volumes. The volumes are:

VOLUME 1. ***Maintenance and Upgrading of Radar and Raingauge Infrastructure***

VOLUME 2. ***Radar and Satellite Products***

VOLUME 3. ***Data Merging for Rainfall Map Production***

Rationale for SIMAR

Water resources in South Africa are not well buffered against natural rainfall variability. Rainfall deficits and excesses readily translate to droughts and floods, respectively. Well-developed water resource infrastructure, which South Africa is fortunate to possess, has to be managed extremely skillfully to successfully balance water surpluses and deficits at an inter-catchment level, as well as to achieve best trade-offs between flood mitigation and storage maximisation at basin level.

The concept of water resource management is no longer restricted to regulating flows, storage and abstractions in and from rivers, dams and aquifers. Water resource management is increasingly becoming concerned with applying measures to ensure resource (ecosystem) sustainability and also with activities in the catchment which impact on both sustainability and availability of water for abstraction and use. A particular focus in the 1998 Water Act is on activities, termed streamflow reduction activities, the licensing and regulation of which are provided for in the Act. To do this objectively requires defendable information on water usage associated with entities such as forests, agricultural lands, natural veld, farm dams, soil conservation schemes, etc. Such water usage is tightly linked, through the catchment water balance, to catchment water availability and thus rainfall, a link which imposes an obligation on catchment management agencies to obtain detailed and accurate rainfall measurements.

Since natural disasters and fluctuations in agricultural production are also closely linked to rainfall, these sectors have a similar need for such detailed rainfall information.

Raingauges have traditionally provided the rainfall measurements required for water resource management purposes. Because the national raingauge network is rapidly becoming too sparse to meet existing and anticipated management requirements, a new rainfall monitoring/information system, incorporating the optimal use of remote sensing, has become necessary to satisfy the needs of South Africa.

This need was envisaged to be best satisfied through an umbrella research and development programme (SIMAR) having the ultimate goal of merging satellite/radar/gauge data to produce **one field** that is acceptable to the water-resources (and hence also agricultural and disaster-management) users.

The specific aim was to produce a daily rainfall map of 24 hour accumulated rainfall to a resolution of 2 km, over the whole subcontinent, accessible on the Internet. This has been accomplished. Furthermore, this primary product can and will be refined where needed to finer time scales over selected areas. This refinement will be of particular interest to the disaster-management users and those involved with the mapping of the tendency for, or forecasting of, flash floods. As improvements to the data streams and modelling techniques become available, they will be incorporated into the products emanating from the research. Follow-on research projects supported by the Water Research Commission are designed to bring about such improvements.

Results of SIMAR component projects

Details of the results deriving from the three component projects included under the SIMAR umbrella are contained in the three volumes which make up the SIMAR final report. Some background information pertaining to these results, and the results *per se*, are summarised below.

VOLUME 1. ***Maintenance and Upgrading of Radar and Raingauge Infrastructure***

Since conventional meteorological infrastructure is dwindling at an alarming rate in South Africa, it became necessary to investigate the complementary use of conventional and less conventional infrastructure in sourcing rainfall data. The complementary sources here considered are surface networks and remote sensing sources, namely radar and satellite. The focus has fallen on maintaining current systems as well as using new technologies and techniques to upgrade systems, where necessary, with a view to securing and sustaining a reliable data flow from the above-mentioned data sources. The specific objectives of this part of the programme were as follows:

- Maintain automated surface gauge networks (Durban and Liebenbergsvlei) as well as investigate the application of new technology to ensure real time availability of data.
- Maintain and upgrade the National Weather Radar Network (NWRN) by improving the monitoring capabilities at each radar system, investigating the possible expansion of the network coverage and pursuing an improved funding base for the radar network.
- Utilise the latest remote sensing technology in order to improve the quality of products to be generated.

- In cooperation with other stakeholders, assist in establishing a real time precipitation database for South /southern Africa.
- Actively seek and promote collaboration with stakeholders, institutions and organisations, on a formal and informal basis, to expand and enhance surface coverage of precipitation measurements.
- Equip and train individuals, especially those from previously disadvantaged communities, with a view to their acquisition of remote sensing and electronic maintenance skills.

The raingauges of the Liebenbergsvlei and Durban networks played a vital role in investigations regarding elimination of ground clutter and in validation of radar-estimated rainfall on the ground. An investigation into the feasibility of using cell phone communication technology and infrastructure resulted in such technology being implemented in the Liebenbergsvlei and Durban networks, and gave rise to the vision of also implementing the technology at all the SA Weather Service second order stations.

Improvements and upgrades were introduced at the majority of radar installations within the network, while also ensuring a reliable power supply to the systems. A remote control and monitoring system, whereby the functioning of individual radar systems can be monitored from a central point, was implemented. This new capability has, for the first time, allowed objective assessments of the reliability of individual radar systems within the NWRN to be made. During the course of this project, the SAWS drastically increased its funding for maintenance and upgrading of the NWRN.

Unfortunately, the Meteosat Second Generation (MSG) satellite did not become operational during the lifetime of the SIMAR project as anticipated, as the MSG programme suffered lengthy delays prior to, and further problems after, the launch of the satellite. Nevertheless, research into utilising Meteosat 7 to fulfill the SIMAR project's objectives, continued. New techniques were developed which will be applied to MSG when it eventually becomes operational.

Close cooperation with the SAWS database developers led to provision being made for the archiving of real-time data generated by the SIMAR programme. The development of the new database has proceeded through different phases and will continue to be developed to accommodate such data products for routine applications and research purposes.

This component project succeeded in promoting data sharing between institutions, albeit on a small scale, and initially limited to operational exchange of data through collaboration with DWAF and Suidwes Agriculture. The pursuit of this objective of institutional collaboration will not end with SIMAR but will be carried on and expanded.

The training of personnel in the maintenance and upgrading of observational systems received high priority in the SIMAR project. The training initiative was also expanded to the international arena with training on SIMAR related subjects presented to students from other African countries such as Botswana and Tanzania.

VOLUME 2. ***Radar and Satellite Products***

The focus of this component project was to provide the two remote sensing-based rainfall fields – the one derived from radar and the other from satellite – to be merged with yet another rainfall field, derived from daily reporting raingauges.

The specific objectives were as follows:

Radar products

- Provide a Meteorological Data Volume (MDV)-based, real-time, radar rainfall map of the radar covered area of South Africa
- Optimize merging in areas of radar overlap and utilize the reflectivity measurements in these areas for additional performance testing
- Improve radar-rainfall algorithms which address the outstanding issues of data quality and integrity (hail, bright band, ground clutter and coastal/orographic rain)
- Include additional radar information as it becomes available and identify the most serious gaps in South Africa's weather radar coverage.

Satellite products

- Investigate and develop suitable rainfall estimation algorithms from satellite data for South Africa, which also address known problems related to coastal/orographic rain
- Incorporate the latest satellite (Meteosat Second Generation, which should have become available during the project period) in order to address issues related to temporal resolution
- Provide an MDV-based, real-time, satellite rainfall map of South Africa
- Integrate raingauge, radar and satellite rain fields to provide the desired daily rainfall maps, making use of the modelling component (reported in *VOLUME 3* of the SIMAR final report).

Despite the fact that the MSG Satellite did not become operational during this project as originally anticipated, SIMAR accomplished major advances in the estimation of rainfall using remote sensing techniques and the integrated mapping of rainfall over South Africa.

Radar rainfall estimation

South Africa's NWRN represents a unique system based on a local solution to the complex problem of networking of several individual radars and merging of their individual data fields. This system, developed in-house, is a combination of South African innovation and shareware/freeware available from various sources in the world. Very few countries in the world operate successful weather radar networks and even fewer a network as elegant and modular as the one in South Africa. The report gives a summary of how this was achieved and highlights the data flow and product generation from the eleven radars within the network.

A major advance in radar rainfall estimation is the unique methodology that was developed to filter the negative impact of ground clutter. This technique, that uses the scan-to-scan coherence in the echo field to dynamically build up a slowly evolving clutter mask, has all but solved the problems of ground clutter contamination. This advance has had a positive impact on the resolution of the rain fields that are archived, displayed and used as input to create the integrated satellite-radar-raingauge rain fields.

The verification of radar performance, and independent procedures and tests to investigate the inter-calibration of network radars, have been fully documented. Of significance is the success with which the sun has been used as an independent calibration source.

Conversion of radar reflectivity into rain rate and the computation of rainfall depth accumulations have been refined considerably. Using the dense Liebenbergsvlei raingauge network as a basis for comparison, the mean reflectivity in the vertical column was found to be a more appropriate input to the Z-R relationship than the customarily-used maximum reflectivity in the vertical column. The mean reflectivity has a smoothing effect on the enhanced or erroneous reflectivity caused by the occurrence of hail, or by the so-called *Bright-Band* and *Anomalous Propagation* phenomena.

Furthermore, methods have also been developed to generate a merged rain field from rain fields generated at the individual radar sites instead of from a merged reflectivity field. This allows the use of different (and more appropriate) Z-R relationships for different regions and also allows use of data with the finest temporal resolution. Rainfall estimates over South Africa obtained in this way has been evaluated using rainfall data from 60 automatic weather stations across South Africa.

The above-mentioned studies and advances all provided a sound foundation for improvements already made to the NWRN rainfall estimation techniques, or for improvements due to be implemented in the near future.

Satellite rainfall estimation

Building on a review of literature on past South African and international experience, a technique (probably the most sophisticated satellite-rainfall estimation technique yet available for South Africa) that makes optimal use of all three channels (IR, Visible, Water Vapour) of the current Meteosat 7 satellite was developed and implemented operationally. Particular attention was also given to the characteristics of the MSG Satellite. Although it did not become operational during the project as originally anticipated, some of the first data examples from this satellite are shown.

The first stage in the evolutionary development of the MSRR (Multi-Spectral Rain Rate technique) was the ITR (Infra-red Power Law Rain Rate technique), which gave rise to the intermediate BSRR (Bi-Spectral Rain Rate technique). The use of all three channels leads to improved methods for filtering out non-precipitating clouds and enhances the estimation of rainfall from maritime clouds. Image processing techniques (including edge detection and speckle removal techniques) were also introduced to better identify rainy pixels from those that are cloudy but not rainy. Systems to reformat and communicate the satellite data in the same MDV format being used for radar data were developed. A novel development in the satellite rainfall estimation was the use of topographical slope to enhance estimated rainfall over mountainous regions. The advantages of using a Geographical Information System to display and process the data and products from the various sources was clearly demonstrated.

Methods to verify the satellite rainfall estimates in terms of their spatial extent and quantitative values through comparisons with radar and raingauge estimates were developed and applied. It became clear that the satellite rainfall estimation technique which was developed achieves the objective of providing useful, large-scale rainfall fields for the southern Africa region.

Rainfall data integration and product distribution
An analysis of the strengths and weaknesses of raingauge-, radar- and satellite-derived rainfall information provided the basis for additional measures to address the major weaknesses in each source. The accuracy (including human-introduced error factors) and coverage of daily raingauge data, in particular, has become a matter that needs to be addressed as a national priority.

The generation of the merged satellite-radar-raingauge field is a stepwise process, starting with the merging of the radar and raingauge fields. Thereafter the satellite and raingauge fields are merged before the two resultant fields are combined.

SIMAR has a dedicated section on the South African Weather Service (METSYS) web page (http://metsys.weathersa.co.za) which displays the various individual daily rainfall fields (radar, gauge and satellite) together with the integrated fields. Archived data relating to these fields are also presented.

VOLUME 3. ***Data Merging for Rainfall Map Production***

This component project was initiated against the background of the following premises and objectives:

- There existed a large collection of daily-read rainfall data in the country, which were (and still are) continuously being added to. The first aim of the research was to be able to interpolate optimal rainfields between raingauges at individual locations and also to suggest the best estimates of catchment (areal) totals of rainfall, both historically and currently.
- The accuracy of radar in pinpointing, in considerable detail, where rain falls was not in question, but some difficulties still existed in terms of estimating rain rates from radar data. The second aim was to combine raingauge and radar data into a meaningful composite to provide an optimal rainfield acceptable to users. However, radars did and continue to cover only part of the country. There are less densely-populated areas with sparse raingauge coverage and no radars, but where satellite surveillance information could be accessed. It was therefore considered important to link satellite, radar and gauge data together to obtain the best estimate of rainfall in these remote areas.
- The third and main aim of the research was to devise a product to enable the publication, on a daily basis, of the 24-hour rainfall over the country. The means of achieving this aim was seen to be optimal integration of gauge, radar and satellite estimated data, which would of necessity improve with commissioning of more radars, upgrading of software and introduction of a new generation of satellites.

Theoretical development
Combining the precision of raingauge data with the coverage of satellite data and the detail of radar data was, in effect, an important objective of this research. The techniques

initially envisaged as a means of achieving this were optimal spatial interpolation using a technique called Kriging and an associated one called co-Kriging.

It turned out that co-Kriging was not a good option because of the large computational load. This load comes from the fact that there are of the order of one million small areas (pixels) approximately 1.5 kilometers square (the typical spatial resolution of a weather radar) covering the subcontinent and the surrounding oceans. The challenge was to be able to map the country's rainfall routinely to that detail. Even the quadrupling of computer speed, between the year 2000 (when the project was proposed) and its end in 2003, did not diminish the need to find a better way to process data, which would be easy to automate. A method of Kriging, exploiting the efficiency of the Fast Fourier Transform, was consequently developed. The process of development necessitated having to deal with a highly technical subject, involving some difficult and advanced mathematical ideas and theory.

Outcome and Technology Transfer
The techniques developed for optimal integration (merging) of data fields and their implementation to date have been most fruitful. The daily rainfall maps on the SAWS:METSYS website bear testimony to this successful outcome.

The Fast Fourier Transform approach to Kriging provided the basis for the coding of an algorithm to accomplish the massive computing task efficiently and speedily. Speed is of the essence in the delivery of the daily rainfall maps in real time. Information on the accumulated rainfall for the 24 hours until 8:00 am SA time, derived from the recording raingauges around the country, arrives at METSYS (Bethlehem) by 9:00 am daily. By that time, the previous 24 hours' satellite and radar images will have been used to produce the best estimates, respectively, of the rainfall totals per pixel over the whole area. The merging of the three fields: gauge, radar and satellite is then done and the result posted on the METSYS web-site by 11:30 am. A thorough description of the practical implementation of this methodology is presented in the body of *VOLUME 2* of the SIMAR final report. Some examples of the website output are reproduced therein.

Conclusions and recommendations

SIMAR has successfully met its objectives and laid the foundation for a national (and potentially regional) rainfall observing system which promises to meet all reasonable requirements regarding spatial and temporal resolution and real-time availability of data.

There are several areas in which the current SIMAR system, with further attention to data availability, research and development, can be improved. These are:

- *Radar inter-calibration* – improved techniques to constantly monitor the complex radar calibrations within the NWRN.
- *Modern electronic techniques* – ongoing development and use of modern electronic technology to improve data collection, communication, processing and storage.
- *Radar and satellite product research* – ongoing research to improve the quality of remote sensed data and derived products.

- *Data exchange and availability* - It is evident that much more work is required on the issues related to institutional willingness to collaborate and share information. The process should occur at institutional level and be formalized through Memorandums of Understanding or other binding means. In addition government agencies should consider making remotely sensed data available free of charge and without any restriction or accessibility issues to researchers. This can only occur if government sponsors the necessary infrastructure to obtain remotely sensed data from an array of platforms to be utilised for research and training purposes.
- *Speeding up and refinement of merging algorithms* – the currently used method of combining gauge, radar and satellite measurements of rainfall can be refined using variants of Kriging which exploit the clustering of measured data and regions to be infilled.
- *Repair of weather radar images of rainfall* – ground clutter and anomalous propagation are nuisance contaminants of images of rainfall estimated by radar. These can be infilled with good estimates of rainfall if they have been identified correctly.
- *Accumulation of rainfall from radar and satellite images* – because the radar and satellite images are instantaneous snapshots of rainfields, the naïve superposition of the images gives a false accumulation field when total depths of rain are required. A method of morphing based on the calculated advection field will overcome this present deficiency.

The SIMAR system would also benefit from certain infrastructural improvements, the most crucial of these being:

- *Raingauge network* – incorporation of all qualifying raingauges in South Africa and the region, irrespective of institutional ownership. The modernization of the raingauge infrastructure through the use of modern electronics and communication systems to provide better temporal resolution on a real-time basis.
- *Radar network* – incorporation of all operational radars and standardisation of operations and data acquisition systems in the region. The expansion of the NWRN to fill areas not covered.
- *Satellite* – immediate exploitation of opportunities presented by the deployment of the MSG satellite.

The above envisaged improvements build on the existing platform of work developed under SIMAR and will make a considerably more acceptable product. Follow-on projects already under way are addressing these issues with energy.

Capacity development

The capacity developed at both technical and professional levels through SIMAR has provided a sound foundation upon which further capacity can be built.

The training of technical personnel in the maintenance and upgrading of observational systems received high priority in the SIMAR programme. Four individuals from the previously disadvantaged groups were trained in maintaining the electronic observational infrastructure thus ensuring the long-term sustainability of the observing systems. Training was conducted in-house, through courses as well as self-development. The training initiative was also expanded to the international arena with training on SIMAR related subjects presented to students from other African countries such as Botswana and Tanzania. As SIMAR products are used routinely by institutions, training will continue well beyond the lifetime of this project. It is especially training in the utilisation and interpretation of SIMAR products where a strong need exists. Users should also be trained and educated in the use of remotely sensed data, its advantages as well as its limitations.

There are two aspects to professional capacity building which were achieved here – indirect (people being exposed to the ideas and concepts but not working on the project) and direct (those people personally involved with aspects of the project). In addition, there was a strong component of Competency Development as a direct result of the project.

Indirect Capacity Development.
In the Hydrology Section of Umgeni Water, where one of the researchers (Scott Sinclair) worked in 2001 and 2002, two PDIs were kept abreast of the developments of the project in both informal and formal (reports, presentations) ways. The 2002 final year class of 28 Civil Engineering Students in Hydrology at the University of Natal, Durban, contained 16 PDIs (of whom 5 were women) and 2 white women. The project co-leader (Geoff Pegram) made frequent reference to the SIMAR in class and repeated the oral presentations given in this regard at the European Geophysical Society in Nice in April 2002. These presentations tempted two students from previously disadvantaged backgrounds to undertake dissertations under the project co-leader's supervision during the second semester of 2001

Direct Capacity Development.
In the second semester of 2001, a female final year student, Deanne Everitt, undertook a dissertation study under the supervision of the project leader entitled "Flood Impacts: Planning and Management". This was an overview study making use of the output from SIMAR, with special focus on the Umlazi catchment in Durban. A later addition to the team was Nokuphumula (Phums) Mkwananzi, a practising Engineer, who registered for an MScEng at Natal University under the supervision of the project co-leader in 2002, worked on the WRC project "Extension of Research on River Flow Nowcasting to include Levels of Inundation" which depended on SIMAR input of rainfields, and completed his Masters in September 2003.

Competency Development
Because of the nature of the Research, a number of people in Umgeni Water, Durban Metro/eThekwini Municipality, SAWS: METSYS and the University of Natal have been exposed to new ideas and potentials for ameliorating flood damages using the ideas that are direct spinoffs from SIMAR; new technology has been developed and existing technology has been improved and refined. Every individual involved has grown in competence and benefited from the project; in the long run the wider community in the region will be beneficiaries.

Knowledge dissemination

Knowledge generated by SIMAR has been disseminated through peer-reviewed articles, conference presentations, workshops and during international visits. These include the annual South African Society for Atmospheric Sciences (SASAS) conferences. The SASAS conference that coincided with the World Summit on Sustainable Development (WSSD) in 2002 provided an international platform for three SIMAR presentations. Members of the SIMAR team also used opportunities during visits to Lesotho, Botswana, Mozambique, Burkina Faso and the Kenya Institute for Meteorological Training and Research as well as the Drought Monitoring Centre to present the progress within SIMAR. The potential agricultural applications of SIMAR products were presented by members of the research team at a workshop organised by an agricultural service provider.

An important means of relatively quick dissemination of the ideas that are the outcomes of research are via presentations at conferences and Symposia. Such presentations at National and International Fora include the following:

National:

1. Burger R.P., P.J.M. Visser, K.P.J. de Waal and D.E. Terblanche (2002). Convective Storm Climatology over the South African Interior. Annual Conference of the South African Society for Atmospheric Sciences. Pretoria, 2002.
2. Deyzel I.T.H. (2002). Application of Satellite Data in Estimating Surface Rainfall. Annual Conference of the South African Society for Atmospheric Sciences. Pretoria, 2002.
3. Kroese N.J., J.N.G. Swart and A.J. Lourens (2002). The Implementation of a real-time reporting raingauge network in South Africa. Annual Conference of the South African Society for Atmospheric Sciences. Pretoria, 2002.
4. Visser P.J.M, J.A. Blackie and S. Boersma (2002). Quality Control and Product Development for the National Weather Radar Network. Annual Conference of the South African Society for Atmospheric Sciences. Pretoria, 2002.
5. Fernandes L. and L. Dyson (2003) Comparison between SIMAR Rainfall and MM5 Rainfall Prognosis for the Rainfall of March 2003. Annual Conference of the South African Society for Atmospheric Sciences. Pretoria, 2003.
6. Kroese N.J. (2003). Meteosat Second Generation (MSG) and its application in South Africa. Annual Conference of the South African Society for Atmospheric Sciences. Pretoria, 2003.
7. Visser P.J.M. (2003). The Detection and Removal of Ground Clutter by Auto-Correlating Volume Scanned Radar Reflectivity Fields. Annual Conference of the South African Society for Atmospheric Sciences. Pretoria, 2003.
8. Nhlapo A.L. (2003). Weather Radar Reliability (*Poster presentation).* Annual Conference of the South African Society for Atmospheric Sciences. Pretoria, 2003.

International:

1. Seed A.W. and G.G.S. Pegram (2001). Using Kriging to Infill Gaps in Radar Data due to Ground Clutter in Real-Time. *Fifth International Symposium on Hydrologic Applications of Weather Radar - Radar Hydrology,* Kyoto, Japan, November.
2. Pegram, G.G.S.and Seed, A.W., (2002). 3-Dimensional Kriging using FFT to Infill Radar Data. Presentation at *27th EGS Assembly*, Nice, France. April.

3. Pegram, G.G.S., Seed, A.W. and Sinclair, D.S. (2002). Comparison of Methods of Short-Term Rainfield Nowcasting. Presentation at *27^{th} EGS Assembly*, Nice, France. April.
4. Sinclair, D.S., Ehret, U., Bardossy, A and Pegram, G.G.S., (2003). Comparison of Conditional and Bayesian Methods of Merging Radar & Raingauge Estimates of Rainfields, Presentation at *EGS - AGU - EUG Joint Assembly*, Nice, France, April.

In yet other ways, SIMAR benefited substantially from international exchanges of knowledge. Initiatives to present data and results led to fruitful discussions and the pursuit of new ideas. In particular, Professor Geoff Pegram was active in fostering Australian and European links, as marked by the following personal invitations:

- 1999 - present : Invited to collaborate with the Australian Cooperative Research Centre for Catchment Hydrology
- 2001 - Mieyegunyah Distinguished Fellow Awardee, Melbourne University - Visiting Research Fellow (12 weeks)
- 2002, 2003 & 2004 - Visiting Research Fellow - Civil and Environmental Engineering Department - University of Melbourne - (8 weeks)
- 2002 - Keynote Speaker: 27^{th} Hydrology and Water Resources Symposium, Melbourne, 20-23 May.
- 2003 - Invited to participate as rapporteur (and future full member of Steering committee) in European Union project: MUSIC / CARPE DIEM Joint Workshop with End Users, at Düsseldorf-Neuss, Germany, May 27 and 28, 2003: "Current Flood Forecasting Practices In Europe"

The knowledge gained by these interactions has benefited not only the participants in SIMAR but has already realized its potential to benefit the post-graduate students working on on-going projects which are out-growths of the Water Research Commission's investment in SIMAR.

ACKNOWLEDGEMENTS

The members of the Steering Committee for this project were:

Dr GC Green	:	Water Research Commission - Chairman
Dr DE Terblanche	:	SA Weather Services
Mr E Poolman	:	SA Weather Services
Mr K Estié	:	SA Weather Services
Mr S van Biljon	:	Department of Water Affairs and Forestry
Mr DB du Plessis	:	Department of Water Affairs and Forestry
Mr JC Perkins	:	Department of Water Affairs and Forestry
Prof GGS Pegram	:	University of Natal
Dr J C Smithers	:	University of Natal
Dr C Turner	:	Eskom
Prof S Walker	:	University of the Orange Free State
Dr D Sakulski	:	National Disaster Management Committee
Ms B van Wyk	:	Rand Water
Mr M Summerton	:	Umgeni Water

We are deeply indebted to the Steering Committee for making this study so successful. In particular, we want to single out the chairman, Dr George Green, for his contribution. The Water Research Commission's vision in appointing experts and interested parties to the steering committees, which guide, advise and monitor the researchers in their endeavours, has borne excellent fruit in this research. In addition, the interest shown by the potential end-users (here represented by DWAF) has sharpened the focus of the research in providing an end-product which will be useful, not just another academic curiosity.

Our thanks go to the Water Research Commission for providing the funding that made this applied research possible. It has enabled considerable collaboration between those who are normally isolated individuals in traditionally compartmentalised organisations.

Finally, the authors of this report are grateful for the kind assistance of several people among whom, requiring special mention, are Karel de Waal, Prof. Geoff Pegram, Nico Mienie, Jan Blackie, Ernst Vermeulen and other staff members of METSYS.

3 December 2003

GLOSSARY OF ACRONYMS

AIPR	Adapted infrared Power law Rain rate
AP	Anomalous Propagation
ASM	Angular Second Moment
AVHRR	Advanced Very High Resolution Radiometer
BSRR	Bi-Spectral Rain Rate
CAPPI	Constant Altitude Plan Position Indicator
DCA	Deep Convective Activity
DEM	Digital Elevation Model
DF	Discriminant Function
GLCM	Grey Level Co-occurrence Matrix
HRV	High Resolution Visible
ICD	Iterative Constrained Deconvolution
IDM	Inverse Distance Moment
IR	Infra-Red
ITR	Infra-red Threshold Rainfall
IWSM	Infrared Water Vapour Spectral Mask
LDA	Linear Discriminant Analysis
MDV	Meteorological Data Volume
NASA	National Aeronautics and Space Administration
NASDA	National Space Development Agency (NASDA) of Japan.
NWRN	National Weather Radar Network
MSG	Meteosat Second Generation
MSRR	Multi Spectral Rain Rate
PR	Precipitation Radar
RDAS	Radar Data Acquisition System
RF	Radio Frequency
RFE	Satellite based Rainfall Estimation
SAWS	South African Weather Service
SIMAR	Spatial Integration and Mapping of Area Rainfall
SEVIRI	Spinning Enhanced Visible and Infrared Imager
TITAN	Thunder Identification Tracking and Nowcasting
TMI	TRMM Microwave Imager
TRMM	Tropical Rainfall Measuring Mission
VIP	Video Integration Processor
VIRS	Visible and infrared Radiometer System
VIS	Visible
WAR	Wetted Area Ratio
WSRR	Warm Stratiform Rain Rate
WV	Water Vapour

TABLE OF CONTENTS

1. INTRODUCTION

Water is the single most important variable affecting life on the planet. Rainfall, the major source of water for human activities, is one of the least understood variables measured by weather services and other institutions. Our ability to measure rainfall accurately and adequately falls far short of the demands required by modern day technologies and lifestyles.

Against this background and the fact that conventional meteorological observing stations are dwindling at an alarming rate in South Africa, the SIMAR (Spatial Integration Mapping of Area Rainfall) programme sought to develop a near real time, spatially high-resolution, rainfall measuring and mapping system for southern Africa based on both surface measurements and measurements using remote sensing techniques.

The aim of this project, a fundamental component of SIMAR, was to utilise and improve the use the remote sensing estimations of rainfall with a view to produce a daily spatial map of area rainfall. The report deals with the methodology to estimate rainfall with remote sensing platforms, such as weather radar and geostationary weather satellite. The specific aims of this project were to:

Radar products:

- Provide an MDV-based, real-time, radar rainfall map of the radar covered area of South Africa as an integral part of the "Real-time mapping of daily rainfall over South Africa for water resource applications" umbrella programme.
- Optimize merging in areas of radar overlap and utilize the reflectivity measurements in these areas for additional performance testing.
- Improve radar-rainfall algorithms which address the outstanding issues of data quality and integrity (hail, brightband, ground clutter and coastal/orographic rain).
- Include additional radar information as it becomes available and identify the most serious gaps in South Africa's weather radar coverage.

Satellite products:

- Provide an MDV-based, real-time, satellite rainfall map of South Africa as an integral part of the SIMAR umbrella programme
- The investigation and development of suitable rainfall estimation algorithms from satellite data for South Africa including addressing the known problems related to coastal and orographic rain.
- Integrate raingauge, radar and satellite rain fields to provide the daily rainfall maps in conjunction with the modeling component of SIMAR.

The focus of this project was to provide the three rainfall fields – one derived from radar, another from satellite and yet another from the daily reporting raingauges – to be used by the SIMAR data integration procedure. Section 2 describes the flow of radar data from the source radar to a merged radar rainfall map. Section 3 discusses performance testing results, radar overlap statistics, ground clutter removal and radar-raingauge comparisons. Section 4 is dedicated to satellite rainfall estimations and represents work almost exclusively done by a single research-team member, Izak Deyzel. The operational products of SIMAR are available on the web at http://metsys.weathersa.co.za.

2. THE NATIONAL WEATHER RADAR NETWORK DATA FLOW

The National Weather Radar Network (NWRN) consists of 10 fully operational weather radar systems (Figure 2.1). The network and the individual radar systems operate similarly to the radar configuration of the VIPOS project (Terblanche, 2000). Just before this project's initiation the NWRN was expanded with the commissioning of the Polokwane (Pietersburg) radar.

A short description of the processes employed to generate a merged radar rainfall field from the NWRN follows. A diagram of the processes is shown in Figure 2.2. Every radar site operates with the in house-developed, PC DOS-based Radar Data Acquisition System (RDAS), which controls the radar antenna and processes the output from the radar receiver using the locally-developed DISPLACE method (Terblanche et al, 1996). The radar systems operate in volume scan mode whereby data from 224 range bins (each bin 900 m in length, thus providing a maximum data collection range of 201 km) are collected for full rotations at one degree resolution in azimuth and at 18 elevations steps. The base-scan of the radar is set at 1^{o} for coastal radar systems and 1.5^{o} for inland systems. Each radar volume scan requires 4 to 5 minutes to complete. RDAS includes software that assists with the calibration of the radar, which depends on the relationship between receiver output and radar reflectivity. This facilitates standard calibration procedures throughout the network and comparisons between the performances of different radar systems. The data from RDAS is transferred to a PC operating under LINUX in which the radar reflectivity data is transformed from spherical coordinates to Cartesian coordinates, referenced to sea level, with a 1 km vertical and horizontal resolution.

The data in horizontal planes at specific heights are called Constant Altitude Plan Position Indicators (CAPPI). CAPPIs are produced in the Meteorological Data Volume (MDV) format, which is the common format used in SIMAR for all grid data and products. MDV is also the inherent data format of the Thunderstorm Identification, Tracking, Analysis and Nowcasting system (TITAN) (Dixon and Wiener, 1993). At the radar site, several processes are followed to eliminate ground clutter, and thereafter the best available radar reflectivity to rain rate algorithm for the specific radar is applied to create a daily radar rainfall field. This process is modular, and improvements in the methodology, such as in the clutter removal, data infilling and rainfall estimation procedures, can be accommodated as they arise. The daily rainfall field, in MDV-format, is transferred via the Frame Relay network of the South African Weather Service (SAWS) from every radar site to a main Linux server for the creation of the merged radar precipitation field. This methodology is somewhat different from the VIPOS configuration. In VIPOS the radar reflectivity data was merged and a common Z-R relationship applied across the merged field. Reasons for this change from VIPOS are discussed in Sections 3.3 and 3.6.

The 1 km resolution daily precipitation data are received from each individual radar and are merged into a daily radar precipitation field. The resolution of the merged precipitation data conforms to the 1024 by 1024 one minute latitude and longitude horizontal grid points. In areas of overlap between radars, the maximum precipitation amount at each pixel from any radar is used in the merging process. This implies that the radar with the best view of a specific atmospheric volume of the atmosphere is used in the final merged field. The merging process is done on the 06:00 GMT rainfall accumulation field from the individual radar and is available half an hour later. Future improvements of the precipitation accumulation process at the radar will aim to provide the daily radar rainfall field at 06:15 GMT (08:15 SAST).

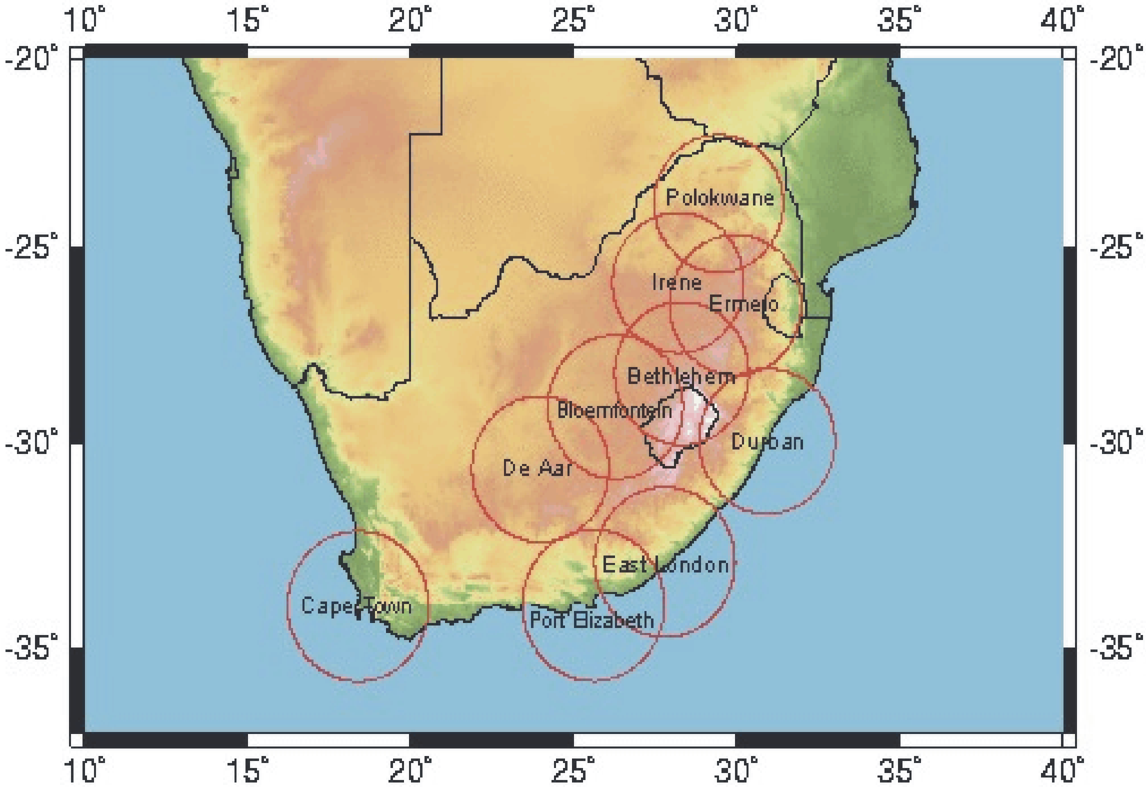

Figure 2.1 The coverage of the 10 weather radar in the National Weather Radar Network. The circles indicate the radar data collection range of 200 km.

3. RADAR PRODUCTS

Weather radar has the distinct feature of sampling precipitating clouds at high spatial and temporal resolution, greatly exceeding the resolution presently possible with raingauges or satellite. However, weather radar suffers from many complexities, owing to the fact that it is an active remote sensing device, often affected by atmospheric conditions, attenuation, the earth's curvature, beam blocking, uneven radar beam filling, clutter contamination, regional climate variability and other factors.

This section of the report focuses on the efforts to improve some of the challenges of using weather radar to estimate precipitation accurately. It commences in Section 3.1 with examples of how radar system performance was scrutinised for accuracy. The systems used to evaluate the overlapping regions between radar are also discussed in Section 3.2 The detection and removal of ground clutter is addressed in Section 3.3, Achievements in this regard can be regarded as a major breakthrough towards significantly reducing errors in precipitation estimation in the NWRN. In section 3.4 radar rainfall and raingauge comparisons are performed. Although the task of accurately estimating precipitation at all radars still demands more work, some methodologies to address this are presented in this report.

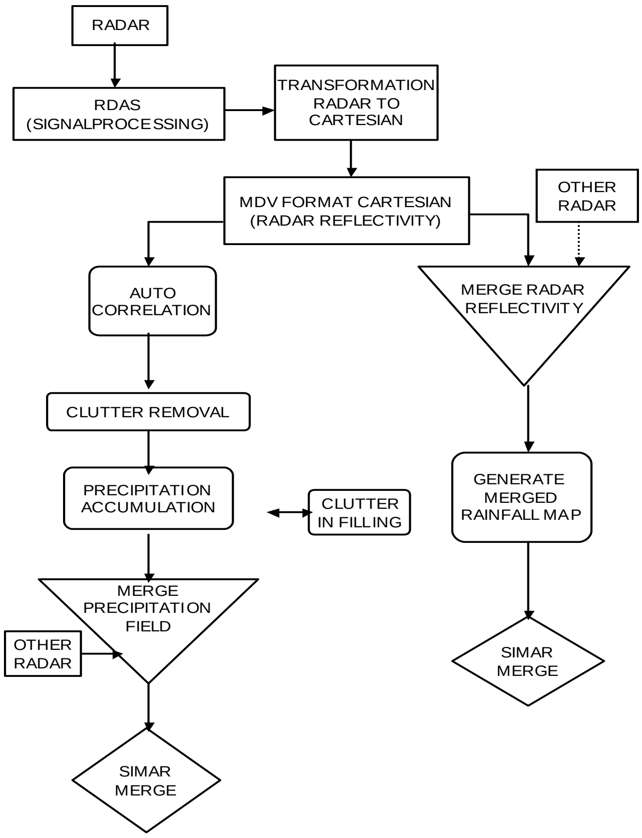

Figure 2.2 The data flow with the clutter removal procedure indicated by the left leg and the previous data flow method without clutter removal on the right leg.

3.1 Radar system performance tests

3.1.1 Radar sun-track calibration

The sun-track radar calibration method establishes a technique to evaluate radar systems at various operating frequencies using a common extraterrestrial source of radio-emission. The radio-emission of the sun at a radar frequency is known and therefore provides an independent measurement of radar sensitivity which can be obtained for each individual radar. Sun-track calibrations of the MRL-5, Irene and Bloemfontein radars are presented. This methodology still needs to be extended to other radars, especially the Durban and Ermelo radars, which seem to have sensitivity defects. This paragraph is divided into three main sections. The first section focuses on the determination of the antenna pointing accuracy. The second section derives the Gain/Temperature ratio of the system, which is a measure of the performance sensitivity of the receiving system. The third section equates the measured received signal from the sun's radio emission to that of the calculated expected signal derived from the flux density of the sun for that day, and determines the true RF signal calibration level for the radar. This is of particular relevance in that it evaluates the entire antenna and receiver system and by implication the propagation path of the transmitter.

In all, five sun-tracks were recorded from the MRL-5 radar in an attempt to establish consistency of the measurements. In large this has been achieved, although there are areas that need to be refined such as the determination of the pointing accuracy of the antenna over the hemisphere. A measured shortfall of an average of two dB's of the measured received signal to that of the calculated expected received signal was found to be due to averaging correction that must be applied when a stable signal generator is used.

Determination of the antenna pointing accuracy
Five sun-tracks were recorded, where the antenna was placed in an angular position bisecting the sun's transition path due to the Earth's diurnal rotation. The received signal level in VIP counts (raw digital sample values in RDAS) was recorded along with the time of maximum received signal. The angular displacement of the antenna from that of the position of the solar disk transit at the time of maximum received signal was noted and summarised in Table 3.1.1. An example of the solar track on 2001/11/12 is shown in Figure 3.1.1.

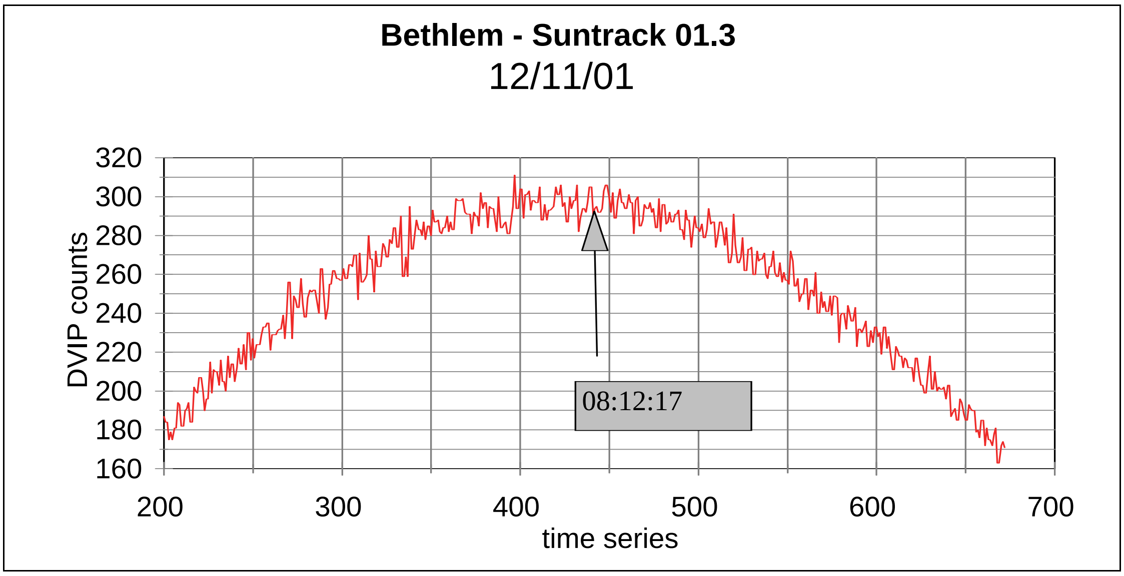

Figure 3.1.1 Example of a solar track VIP count for the MRL-5. Time series in seconds.

Table 3.1.1 Solar position and antenna direction position measurements

Sun Track	**Antenna Position**		**Solar Max**		**Difference Degrees**	
Date	**Az**	**El**	**Az**	**El**	**Az**	**El**
26/09/2001	39.1	293.6	293.7	39.2	0.1	0.1
9/11/2001	78.7	55.8	77.9	56.2	0.8	0.4
12/11/2001	71.3	64.6	70.5	65.0	0.8	0.4
10/1/2002 a	83.2	63.4	82.4	64.0	0.8	0.4

10/1/2002 b	271.7	55.6	272.0	55.6	0.3	0.0

Inferences can be drawn from Table 3.1.1 that the MRL-5 antenna accuracy is good in the Western hemisphere but deteriorates in the Eastern hemisphere.

Determination of the Gain/Temperature ratio

Table 3.1.2 Estimation of the MRL-5 radar system temperature.

MRL-5 antenna gain	39 dB
The antenna noise temperature viewing an average background sky at 30 degree elevation at 2880 GHz is estimated to be	30 ^{o}K
$T_{a\,=}$ 30(1/L)	14 ^{0}K
T_{feed}	160 ^{0}K
T_{paramp}= 1.5 dB noise figure	120 ^{0}K
$T_{paramp\ gain\ =}$ 12 dB	8 ^{0} K
T_{system}	302 ^{0}K
Expected G/T. = 7943.28/302	14.2 dB

Table 3.1.3 The measured Gain/Temperature ratio of the MRL-5 radar.

DATE	**Gain/Temperature Ratio**
26/09/2001	13.44 dB
9/11/2001	12.38dB
12/11/2001	14.01 dB
10/1/2002 a	14.04 dB
10/1/2002 b	13.03 dB

The measurement on 09/11/2001 was particularly noisy and it should be viewed with suspicion. Exacerbating the inaccuracy of the measurement was the positioning of the antenna so as to allow the sun to drift through the maximum of the main beam. The latitude and longitude of the radar used to position the antenna differed slightly to that used to calculate the sun’s transit.

Antenna co-ordinates used at the radar:
Latitude -28, 05, 54 S
Longitude 28, 09, 47 E

Antenna co-ordinates determined by the latest survey:
Latitude -28, 05, 52.5 S
Longitude 28, 09, 48.6 E

This discrepancy only became evident during the sun tracks and the surveyed co-ordinates are now used.

The measurement of the solar flux density.

The received daily solar flux density as seen on Earth is calculated for the system under test and then compared to that of the actual measured received signal.

The MRL-5 parameters for the S-band system are:
Antenna = 4.5 metre diameter
Gain = 39 dB
Radome one-way loss = 0.25 dB
Beam width = 1.5 degree
Waveguide loss = 2.0 dB
Receiver bandwidth = 1.5 MHz

Table 3.1.4 shows that the average of the signal difference is –1.92 dB. This is consistent with the expected fluctuation for the averaging of a coherent signal. There is confidence in the technique to obtain measurements to within one dB of that calculated and it has been achieved at the MRL-5 radar.

Table 3.1.4 The received daily solar flux density as seen on Earth calculated for the system under test and compared to that of the actual measured received signal.

	Solar Flux Density $W.m^{-2}. Hz^{-1}$	Max mean DVIP count	Received Signal dBm	Calculated Received Signal dBm	Signal difference dB
26/09/2001	$259.8 * 10^{-22}$	315	-101.38	-99.48	-1.9
9/11/2001	$234.01 * 10^{-22}$	250	-102.8	-99.93	-2.87
12/11/2001	$211.57 * 10^{-22}$	300	-101.68	-100.29	-1.31
10/1/2002 a	$215.32 * 10^{-22}$	310	-101.58	-100.29	-1.29
10/1/2002 b	$215.32 * 10^{-22}$	260	-102.53	-100.29	-2.24

Irene radar measurements

Two sun-tracks were done on the Irene system with the following results shown in Table 3.1.5.

Table 3.1.5 Solar position and antenna direction position measurements for MRL-5 radar.

Sun Track	**Antenna Position**		**Solar Max**		**Difference Degrees**	
Date	**Az**	**El**	**Az**	**El**	**Az**	**El**
21/11/2001	92.0	46.8	92.7	45.6	0.7	1.2
10/01/2002	91.9	54.5	92.6	53.2	0.7	1.3

Table 3.1.6 The measured Gain/Temperature ratio of the MRL-5 radar against the expected value of 19.7 dB

DATE	Gain/Temperature Ratio
21/11/2001	10.51 dB
10/01/2002	9.87dB

From Table 3.1.5 it can be concluded that with regard to azimuth, the Irene radar is performing well, while the elevation is overestimated at high elevation angles. This can lead to underestimating storm tops close to the radar.

Table 3.1.7 The received daily solar flux density as seen on earth calculated for the system under test and compared to that of the actual measured received signal with the receiver bandwidth assumed at 1.5 Mhz..

	Flux Density Joules /deg K	**Max mean DVIP count**	**Received Signal dBm**	**Calculated Received Signal dBm**	**Signal difference dB**
21/11/2001	$282.52 * 10^{-22}$	147	-109.67	-100.67	-9.51
10/01/2002	$291.7 * 10^{-22}$	137	-110.02	-100.02	-10

There appears to be an excessive loss in both the G/T and the measured solar flux for the Irene radar. Similar to the MRL-5, a 2dB difference can be subtracted from the signal difference due to the averaging of a coherent signal, resulting in a –8 dB signal difference for Irene radar.

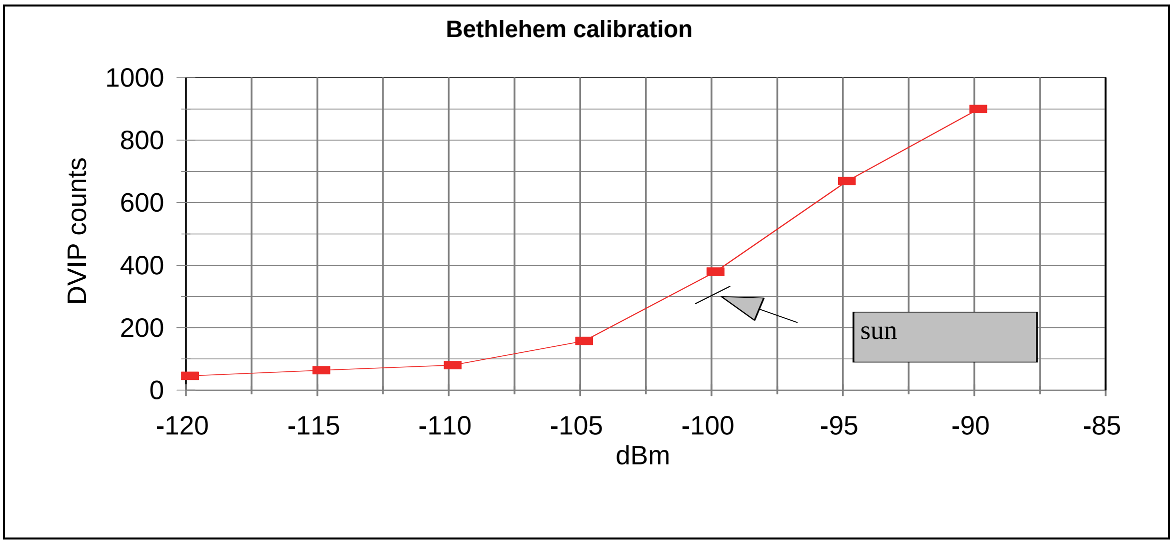

Figure 3.1.2 Comparison of sun-calibration with signal generator calibration for MRL-5.

Bloemfontein measurements

Three sun-tracks were done on the Bloemfontein system with the following results (Table 3.1.8).

Table 3.1.8 Solar position and antenna direction position measurements on 2001/02/22

Sun Track TIME (GMT)	**Antenna Position**		**Solar Max**		**Difference Degrees**	
	Az	**El**	**Az**	**El**	**Az**	**El**
8:58:5	53.1	62.1	52.5	62.3	0.6	0.2

9:50:00	27.8	69.4	26.9	69.5	0.9	0.1
12:01:10	300.1	58.2	299.1	57.6	1.0	0.6

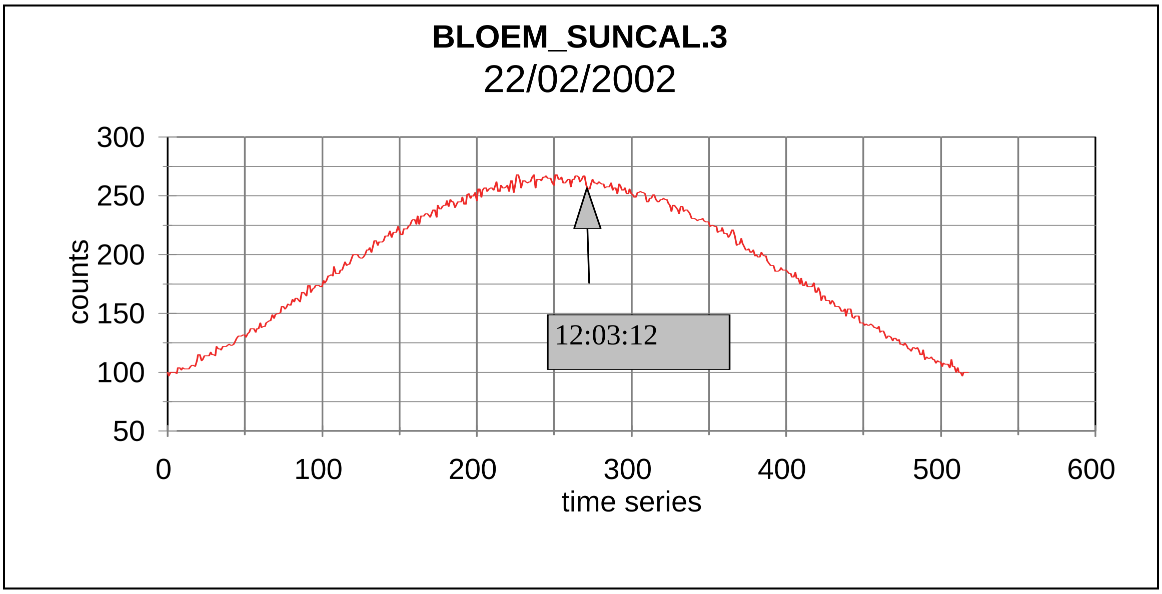

Figure 3.1.3 VIP counts for Bloemfontein radar from the sun track as the sun crossed the antenna's main beam.

Noting the increase in the VIP received counts when the sun is in the antenna main beam to the received level from a quite sky (Figure 3.1.3) determines the Gain/Temperature ratio of the radar system. This is a significant ratio and allows comparison to other systems. The C-band radar situated at Bloemfontein recorded a Gain/Temperature ratio of 19.01 dB, compared to 10.51 dB for the MRL-5. The reason for the superior figure for the C-band radar is the narrower beamwidth (more gain), less waveguide loss and a better noise figure.

In determining the calibration accuracy, the calculations indicated a received signal level of -98.38 dB, to an actual measured received level of -98.57 dB, after the correction for the signal averaging correction of 2 dB, resulting in a difference of -0.19 dB. This value shows that the Bloemfontein radar system was operating within specification on the date of this test.

3.2 Radar overlap statistics

Making comparisons between raingauge data and radar rainfall estimates is a complex issue, because of weather radar system characteristics and the large differences in sampling volumes and techniques between the two measuring devices. This complexity is increased when a radar network is used. The mosaic field is then generated by using the maximum reflectivity value available from any of the radars covering overlapping regions. When radar is under- or overestimating reflectivity intensity due to system and/or calibration errors, the final mosaic field will be affected. This phenomenon can be observed when storms move into or out of the overlap region and a significant change in intensity occurs. These errors lead to a sharp discontinuity in a rainfall field or reflectivity field at the boundary of the overlap region. Another aspect to consider is that the sensitivity of radars of the same wavelength differs. When the wavelengths differ, the radar sensitivity or minimum detectable signal differs even more. In general, a longer wavelength radar, such as the S-band MRL-5 radar, is less sensitive than a shorter wavelength radar such as the Enterprise C-band radar. However, at longer ranges, such as in overlap regions, the MRL-5 will suffer less from attenuation than the Enterprise (Bloemfontein/Irene/Ermelo) radars.

By investigating the overlap area of two radars, the following information can be obtained:

- The under or over estimation of a radar
- The antenna alignment with respect to each other
- Different view aspects of the same rain event
- Sensitivity of the individual radar.

Software was developed for analysing the overlapping areas between radars. A specific time is chosen and the closest corresponding volume scans from the radars are selected. A CAPPI altitude map of the overlap area is created to ensure that only the region observed by both radars is used. For the region between the Bloemfontein radar and the MRL-5, the 7 km CAPPI above sea level and higher is used. This represents an (eye shaped) area with a width of about 40 km, while the distance between the two radars is approximately 230 km. Therefore, the overlap region is between ranges of 90 to 130 km from both radars.

Figure 3.2.1 shows the overlap reflectivity comparisons between the MRL-5 and the Bloemfontein radar on 8 December 2001 at 13:45 GMT. Only positions where both radars detected reflectivity were included. Due to the sensitivity limit of the MRL-5 at this range, a lower limit of 13 dBZ was placed on the radar reflectivity values to be included. When the small time difference of 90 seconds between volume scans are considered, the regression line is very encouraging. The MRL-5 radar detects on average 5 dBZ more in the overlap region compared to the Bloemfontein radar. Data from the MRL-5 will therefore dominate this overlap area when the mosaic is created. At reflectivity below 20 dBZ, the Bloemfontein radar is more sensitive and detects smaller hydrometeors. Routine analysis between all radar overlap regions is now possible.

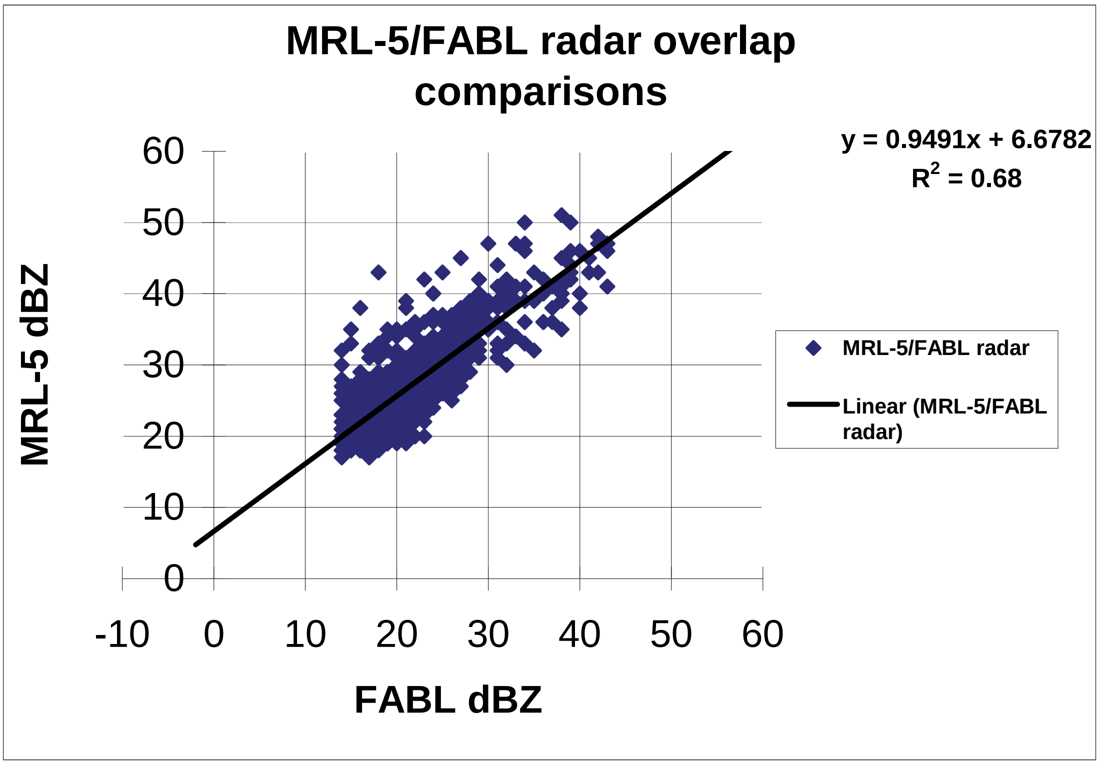

Figure 3.2.1 Bloemfontein and MRL-5 radar overlap for 8 December 2001 at 13:45 GMT

3. 3 Ground clutter removal

The ability of weather radar to estimate rainfall at high spatial and temporal resolution, has made it an attractive tool for water management. However, ground clutter is responsible for huge overestimations of rainfall during both rainless and rainy days. The method used previously within the NWRN, utilised the TITAN system to develop a clutter map over a short time period. The clutter map generates a mask of cluttered areas during a rainless period (no atmosphere-based returned signals) over the whole area of radar coverage. However, ground clutter is not temporally and spatially stationary. Due to continued changes in the atmosphere refractivity index resulting from temperature, moisture and pressure variations, ground clutter detection and removal by a clutter map, is often ineffective. Another option for clutter removal is presented by satellite images (IR and VIS) which assist in identifying no-rain days, when radar echoes can be ignored. Difficulties exist in the transitional situations where unambiguous answers cannot be provided from satellite images on the question of a positive precipitation event or not. The solution needs to be generated using information provided by the radar. Doppler processing capabilities on radars could assist greatly in detecting non-moving objects, while the signal to signal variance can provide insight into the properties of the target. However, Doppler radar is often still not able to identify ground clutter well under variable conditions and has particular problems with sea clutter. In the South African radar network, no radar has an operational Doppler facility and this option is in any case not available. Another clutter removal option which has been investigated is the application of statistical methods during sampling and processing of returned signals, using the auto-correlation between signals (Sugier J. et. al, 2002). This process is restricted by the fast-rotating antennas of operational weather radars.

The new scheme applied in the NWRN makes use of a similar principle, as it uses the auto-correlation of radar reflectivity between volume scans. The objective is to generate a daily "clutter" map which eliminates all precipitation over the locations detected as possessing ground clutter (possible ground clutter-contaminated precipitation) during any time over the accumulation period of 24 hours. Two problems are solved by this method. Firstly, it ensures that once a pixel is suspected of being contaminated by ground clutter during the rainfall accumulation process, it will be flagged for infilling from neighbouring points at the end of the accumulation process. Secondly, it avoids exaggerated daily radar rainfall estimations reaching values of several thousands of millimetres which can result from persistent ground clutter. This exaggeration would have a profound impact on the scaling of previously MDV-formatted files, resulting in a huge loss in resolution and precision of the stored data. Errors would also be transferred to the merged field and therefore seriously affected the inter-comparisons between radar, raingauge and satellite rainfall fields.

3.3.1 Method to detect and remove ground clutter from daily rainfall maps

The new method of clutter detection relies firstly on the premise that the radar reflectivity variability of ground clutter between volume scans is less compared to precipitating storms. Secondly, the variability of the radar reflectivity auto-correlation field of stratiform and convective storms display a smoothly correlated pattern in 3-D space compared to a highly variable spatial distribution of ground clutter. The extinction coefficient x determines the period for correlation to be considered. The following equation is executed on each pixel of the radar field:

$$E_T = X_T X_{T-1} x + E_{T-1}(1-x)$$

where E_T refers to the auto-correlation of radar reflectivity at volume scan at time T and x refers to the extinction coefficient. To prevent slow-moving storms from being flagged as ground clutter, an extinction factor of between 0.03 and 0.025 was used, depending on the radar. This allowed the decorrelation time for the autocorrelation to decrease from 1.0 to 0.3 after 3 hours or 40 volume scans. The resulting field of E_T has similar dimensions as the radar reflectivity field. Once the auto-correlation E_T at a location exceeds an empirically-determined threshold (relating to an average reflectivity of 37.4 dBZ over 40 volume scans), the location is automatically flagged as containing ground clutter for that day. If the vertical difference of the time series auto-correlation value exceeds another empirically-tested threshold relating to an average difference of 22.3 dBZ over 40 volume scans, or the horizontal difference exceeds a threshold relating to an average horizontal difference of 14.14 dBZ, the location is also flagged as containing clutter for the day. Once a location has been flagged as a ground clutter location, it is excluded from rainfall accumulation for that day. A final Gaussian filtering over a 5 by 5 grid area is performed to remove isolated clutter pixels left in the rainfall field. This ensures the removal of remnants of cluttered pixels on no-rain days. On days with rainfall, the rainfall pattern is more contiguous and isolated rainfall pixels are unlikely.

3.3.2 Results of ground clutter removal

The clutter identification and removal procedures were tested at radar sites with extensive clutter problems, these being the Cape Town, Port Elizabeth, Durban and Bethlehem (MRL-5) sites. The data were selected to correspond with days with widespread precipitation and days without any precipitation. The no-rain days show the effectiveness of the clutter removal procedure. Three types of radar reflectivity data were used to perform the rainfall accumulation:

- radar reflectivity data without any clutter removal process
- radar reflectivity data with the TITAN clutter map activated
- radar reflectivity data with the clutter removal method described in 3.3.1

The **clutter remove without filter** refers to data where the ground clutter flag was dynamically turned on as ground clutter was detected or off when the spatial auto-correlation criteria were not met. Accumulating these data to generate a radar-estimated rainfall field, still results in erroneous rainfall values within the masked area, although the errors are dramatically reduced. The filter is applied to the accumulated rainfall field and the clutter-flagged pixels removed from the rainfall field. The **area of clutter mask** refers to the final mask for ground clutter as created after a day by the auto-correlation criteria. The **mask** is defined as all the locations or pixels in the field which met the criteria to be flagged as ground clutter during that day. The reference to **masked area** is for those results from over the masked area only.

Durban radar clutter removal results

Table 3.3.1 Results for 2003/04/05 for Durban radar (a day without rain).

	Area with radar "rain-fall" (km2)	**Area of clutter mask (km^2)**	**Maximum rainfall value in domain (mm)**	**Maximum rainfall in masked area (mm)**	**Average rainfall in domain (mm)**	**Average rainfall in masked area (mm)**
Raw radar	440	440	3060	3060	209.4	209.4
Clutter map (TITAN)	404	404	3040	3040	189.8	189.8
Clutter remove without Filter	598	265	13.7	13.7	1.08	1.52
Clutter remove with Filter	38	-	3.7	-	1.29	-

.

The estimation of rainfall with ground clutter using raw data (no clutter removed) for Durban radar on 2003/04/05 resulted in daily maximum rainfall exceeding 3000 mm (Table 3.3.1). The TITAN clutter removal procedure (Clutter map) did not reduce these huge rainfall over-estimations. When the mask is used to cut the clutter out and the filter applied to remove isolated single pixels, the error area is reduced to only 38 km^2, while the estimated maximum rainfall is only 3.7 mm. Another important factor is the increase in area with rainfall before filtering from 404 km^2 to 598 km^2. This is due to the improved scaling of the MDV data format through elimination of ridiculous clutter-induced rainfall values. The reduction of the error area by clutter removal was 91%. The reduction in the rainfall amount error was 99.5 %.

Table 3.3.2 Distribution of rainfall on 2003/04/05 after filtering and clutter removal.

Rainfall interval(mm)	0	0.47	0.94	1.41	1.88	2.35	2.82	3.29	3.76

Percentage of area greater than interval	100	78	55	39	26	13	5	2	0
Area(km^2)	38	30	21	15	10	5	2	1	0

Table 3.3.2 shows that of the remaining clutter, 61% has values below 1.41 mm and 95% below 2.82 mm. The small remaining area with "rainfall", which in this case is still clutter-induced, can easily be disregarded.

Table 3.3.3 Results for 2003/05/12 for Durban radar on a day with widespread rainfall.

	Area with radar rainfall (km2	**Area of clutter mask (km^2)**	**Maximum rainfall value in domain (mm)**	**Maximum rainfall in masked area (mm)**	**Average rainfall in domain (mm)**	**Average rainfall in masked area (mm)**
Raw radar	28374	848	2860	2860	29.9	127.6
Clutter map (TITAN)	28374	848	2860	2860	29.4	111.5
Clutter remove without Filter	76694	480	162	140	10.8	21.8
Clutter remove with Filter	76356	-	162	-	10.7	-

Table 3.3.4 Distribution of rainfall on 2003/05/12 for the Durban radar.

Rainfall interval(mm)	0	16.4	32.8	49.2	65.6	82.0	98.4	114.8	131.2	147.6	164
Percentage greater than interval	100	21	6	2	1	0.4	0.2	0.1	0.05	0.01	0
Area (km^2)	76356	16316	4523	1561	645	326	158	99	41	9	0

On 2003/05/12 for Durban radar (Table 3.3.3) the area with rainfall increased by a factor of 2.67, after the clutter was removed. The MDV-format scaling of the raw rainfall data accumulation forced low rainfall values below 5 mm for the day to be scaled down to no rain. The maximum rainfall after clutter removal is only 160 mm and the MDV scaling does not adversely affect low rainfall values in this case. The reduction in the rainfall error was 60.8%. If the ground clutter errors are not removed, large discrepancies would result in daily radar-raingauge comparisons. In fact, in many instances before clutter removal, the radar rainfall field would not have indicated any rainfall, owing to the scaling of the MDV-format. The clutter remove procedure removed some rain over the ocean. Low level convective development over the warm Agulhas current was perceived as ground clutter. The ocean "clutter" coincides with the regions of maximum estimated rainfall over the ocean. Different rainfall estimation algorithms for both radar and satellite are required over the oceans. Table 3.3.4 shows that most of the rainfall on this day was below 16.4 mm. The MDV-format scaled most of the low rainfall to no rain in the raw radar data case.

Table 3.3.5 Results of radar rainfall fields 2003/06/04 for Durban radar with widespread light rainfall.

	Area with radar rainfall (km2	Area of clutter mask (km^2)	Maximum rainfall value in domain (mm)	Maximum rainfall in masked area (mm)	Average rainfall in domain (mm)	Average rainfall in masked area (mm)
Raw radar	1030	336	3620	3620	112.2	302.6
Clutter map (TITAN)	995	301	3620	3620	98.7	280.2
Clutter remove without Filter	37504	213	26.6	15.8	2.49	4.2
Clutter remove with Filter	35394	-	27.0	-	2.38	-

Table 3.3.5 shows the results for 2003/06/04 with widespread light rainfall. The rainfall error reduction after clutter removal was 97.7%. The improved scaling of the MDV data increased the area identified with rainfall dramatically from 1030 km^2 to 35394 km^2. The MDV scaling resulted in destroying the radar rainfall field when the raw radar and the TITAN clutter map were applied.

MRL-5 radar clutter removal results

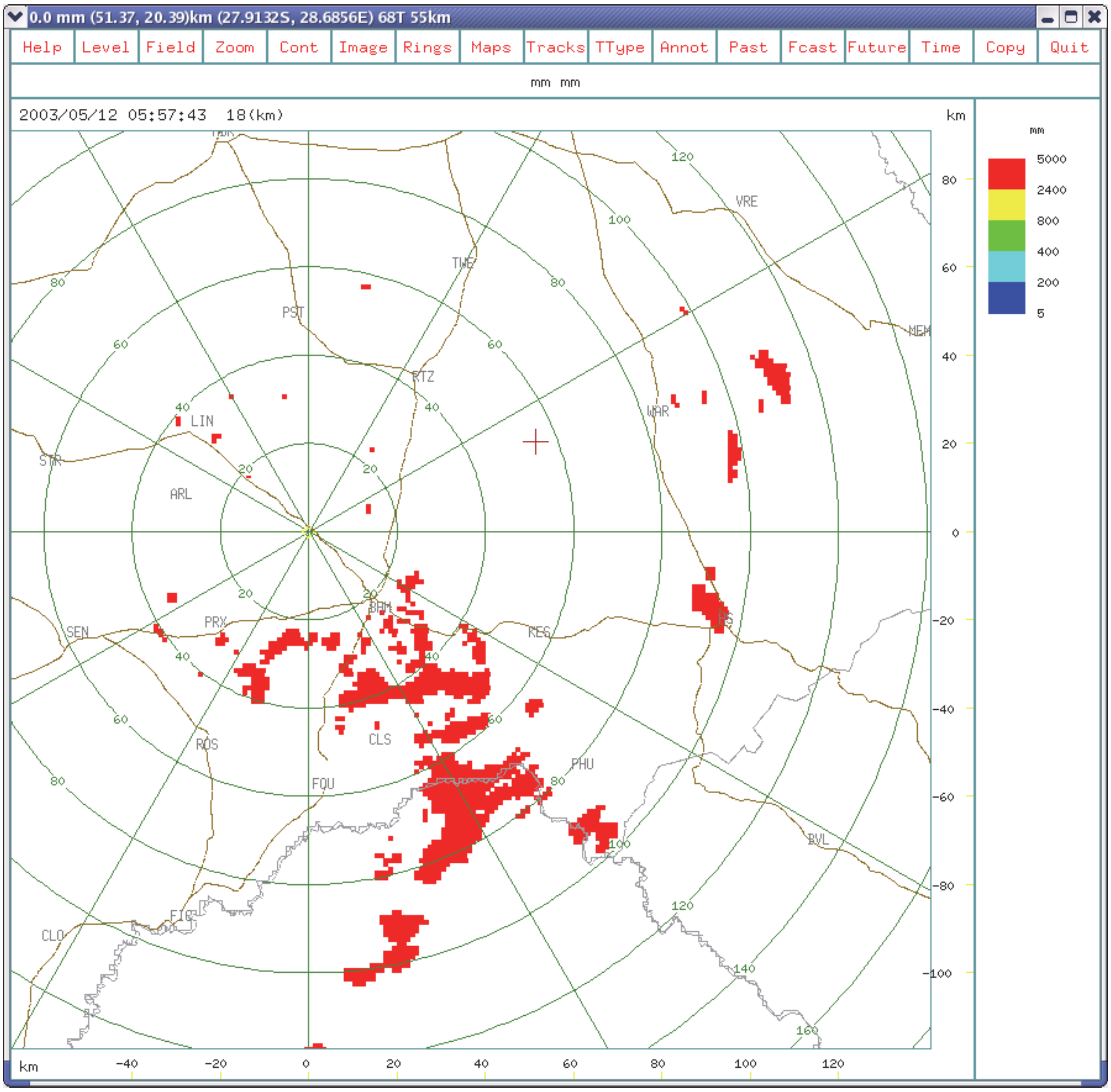

Figure 3.3.1 The clutter mask generated for the MRL-5 radar on 2003/05/12.

Fig 3.3.1 shows the clutter mask generated for the MRL-5 radar on 2003/05/12. Extensive ground clutter was detected at a range of 100 km. The ground clutter from the Rooiberge and Maluti Mountains is well demarcated. Around Harrismith the effect of the Platberg and the higher elevation around Memel in the top right part of the image is also shown. The day experienced widespread convective development.

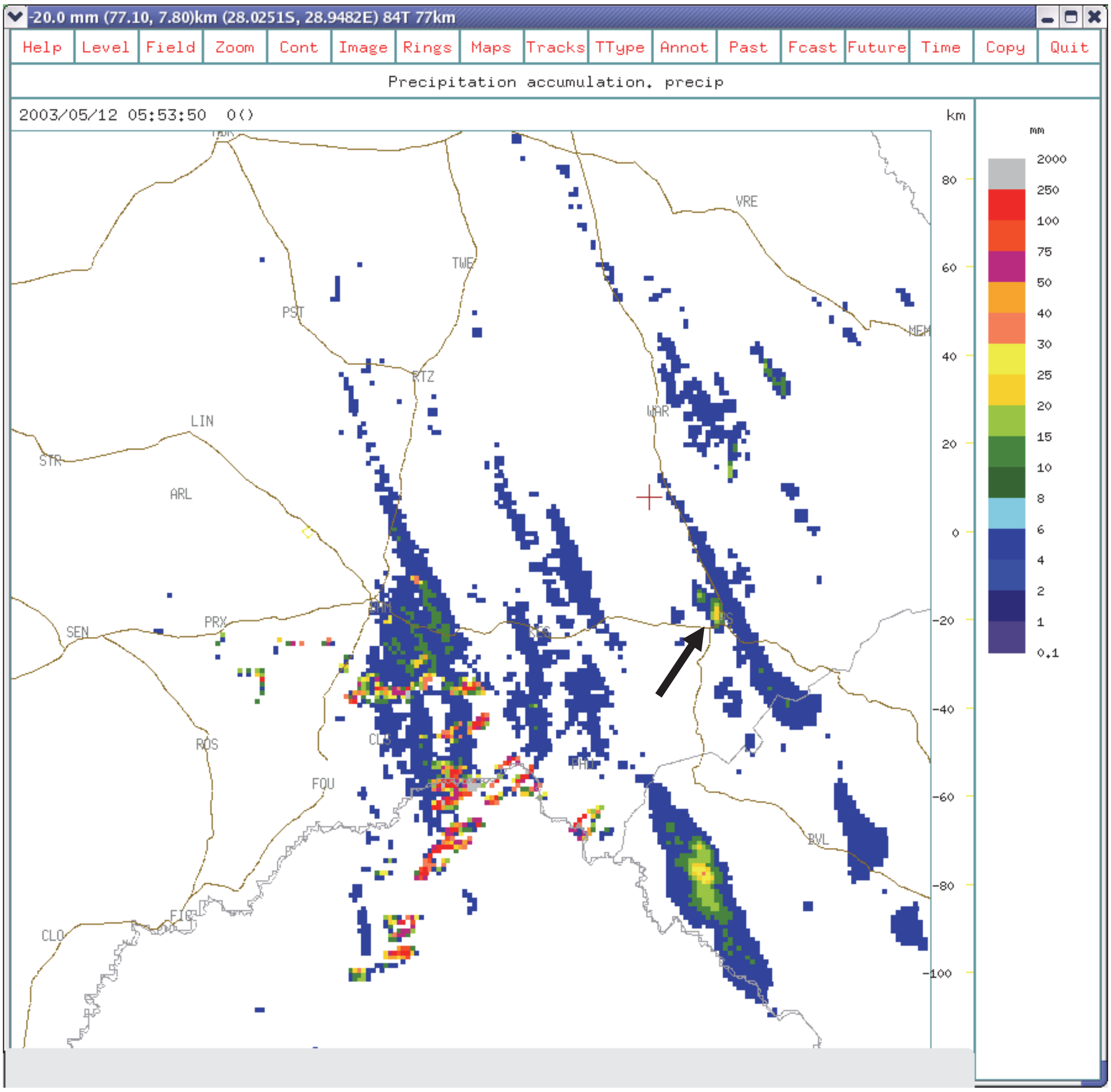

Figure 3.3.2 Radar rainfall estimation from radar reflectivity data with the TITAN clutter map applied for 2003/05/12.

Figure 3.3.2 depicts high rainfall values exceeding 2500 mm on 2003/05/12 for the MRL-5 radar when applying the TITAN clutter map. The ground clutter affects a must greater area than only the estimated extreme rainfall areas. An important feature of this display is the lack of colour resolution, despite the extensive colour palette. This is due to the scaling of MDV formatted file with extreme values in the data. The area of high rainfall close to Harrismith (indicated by an arrow in Figure 3.3.2) looks very much like a rainfall event. However, it is correctly identified as ground clutter.

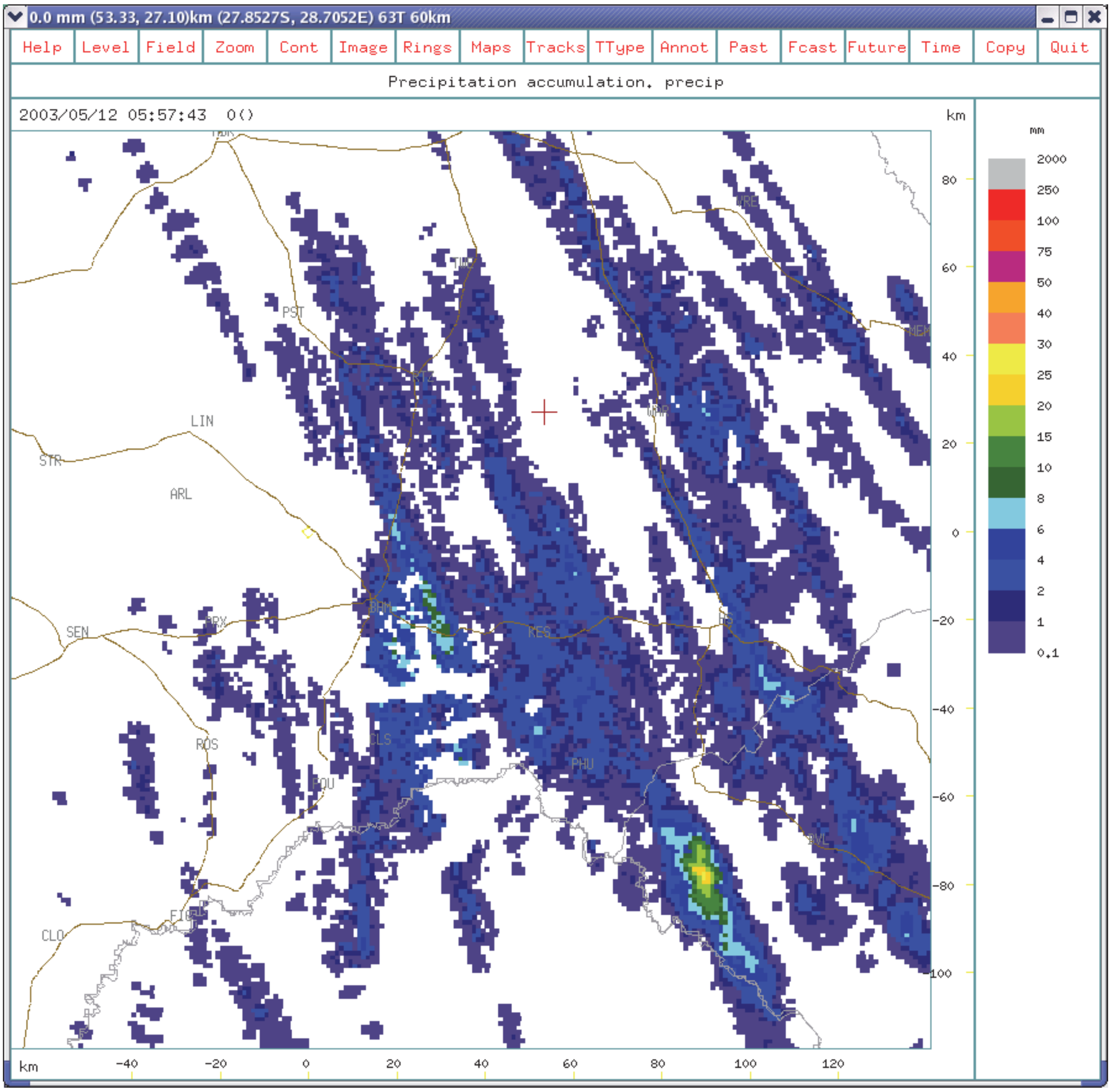

Figure 3.3.3 Radar rainfall estimated with the clutter mask applied and a filter for isolated pixels on 2003/05/12 for MRL-5 radar.

In Figure 3.3.3 a very dramatic improvement is observed to the resolution of the data as the color legend is now fully used by improved MDV scaling. Notice the observing of low rainfall values in the image compared to Figure 3.3.2. From the spatial data outside the masked area, sufficient information is available to determine the rainfall in the masked areas.

Table 3.3.6 Results of radar rainfall estimation on 2003/04/19 by the MRL-5 radar (a no-rain day).

	Area with radar rainfall (km2)	**Area of clutter mask (km^2)**	**Maximum rainfall value in domain (mm)**	**Maximum rainfall in masked area (mm)**	**Average rainfall in domain (mm)**	**Average rainfall in masked area (mm)**
Raw radar	542	537	3000	3000	322.9	325.7
Clutter map (TITAN)	509	504	3000	3000	327.5	330.6
Clutter remove without Filter	771	43	7.1	3.47	1.1	0.8
Clutter remove with Filter	321	-	7.1	-	1.1	-

Table 3.3.7 Rainfall distribution on 2003/04/19 after clutter removal.

Rainfall interval(mm)	0	0.81	1.62	2.43	3.24	4.05	4.86	5.67	6.48	7.29
Percentage greater than interval	100	45	19	8	4	2.5	2.1	0.9	0.3	0
Area(km^2)	321	147	60	27	13	8	7	3	1	0

Table 3.3.6 shows the results of a no-rain case on 2003/04/19 for the MRL-5 radar. The area error reduction after clutter removal is 59%, while the rainfall error reduction is 99.6%. Table 3.3.7 shows that most of the remaining radar rainfall values are below 0.8 mm. Most of this rainfall results from remnants of aircraft fight routes and small locations of anomalous propagation. The MRL-5 radar, with a 1.5^o beam width, is more prone to anomalous propagation effects. Mountain-induced clutter is removed very effectively.

Table 3.3.8 shows a reduction of 96.0% in the rainfall estimation error by the MRL-5 radar for a rain day (2003/05/12) after clutter removal. The area covered by rainfall is dramatically increased due to improved MDV-scaling.

Table 3.3.8 Results for radar rainfall estimation by the MRL-5 radar on 2003/05/12.

	Area with radar rainfall (km2)	**Area of clutter mask (km^2)**	**Maximum rainfall value in domain (mm)**	**Maximum rainfall in masked area (mm)**	**Average rainfall in domain (mm)**	**Average rainfall in masked area (mm)**
Raw radar	2541	557	2620	2620	77.8	276.1
Clutter map (TITAN)	2495	532	2620	2620	76.6	278.0
Clutter remove without Filter	33349	104	82.0	16.5	3.0	4.8

Clutter remove with Filter	32543	-	82.0	-	3.1	-

Cape Town clutter removal results

Table 3.3.9 Results of radar rainfall estimation by the Cape Town radar on 2003/04/19, a day with light rain.

	Area with radar rainfall (km2)	**Area of clutter mask (km^2)**	**Maximum rainfall value in domain (mm)**	**Maximum rainfall in masked area (mm)**	**Average rainfall in domain (mm)**	**Average rainfall in masked area (mm)**
Clutter map (TITAN)	1207	863	326	326	11.9	15.8
Clutter remove without Filter	2496	1598	3.54	3.54	0.15	0.20
Clutter remove with Filter	2196	-	2.52	-	0.48	-

Table 3.3.9 shows that compared to the application of the TITAN clutter map, the rainfall error reduction on 2003/04/19 for Cape Town radar after clutter removal was 95.2 %. Raw radar data were not available for this day. Rainfall over the Western Cape is often very light and ground clutter from the mountains affects the estimation of rainfall. Unfortunately, few events with significant rainfall were available from the radar during the 2003 season to provide a more comprehensive study of the region. Nevertheless, it was found that the mountainous ground clutter is sufficiently removed. Clutter from non-stationary anomalous propagation does leave some small pockets of erroneous rainfall, but as observed below, these pockets are very small (<0.0025 %) compared to the domain of the radar.

Table 3.3.10 Results of radar rainfall estimation by the Cape Town radar on a no-rain day (2003/05/16).

	Area with radar rainfall (km2)	**Area of clutter mask (km^2)**	**Maximum rainfall value in domain (mm)**	**Maximum rainfall in masked area (mm)**	**Average rainfall in domain (mm)**	**Average rainfall in masked area (mm)**
Raw radar	901	899	585	585	79.2	79.4
Clutter map (TITAN)	710	650	176	176	7.7	7.8
Clutter remove with Filter	43	-	2.8	-	0.82	-

Error area reduction after clutter removal on 2003/05/16 at Cape Town radar was 95.2 %, while the rainfall error reduction after clutter removal was 99.0%.

Port Elizabeth radar clutter removal results

Table 3.3.11 Results from the Port Elizabeth radar for a rain day (2003/04/29).

	Area with radar rainfall (km2)	**Area of clutter mask (km^2)**	**Maximum rainfall value in domain (mm)**	**Maximum rainfall in masked area (mm)**	**Average rainfall in domain (mm)**	**Average rainfall in masked area (mm)**
Raw radar	27297	1334	1270	1270	13.8	60.6
Clutter map (TITAN)	45506	1402	600	600	8.1	28.9
Clutter remove with Filter	85428	-	88.5	-	4.35	

Table 3.3.12 Rainfall distribution after clutter removal for 2003/04/29 for the Port Elizabeth radar.

Rainfall interval(mm)	0	8.9	17.9	26.8	35.8	44.8	53.7	62.7	71.6	80.5	89.5
Percentage greater than interval	100	8.9	1.8	0.7	0.3	0.06	0.01	0.01	0.00	0.00	0
Area(km^2)	85428	7609	1566	597	252	54	11	8	5	3	0

Table 3.3.11 shows that the reduction in rainfall as estimated by the Port Elizabeth radar for 2003/04/29 was 68.5% after clutter removal. The Port Elizabeth radar detects a lot of ground clutter. Sand dunes to the east of Algoa Bay and mountains in the interior are responsible for ground clutter. Ground clutter over the land is completely eliminated by the clutter filtering method. However, anomalous propagation from the ocean allows the islands in Algoa Bay to spuriously appear and result in remnants of small areas of erroneous rainfall cells. Table 3.3.12 shows that most of the rainfall area as detected by radar received less than 8.9 mm. The dramatic increase in rainfall area with the clutter removed from the raw-data radar rainfall field is evident, and is due to improved scaling of the data in the MDV-format.

Table 3.3.13 Results for the Port Elizabeth radar on 2003/04/19 (a no-rain day).

	Area with radar rainfall (km2)	**Area of clutter mask (km^2)**	**Maximum rainfall value in domain (mm)**	**Maximum rainfall in masked area (mm)**	**Average rainfall in domain (mm)**	**Average rainfall in masked area (mm)**
Raw radar	449	443	1310	1310	82.9	84.0
Clutter map (TITAN)	480	409	500	500	22.8	26.3
Clutter remove with Filter	89	-	12.8	-	1.6	-

Table 3.3.13 shows an area error reduction of 80.2% on 2003/04/19 for the Port Elizabeth radar after clutter removal. The rainfall error reduction after clutter removal is 98.1%.

The remaining clutter is over the ocean. All the clutter over land was effectively removed in this case.

3.4.1 Raingauge-radar comparisons

The generation of a mosaic rainfall field from the National Weather Radar Network (NWRN) requires a broader investigation of rainfall data derived from raingauges and radar. This involves the verification of the ability of every radar to sample rainfall adequately, because an error by any radar will affect the acceptability of the end product. In this section of the report, data from the MRL-5 radar and the Durban radar are compared with raingauge network measurements. Finally, automatic weather station data are used to test the ability of other radars in the network to measure rainfall. This procedure assists in the detection of radar-specific errors, with the objective to minimise them and thereby improve the final mosaic rainfall product.

3.4.1 MRL-5 and Liebenbergvlei raingauge comparisons

In the VIPOS (WRC Report No 954/1/01) report, a case study based on data from the MRL-5 radar and surface rainfall measurements from the Liebenbergvlei raingauge network for 24 January 1996 was documented. This case study supported the use of maximum vertical radar reflectivity in the Marshall-Palmer equation ($Z= 200 R^{1.6}$) to determine rain rates for a mosaic radar reflectivity field. This method and algorithm have therefore been applied since the inception of mosaic radar-rainfall compilation and the networking of radars. A detailed study on the performance of this algorithm is therefore appropriate.

Twelve days in the 2000/2001 summer season during which significant rainfall occurred over the Liebenbergsvlei catchment were chosen to compare the rainfall measured by raingauges with the rain as estimated by the MRL-5 over each guage location. To provide a more representative radar rainfall value at a particular location, an average over the 9 adjacent radar pixels centered on the gauge position was taken.

During the MRL-5 calibration performed on 25/8/2001, a 1.8 dB surplus in radar reflectivity was noted, due to a previous overestimation of the radar system. This 1.8 dB overestimation in radar reflectivity for the 2000/2001 season, relates to an overestimation of about 27-30% in rain rates. In all subsequent calculation a 1.8 dB correction was applied. Table 3.4.1 shows the sensitivity of rain rate estimations through the Marshall-Palmer Z-R relationship for a 1.8 dB error.

Table 3.4.1 The impact of a 1.8 dB error in the radar system on rain rate estimations.

dBZ	Marshall-Palmer	dBZ – 1.8	Marshal-Palmer
20	0.64 mm/hr	18.2	0.50 mm/hr
30	2.73 mm/hr	28.2	2.11 mm/hr
40	11.53 mm/hr	38.2	8.90 mm/hr
50	48.62 mm/hr	48.2	37.52 mm/hr

The use of the maximum vertical radar reflectivity suffers from 2 deficiencies:

- Accentuating the errors produced by melting hydrometeors (Bright Band)
- Causing rainfall overestimation in convective storms with a large reflectivity overhang.

Some advantages of using the vertical maximum radar reflectivity are:

- Reducing the effects of ground clutter and anomalous propagation
- Reducing overestimation owing to hail in storms.

To reduce the potential of errors, it was decided to investigate the average radar reflectivity between the 3 km asl CAPPI (or the lowest valid CAPPI layer) and the 8 km CAPPI layer as input to the Marshall-Palmer Z-R relationship instead of the maximum vertical radar reflectivity.

Of the 12 days selected, 5 can be categorised as convective precipitation days and 7 days as having Bright Band features, indicating stratiform precipitation. The Bright Band problem is more pronounce during stratiform than convective rainfall accumulations over 24 hours. Table 3.4.2 shows the result of daily raingauge measurements over the Liebenbergvlei compared with the daily radar rainfall estimation. The operational method of maximum vertical reflectivity and the vertical average method were used for the latter and radar/gauge ratios for both methods are shown.

The large radar/gauge ratio of 2.98 of the composite (maximum reflectivity) method indicates serious overestimation. The overestimation is reduced to 1.33 using the average radar reflectivity method. The case on 2001/02/07 was not well sampled by the raingauge network, resulting in an apparent huge radar overestimation of 4.25 with the average reflectivity method. This is a similar problem to that highlighted for 13 March 1995, when it was proven that even a dense raingauge network has a high probability of underestimating rainfall yielded by the complex fields made up of isolated convective storms. The use of vertical maximum reflectivity more consistently caused huge overestimations in the radar determined rainfall field for the MRL-5. The option of averaging rainfall is therefore favoured and will be included in the next version of TITAN. In the mean time, the averaging method is being implemented as part of the new rainfall estimation method for the MRL-5.

All the days on which the radar/gauge ratios for the average reflectivity indicated a value below 1.2 were classified as convective precipitation days. Most of the stratiform precipitation days produced ratios of between 1.2 and 1.6. It can be concluded that the average method provides a good approximation for convective rainfall, but is less successful for statiform precipitaion. Since lower rainfall rates are expected to contribute more towards rainfall totals in the case of stratiform precipitation, one is inclined to hypothesize that the rain rate for lower reflectivity values (< 50 dBZ) could be over-estimated by the averaging method, possibly from the remaining effects of the Bright Band, while at higher reflectivity values (>50 dBZ) the averaging method performs well.

Table 3.4.2 The comparisons between the Liebenbergvlei raingauges and the radar estimates of rainfall for selected days.

Date	***Rainfall* Type**	***Network Gauges* (mm) A**	***Radar average – 1.8 dB (mm)***	**B/A**	**Radar average (1.8 dB not corrected)**	**Radar composite- 1.8 dB corrected (mm) C**	**C/A**

			B				
2000/10/22	Convective	6.4	6.4	**1.00**	8.6	14.1	**2.20**
2000/10/23	Stratiform	10.5	15.0	**1.42**	19.7	29.1	**2.77**
2000/11/29	Convective	7.9	11.2	**1.42**	14.9	21.9	**2.77**
2000/12/03	Convective	2.3	2.6	**1.13**	5.8	9.6	**4.17**
2000/12/16	Stratiform	26.3	34.1	**1.31**	44.6	72.5	**2.75**
2001/01/12	Convective	7.3	8.4	**1.15**	11.1	15.0	**2.05**
2001/02/07	Convective (isolated)	1.6	6.8	**4.25**	9.3	14.2	**8.87**
2001/02/08	Stratiform	17.6	26.6	**1.51**	34.7	56.6	**3.21**
2001/02/17	Convective	14.8	15.1	**1.02**	19.8	32.5	**2.20**
2001/02/18	Stratiform	24.2	30.8	**1.27**	40.2	64.3	**2.65**
2001/03/22	Stratiform	9.8	15.6	**1.59**	20.7	49.5	**5.05**
2001/03/23	Stratiform	37.8	49.6	**1.31**	64.3	117.5	**3.10**
Totals		166.5	222.2	**1.33**	257.5	496.8	**2.98**

To investigate the possible correction of the Marshall-Palmer Z-R equation to improve the rainfall estimation of the averaging method, an investigation into the rain rate distributions of the gauges compared to that by the radar was performed. Figure 3.4.1 shows examples of obtaining the linear regression functions for the logarithmic rain-rate frequency distribution and rain rates of the gauges and the radar (Marshall-Palmer with averaging method), respectively.

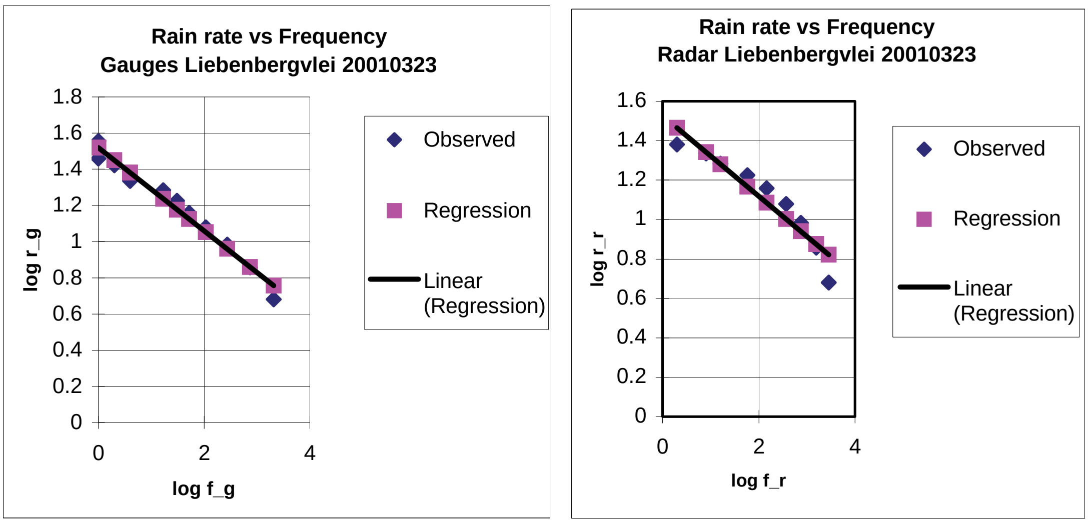

a) b)

Figure 3.4.1 Scatter plot of the log (rain rate frequencies) and log(rain rates) for (a). the rain gauges and (b) the average radar reflectivity for 23 March 2001.

Through linear regression, linear equations are obtained :

$$\log r\_g = m_1 \log f\_g + C_1 \quad (1)$$
$$\log r\_r = m_2 \log f\_r + C_2 \quad (2)$$

where g refers to gauges and r to radar, m is the linear regression function gradient and C the y-offset. To obtain the relationship between log r_g and log r_r, the following equation applies:

$$\log r\_g - \log r\_r = a \log r\_g + b$$

where $a = (m_1 - m_2)/m_1$ and $b = (1 - a) C_1 - C_2$,

which then results in the following equation:

$$R = \left(\frac{Z}{200 \cdot 10^{-1.6b}} \right)^{\frac{1}{1.6(1-a)}}$$, which can be rewritten as $Z = A R^B$.

(3)

This equation is solved to provide new Z-R relationships for each day. Examples of the results for each day are shown in Table 3.4.3.

Table 3.4.3 The new Z-R relationships determined for each day.

Date	**A**	**B**
20001216	240	1.52
20010208	311	1.46
20010217	250	1.6
20010218	268	1.52
20010323	388	1.42
AVERAGE	290	1.5

From the above data it appears that a more favourable Z-R relationship to be used is $Z = 300 R^{1.5}$. Results of recalculating the radar estimated rainfall with this new Z-R relationship using the average radar reflectivity, are provided in Table 3.4.4 The overall gauge/radar ratio is reduced from 1.33, when the Marshall-Palmer Z-R was used, to 1.19 for the $Z= 300 R^{1.5}$. $Z= 300 R^{1.5}$ was again tested for other days in the 2000/2001 season and results are shown in Table 3.4.5. The poor ratio for 2000/12/25 was once again due to poor sampling by the gauges of rainfall from isolated convective storms. Overall it was found that the radar rainfall estimation was much improved by using the average reflectivity and applying the relationship $Z= 300 R^{1.5}$.

Table 3.4.4 The rainfall estimated by $Z= 300 R^{1.5}$ using the radar reflectivity average.

Date	***Gauges* mm**	***Radar Average* $Z= 200 R^{1.6}$**	**Radar/Gauge Ratio for $Z= 200 R^{1.6}$**	**Radar Average $Z= 300 R^{1.5}$**	**Radar/Gauge Ratio for $Z= 300 R^{1.5}$**
2000/10/22	6.4	6.4	1.	5.6	0.88
2000/10/23	10.5	15.0	1.42	13.0	1.23

2000/11/29	7.9	11.2	1.42	10.5	1.32
2000/12/03	2.3	2.6	1.13	3.7	1.60
2000/12/16	26.3	34.1	1.31	30.3	1.15
2001/01/12	7.3	8.4	1.15	7.9	1.08
2001/02/07	1.6	6.8	4.25	6.0	3.75
2001/02/08	17.6	26.6	1.51	24	1.36
2001/02/17	14.8	15.1	1.02	14	0.94
2001/02/18	24.2	30.8	1.27	27.0	1.11
2001/03/22	9.8	15.6	1.59	13.3	1.35
2001/03/23	37.8	49.6	1.31	42.9	1.13
Totals	**166.5**	**222.2**	**1.33**	**198.2**	**1.19**

Table 3.4.5 Results of test days using the $Z = 300 R^{1.5}$ equation with the averaging method.

Date	**Gauge**	**Radar $Z = 300 R^{1.5}$**	**Ratio**
2000/12/25	10.1	16.5	1.63
2001/01/25	12.2	12.9	1.06
2001/01/30	10.1	9.2	0.91

3.4.2 Durban radar and raingauges comparisons

The Durban raingauge network was installed during December 1999 to investigate the ability of coastal radar to estimate rainfall. Coastal precipitation is presently sampled by METEOSAT based techniques. From experience gained with the RASCOAST project (Van Heerden and Steyn,1999), the ability of weather radar was also suspect. Errors in rainfall measurement at the coast are caused by:

- Enhancement of precipitation by orographic effects.
- A drop size distribution which can differ significantly from the Marshall–Palmer distribution, resulting in a different Z-R relationship for the coast.
- The mainly hygroscopic processes involving cloud condensation nuclei of ocean origin, which cause low cloud tops with significant precipitation being formed at altitudes below the radar base scan and at temperatures above the satellite infra-red temperature threshold for warm rain.

The Durban raingauge network consists of 16 tipping rain gauges. This report presents the first opportunity to use data from this network to investigate the performance of the Durban radar in measuring precipitation. Two raingauges (D011, D012) were excluded from the analysis, due to persistent ground clutter interference experienced by the radar in their vicinity. These gauges are both located further inland, to the west of the network (Kloof and Chef Mushroom). Days with significant rainfall were selected to get the widest distribution of rain rates. This was done because the radar detected rainfall poorly on days with rainfall less than 5 mm. Table 3.4.6 shows that the Durban radar significantly underestimates precipitation in most cases, despite the fact that the Durban gauge network is within 30 km from the radar. Table 3.4.7 show Z-R relationships needed to fit the rain rate frequencies.

Table 3.4.6 The comparison of Durban radar-estimated rainfall with data from the Durban rain gauge network.

Date	Gauges	Durban Radar	Radar/Gauge ratio
18/11/2000	38.3	26.3	0.68
19/11/2000	29.8	16.1	0.54
3/2/2001	16.8	11.9	0.71
13/2/2001	17.2	17.3	1.00
18/2/2001	38.3	19.8	0.52

Table 3.4.7 The Z-R ($Z = A\ R^B$) equations calculated for each day.

Date	A	B
2000/11/18	20	0.62
2000/11/19	Undefined (poor rain rate distribution)	Undefined
2001/02/03	80	1.84
2001/02/13	12	2.16
2001/0218	840	0.9

The underestimation is also observed when the rain rates are compared. In all the cases above, the top end of rain rates observed by the radar were half of that measured by the gauges. The values of A in Table 3.4.7 which are less than 200 also point to an underestimation and a potential radar calibration error of more than 3 dB.

The days were selected to represent different types of synoptic conditions to facilitate investigating the linkage between on- and off-shore flows and the results of radar rainfall estimation. The study unfortunately only succeeded in identifying errors in radar rainfall estimation. Refinements on the basis of circulation linkages will therefore have to be postponed until sources of error are eliminated. A proper sun calibration of the radar system is suggested.

3.5 Mosaic radar field and raingauge comparisons

Daily rainfall maps are generated operationally from the mosaic of the 10 radars in the South African National Weather Radar Network. From this mosaic field, 4 other products are generated for potential application in agriculture, namely:

- Running 1 month rainfall accumulations.
- Running 10 days rainfall accumulations.
- Number of days with rainfall exceeding 5 mm in the previous running month.
- Number of days lapsed since it last rained more than 5 mm.

The need for these products emphasises the importance of obtaining quality data from all radars on an uninterrupted basis. Poor radar performance, such as that discussed in the previous paragraph (3.4.2) in connection with the Durban radar, is exacerbated when radar-estimated daily rainfall is accumulated for a month. Gaps in data from radars when not operational affect the quality of these long-period accumulations. Raingauge networks, such as at Liebenbergsvlei and Durban, can provide backup, but such dense networks represent a luxury which is highly unlikely to be repeated at other radar sites.

There are 120 automatic weather stations (AWS) county-wide in the SAWS network, all recording rainfall at 5 minute intervals, which coincides with the radar mosaic field's temporal frequency. Although the AWS are few in number, their data can nevertheless, as a starting point, greatly assist in improving the rainfall measurement by network radars. Initially 60 of the 120 AWS locations were identified to fall within the domain of the radar mosaic. However, this number was reduced to 30, when a limit on the range from the radar to the AWS of 150 km was used. This again reflects the poor distribution of rain gauge data with a high temporal collection rate for data storage and collection.

Presented below are the rainfall accumulation graphs for radar-estimated rainfall and selected AWS raingauges over the period 1 October 2001 to 30 November 2001. Note there is a one day lag between radar and gauges due to the different recording times.

POLOKWANE RADAR

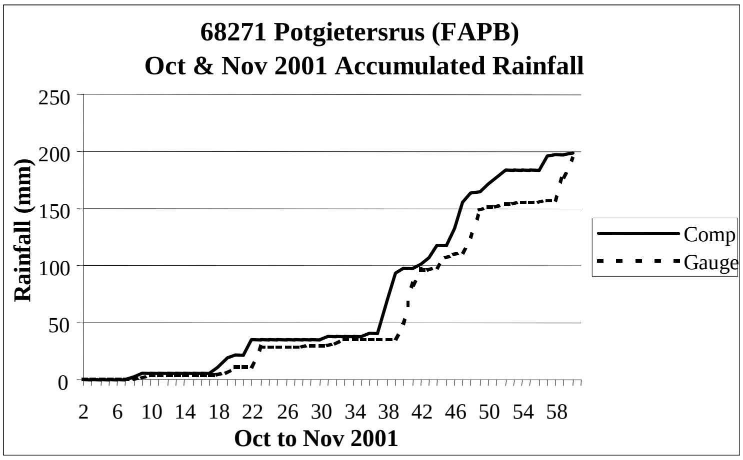

IRENE RADAR

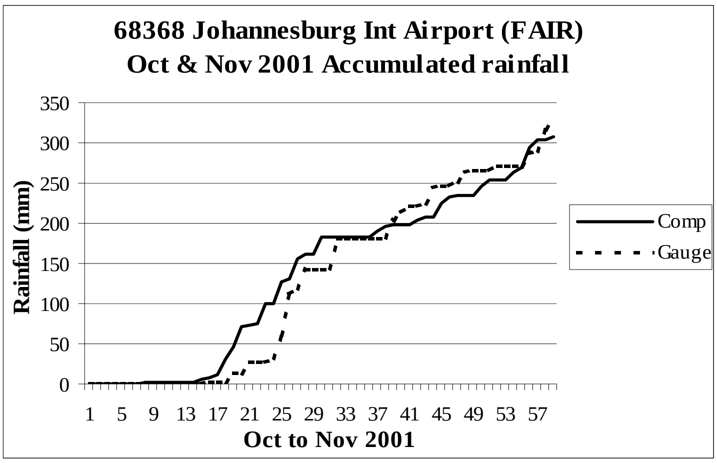

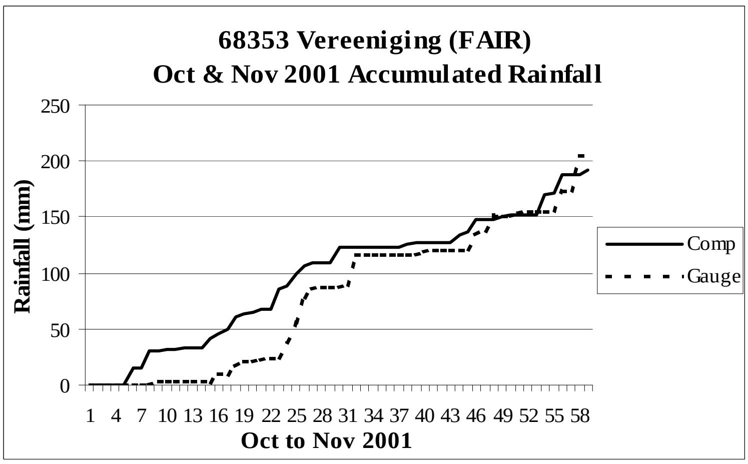

BLOEMFONTEIN RADAR

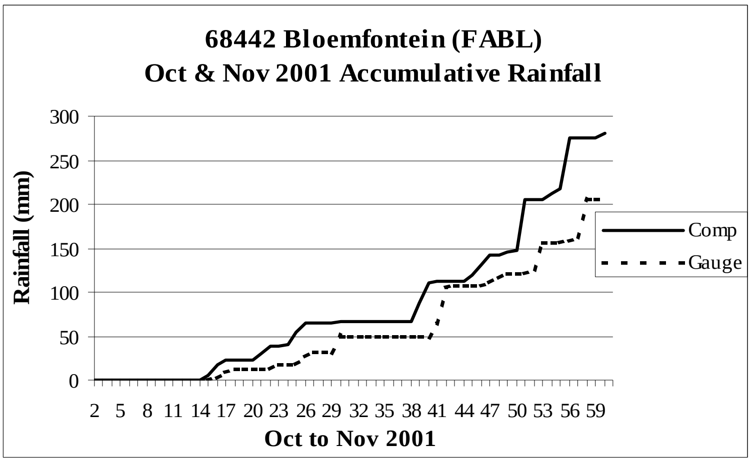

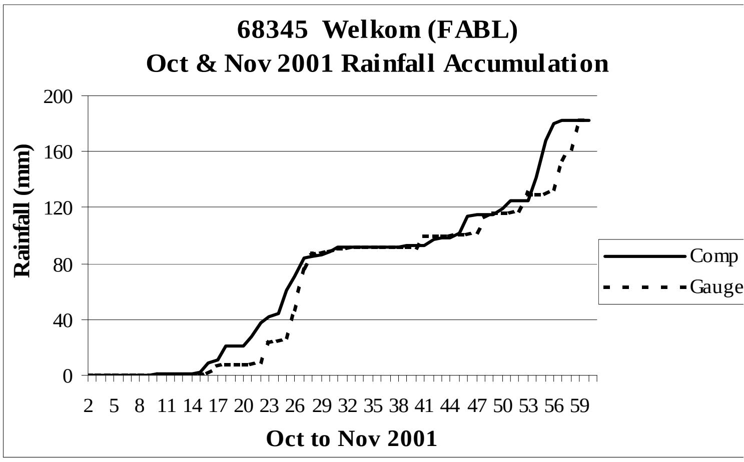

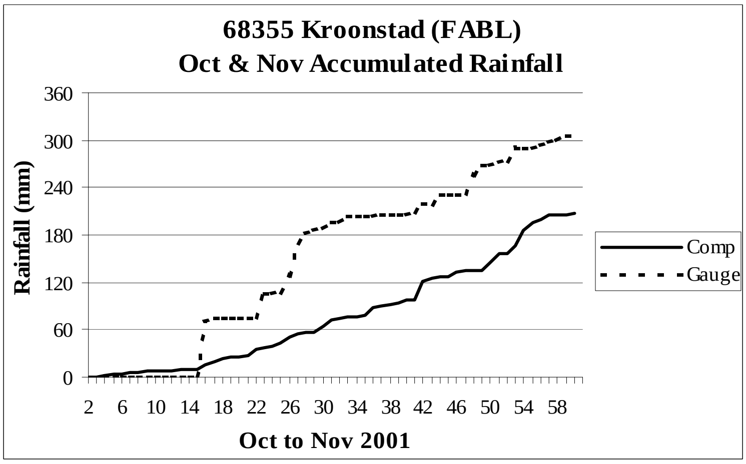

ERMELO RADAR

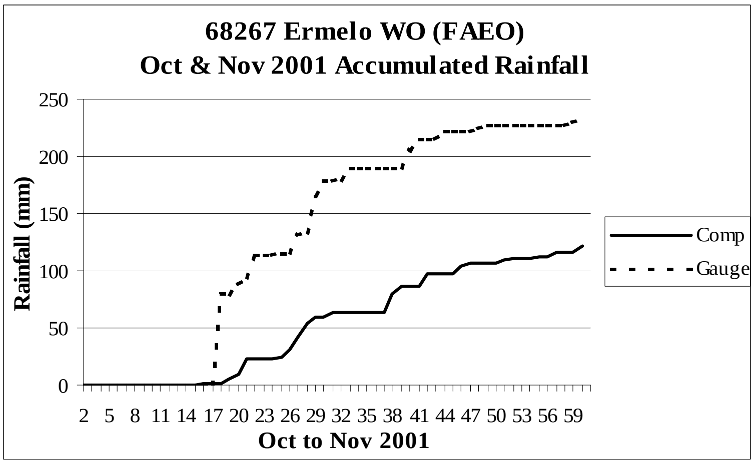

PORT ELIZABETH RADAR

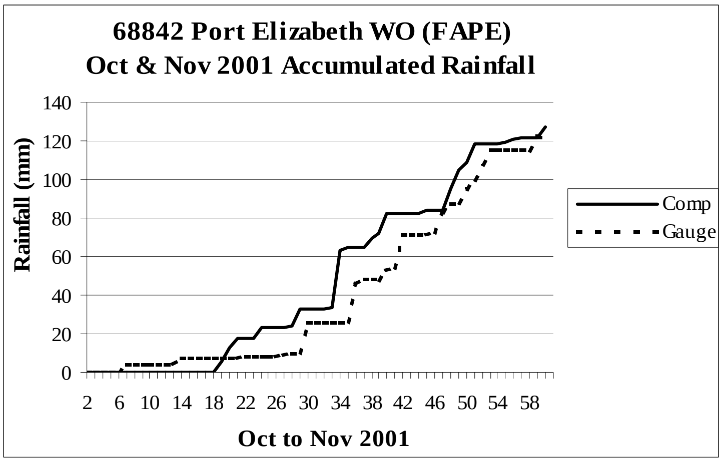

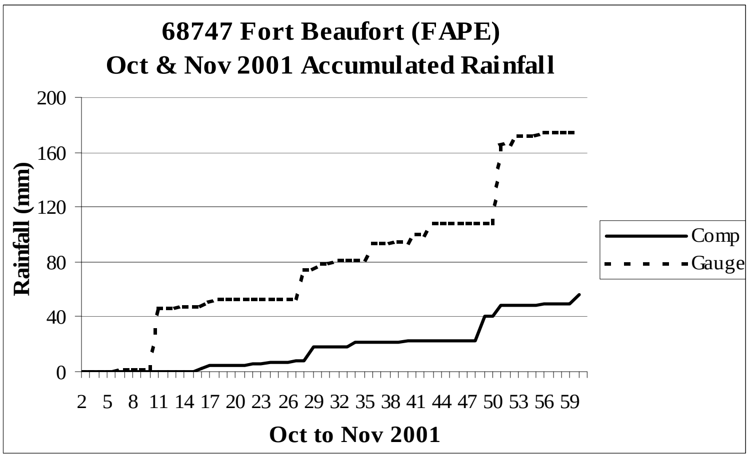

DURBAN RADAR

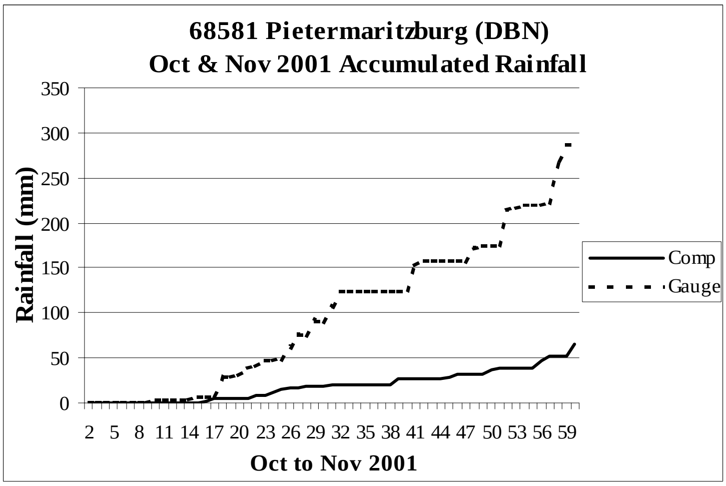

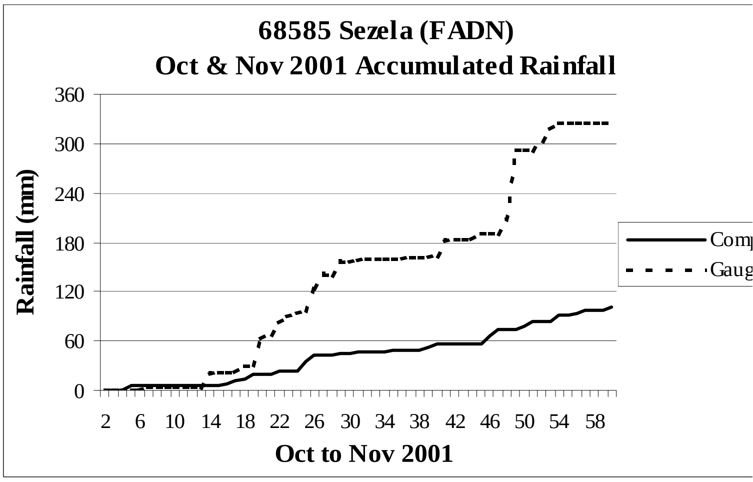

The radar and raingauge comparisons were made using the maximum vertical radar reflectivity averaged over the 9 surrounding pixels centered on the gauge. In general it can be concluded that the Pietersburg, Bloemfontein, Port Elizabeth and Irene radar are performing reasonably well. Kroonstad (Bloemfontein) and Fort Beaufort (Port Elizabeth) are both more than 100 km from the nearest radar, but the general rainfall trends are encouraging at that range. The Durban and Ermelo radars again show that they suffer from underestimation.

3.6 Differences between the mosaic rainfall fields and the MRL-5 rainfall fields

Most of METSYS radar products are derived from the mosaic radar field. Past radar-rainfall studies have mostly been done on data from the MRL-5 radar. There are several differences between a single radar field and the mosaic:

- The single radar data are stored in a 1 by 1 km grid, while the mosaic data are stored in a 1 by 1 minute earth coordinate grid. On average 3 MRL-5 pixels are accommodated in one mosaic pixel. This is done by taking the largest of the single radar values within the mosaic pixel as the mosaic value.
- The single radar rainfall is integrated over every volume scan of between 2 and 5 minutes, which results in the inclusion of about 14 scans every hour for rainfall integration. The mosaic rainfall is integrated at a 5 minute interval, which leads to a maximum of 12 volume scans to be processed in an hour. The mosaic thus disregards at least 2 volume scans per hour compared to the single radar in estimating the rainfall. The rainfall amount and rainfall area would therefore be less for the mosaic field compared to the single radar field.
- The MDV file establishes an offset and bias according to the maximum rainfall value in the field. The mosaic covers the entire country and therefore the scale factors of the mosaic data are not the same as that of the single radar, unless the maximum rainfall value falls within that radar's domain. This causes rounding off problems for the rainfall field if low rainfall values occur within the radar domain and large rainfall values occur in the remainder of the mosaic rainfall field.

It is clear that spatial and temporal errors can occur in the process of going from a single radar to a mosaic rainfall field. The questions to be answered are: how large is this problem and do large overestimations or underestimations occur in the mosaic rainfall due to the current interpolation and integration methods?

Investigation method

The MRL-5 radar is used as an example of the single radar. For simplicity, CAPPI masks were generated for the MRL-5 domain. The mask allows one to extract a circular band from the radar field that corresponds to both the mosaic and MRL-5 field. The northwest quarter of the CAPPI band was used, because of the lack of ground clutter in that area. A similar process was followed for both the mosaic and MRL-5 radar. Therefore, the same surface area is covered by the selection. If the 5 km CAPPI is selected, values for the region covering the northwest sector in both fields are calculated. Any data in the outer or inner circle of the 5 km CAPPI band are excluded. The result is information for an area in the shape of an arch from 270 to 360 degrees. If the CAPPI height is increased, this arch moves out in range. The inner circle also moves out in range accordingly.

Results

In our case, this data arch could represent a catchment or a district. Presented here are the sizes of the areas of the mosaic (latitude longitude minutes) and MRL-5 (1 by 1 km) radar respectively expressed in pixel amounts.

Table 3.6.1 The number of pixels in each CAPPI arch area.

CAPPI level	**MOSAIC**	**MRL-5**	**Size Ratio**
3 km	475	1396	2.93

4 km	921	2774	3.01
5 km	1247	3749	3.03
6 km	1483	4492	3.02

As can be observed in Table 3.6.2 there are on average 3 MRL-5 pixels in one mosaic pixel. The difference from 3 to 6 km is due to the fact that the longitude width in km increases towards the north, causing more (km by km) pixels to be included for one earth angular coordinate pixel.

Table 3.6.2 Average rainfall over the CAPPI area selected, as calculated for both the mosaic and MRL-5 data fields during December 2000.

	3 km MLR-5	**3 km Mosaic**	**4 km MLR-5**	**4 km Mosaic**	**5 km MRL-5**	**5 km Mosaic**	**6 km MRL-5**	**6 km Mosaic**
1/12/2001	11.94	11.42	9.23	8.82	13.02	11.86	2.98	2.22
2/12/2001	0.65	0.17	0.22	0.07	0.65	0.29	0.59	0.13
4/12/2001	9.88	13.84	10.99	18.33	5.64	4.52	4.53	6.17
7/12/2001	40.27	36.86	48.17	46.82	20.39	18.77	8.48	8.27
17/12/2001	98.86	94.75	77.93	76.41	24.84	24.21	13.44	14.03
24/12/2001	5.39	3.79	6.70	5.63	7.23	5.99	5.75	4.85
27/12/2001	1.34	0.96	10.02	11.22	14.38	15.47	8.85	10.70

From Table 3.6.2 the following were found:

- In general the mosaic and MRL-5 radar fields correspond well.
- The larger the area rainfall, the smaller the differences between the two fields.
- With low rainfall, the differences are larger. This problem is mainly due to the scaling differences which arise during MDV file generation.
- Instances where the rainfall of the mosaic field exceeds that of the MRL-5 field, such as on 4/12/2001 for the 4 km CAPPI band, can be attributed to temporal integration problems in the mosaic field. The software that generates the mosaic field allows the use of the same radar reflectivity field for 15 minutes if the data is not updated. This causes “stationary” storms in the merged field for a period of 15 minutes or more, resulting in localized high rainfall values for the mosaic field. This explanation is further supported by the fact that in all cases where the rainfall for the mosaic field exceeded that of the MRL-5 field, the wetted area ratios (WAR) of the mosaic field were several percentage points less than the WAR for MRL-5 field. The smaller WAR is caused using the same radar field for rainfall estimation over a period exceeding several volume scans.
- The values in the MRL-5 field generally exceed those of the mosaic field, albeit by a small margin. This is confusing, since, owing to the use of the maximum value in the interpolation process for the mosaic field, one would expect the averaged mosaic field to exceed the MRL-5 field. The scaling of the MDV-field might once again be responsible for this.

The proper fit of the masks were also investigated. Differences can be caused only by matching the mask field wrongly by one pixel in the x or y direction. In planning the mask field for both the mosaic and MRL-5, the rainfall average changed by less than ten percent at rainfall values less than 5 mm, while the changes for rainfall values exceeding 10 mm were less than 1 percent. The conclusion is that the possible mask offset has a very small effect on the end result. The largest differences occur at low rainfall values, to which most of the discrepancies between the total values for the month.(132 mm for the mosaic and 156 mm for the MRL-5) can therefore be attributed. If rainfall below 5 mm is excluded, the monthly rainfall is in closer agreement (100 mm for the mosaic and 105 mm for the MRL-5). The scaling in MDV files is most likely the main reason for the differences in monthly totals

Table 3.6.3. The comparisons of rainfall for the month of December 2000 between the MRL-5 field and the mosaic field.

DAY	**1**	**2**	**3**	**4**	**5**	**6**	**7**	**8**	**9**	**10**
Mos	11.86	0.29	2.37	4.51	1.37	10.87	18.27	2.89	2.87	9.95
MRL	13.02	0.65	2.50	5.64	2.54	NA	20.39	3.80	3.83	9.81
DAY	**11**	**12**	**13**	**14**	**15**	**16**	**17**	**18**	**19**	**20**
Mos	1.34	2.08	0.04	0.03	0.09	1.25	24.21	0.69	2.90	2.54
MRL	3.55	3.62	0.11	0.13	0.19	2.47	24.84	1.14	3.52	4.27
DAY	**21**	**22**	**23**	**24**	**25**	**26**	**27**	**28**	**29**	**30**
Mos	4.36	0.06	5.71	5.99	0.17	0.04	15.47	0.69	1.90	0.59
MRL	4.34	0.20	6.04	7.23	0.44	0.14	14.38	0.95	3.46	1.92

The process of merging single radars into the mosaic field is, according to these results, not a significant issue compared to other problems faced when using radars. Current practice is for the rainfall field computed for each radar to be transmitted to Bethlehem, to enable creation of the final rainfall field at 06:00 GMT. In merging the final daily fields from the various radars, the 12-scan limitation placed on the data in generating the mosaic field has been removed and larger existing discrepancies between the individual radar and mosaic fields are eliminated. The MDV scaling problem has now also been addressed more effectively by the removal of most of the ground clutter from the precipitation field.

4. SATELLITE PRODUCTS

4.1 Satellite information as data source for SIMAR

Key questions to be addressed in this section are the following:

- Why use satellite data as source for rainfall estimation for SIMAR?
- What do satellites measure?
- What are the different methods for applying satellite data for rainfall estimation?
- How does these techniques relate to the SIMAR satellite rainfall technique?
- What types of data sets are available, what do this mean and how can this be used in SIMAR?
- What are the future prospects for satellite data and rainfall determination?

4.1.1 Introduction

The objectives of satellite rainfall estimations are to address issues such as rainfall occurrence, amount and distribution at all temporal scales for a number of applications in meteorology, climatology, hydrology and environmental science. Rain gauge data are still widely accepted as the most precise source of rainfall information, but their uneven, sparse distribution and limited sampling area represent a substantial problem when dealing with effective spatial coverage of rain systems. In turn, although superior in observing the spatial coverage of rainfall, the radar coverage in South Africa is not adequate for representing a national rainfall map. The lack of rainfall information over the oceans, especially in the Southern oceans, and data sparse regions warrant another source of data. This inadequacy of the current observation network has inspired a search for alternative tools to remotely estimate precipitation. As a consequence, rainfall estimation from satellite platforms is expected to address these limitations.

Satellite-based rainfall-estimations (RFE) provide a cost-effective data source over temporal and spatial scales, not possible from any other in-situ or remote sensing system (Rozumalski, 2000). An important inherent advantage of remote sensing is that the view from space provides a means of extracting data from any point or area on the Earth's surface, regardless of country boundaries and inhospitable conditions. Unlike separate ground observations, which have individual variance of calibration and accuracy, space borne sensors are a single source of data and therefore the errors of sampling and calibration are maintained at a known uniform level for every pixel (Cresswell, 1998). While space borne sensors cannot actually observe the precipitation reaching the Earth's surface, they can measure other variables that highly correlate with surface rainfall, such as cloud top temperature (Ebert and Marshall, 1995). Unfortunately this is also an inherent disadvantage of using satellite data, in that precipitation is only indirectly inferred from cloud observations as observed from space (Kurino, 1997). Non-precipitating high clouds may therefore obscure precipitating low clouds and the underlying dynamics of the precipitation process, thus leading to erroneous estimation of the precipitation. In the case of baroclinic systems the cloud canopy identified as precipitating may not necessarily correspond to the actual spatial distribution of the rainfall at the surface. All these shortcomings must be kept in mind whilst developing a satellite rainfall estimation technique.

With the progress made with MSG, this inherent limitation should be diminished as the surpassed sampling frequency and additional channel information allow for a more direct approach to rainfall determination.

4.1.2. Background to Satellite data

Meteorological satellites measure radiation coming from the Earth and its atmosphere. This radiation may be reflected solar radiation, i.e. by clouds, water vapour, aerosols, or it may be terrestrial radiation emitted by the Earth. The Earth's atmospheric gases are affected differently by different wavelengths of radiation. Meteorological satellites have been designed to take advantage of these responses to observe different aspects of the Earth and its atmosphere (Grimes, 1999). The radiometer measures the intensity of the radiant energy coming from the Earth's surface and atmosphere in a specific wavelength band (channel). When the radiometer collects a certain amount of energy it registers a count, which is proportional to the intensity of the radiation received. The relationship between radiation and counts is established by the radiometer's calibration. The area viewed by the radiometer is called a footprint and its total radiation is assigned to a pixel centred at the middle of the footprint. In order to build an image of Earth of a reasonable size, a scanning system is employed to physically change the direction in which the radiometer is pointing. A complete image is built up when all the pixels in the image have been assigned a value by the radiometer (Grimes, 1999).

There are two important kinds of meteorological satellites, geostationary- and polar-orbiting. The geostationary satellites are in an Earth-synchronous orbit, whilst the polar orbiting satellites are in a north-south orbit around the Earth. The lower height of the polar-orbiter allows it to observe more detail in weather systems and therefore its spatial resolution encompasses that of a geostationary satellite. Taking the temporal characteristics of rain systems, especially convective storms, into account data from geostationary satellites are preferred for precipitation estimations since, although not the ideal, it's temporal sampling will be more representative of the precipitation observed at the surface than the six- to twelve-hourly frequency of the observations made by polar-orbiters.

4.1.3. Methods for estimating surface rainfall from satellite data

During the past three decades, there have been numerous attempts to utilize satellite measurements for precipitation estimations (Csiszar et al., 1997). A summary of various techniques for rainfall estimation from polar orbiting and geostationary satellites will be briefly discussed and will serve as background regarding the rainfall estimation scheme implemented for SIMAR.

One of the earliest satellite rainfall algorithms (Arkin, 1979; Arkin and Meisner, 1987) utilized the observed strong correlation between the frequency of cold cloud top temperatures below a regional-specific threshold temperature and rainfall rates observed at the surface in the tropics. For convective cells a correlation exist between the area occupied by a storm, its height, its life duration and the volume rain rate (Sauvageout, 1992). Cloud top temperature as inferred from IR radiances relates directly to convective cloud height (Scherer et al., 1971; Scofield, 1987) and can therefore be used to estimate the precipitation falling at the surface. It has been found (Lovejoy and Austin, 1979; Tsonis and Isaac, 1985; Bellon and Austin, 1986) that combining visible and infrared brightness temperatures, non-precipitating clouds can be screened out from the cloud top temperature field before applying the rainfall algorithm. However, due to the need to monitor precipitation on the highest possible temporal frequency, and in order to avoid deceptive biases in estimates of daily precipitation due to missing VIS data during nightfall (Porcu et al., 1999), it is commonly preferred to use IR data for its surpassed temporal resolution. Both in the VIS and IR spectral bands, clouds are opaque and precipitation is inferred from cloud top structure, making it an indirect method at best.

Satellite microwave (MW) data provide a direct approach for precipitation estimation through the emission-based retrieval of atmospheric liquid water over ocean or scattering-based retrieval of precipitation-sized ice above the freezing level over land or ocean. The emission-based retrieval method is based on the enhancement of low frequency 6 - 37 GHz microwave emission from large raindrops over the ocean (Petty and Katsaros, 1990; Prabhakara et al., 1992). The scattering-based method is based on the scattering of high frequency 85 GHz microwave radiation from ice crystals in convective storms (Spencer et al., 1989; Grody, 1991). Unfortunately the passive microwave techniques have poorer spatial resolution than IR techniques (Ebert and Le Marshall, 1995) and low temporal resolution for they are usually flown on polar orbiters, such as the U.S. Defense Meteorological Satellite Program (DMSP) Special Sensor Microwave Imager (DMSP SSM/I). Therefore it is not useful for short-term precipitation estimations, unless combined with geostationary IR or other polar orbiting data. The results of Adler et al. (1993) and Negri and Adler (1993) showed that half-hourly geostationary IR-based rainfall analysis could be vastly improved by using an MW algorithm sensitive to vertical cloud structure and inhomogeneities as calibration routine.

The Advanced Very High Resolution Radiometer (AVHRR) on board the polar orbiting satellite series NOAA, allows multi-spectral radiance measurements from which various physical properties of clouds can be determined (Csiszar et al., 1997; Ebert and Le Marshall, 1995). From the parameters measured by AVHRR it has been found (Csiszar et al., 1997) that cloud top temperature alone is a weak indicator of surface precipitation. It is widely accepted that a multi-spectral approach to rainfall estimation produces reliable spatial fields. Rosenfeld and Gutman (1994) have shown that cloud optical thickness and effective droplet radius derived from AVHRR data can be successfully applied in the identification of precipitating clouds, especially in the case of low/warm clouds. These microphysical properties of clouds are directly related to surface rainfall (Ebert and Le Marshall, 1995) and the accuracy of its quantitative estimation may therefore surpass that of the indirect IR or VIS rainfall estimation methods. The low temporal sampling of polar orbiters cannot adequately represent daily rainfall estimations. Hybrid-techniques, combining multi-spectral polar swath data with geostationary is a more effective method, than using either one of the two data sources.

TRMM is another data source of satellite rainfall and has proved itself in producing some of the most reliable and accurate rainfall fields to date. The Tropical Rainfall Measuring Mission (TRMM) is a joint mission between the National Aeronautics and Space Administration (NASA) of the United States and the National Space Development Agency (NASDA) of Japan. The objectives of TRMM are to measure rainfall and energy (latent heat of condensation) exchange of tropical and subtropical regions of the world. Since its launch in late 1997 TRMM has represented a major step towards the future of MW combination with VIS/IR sensors. The primary rainfall instruments on TRMM are the TRMM Microwave Imager (TMI), the precipitation radar (PR) and the Visible and infrared Radiometer System (VIRS). The TMI is a nine-channel passive microwave radiometer based upon the SSM/I, which has been flying aboard the DMSP satellites since 1987. The precipitation radar (PR) provides 1) three-dimensional structure of rainfall, particularly of the vertical distribution; 2) quantitative rainfall measurements over land as well as over ocean; and 3) improvements in the overall TRMM precipitation retrieval accuracy by combined use of active (PR) and passive (TMI and VIRS) sensor data. The VIRS is a five-channel imaging spectral radiometer with bands in the wavelength range from 0.6 to 12 µm. The VIRS data is used to study precipitation using visible and IR techniques. The VIRS is similar to the AVHRR that has flown since 1978 on the NOAA series of spacecraft, with the same applications in multi-spectral rainfall determination. These TRMM sensors are utilized in producing global precipitation fields, with the aid of merged global geostationary IR information.

4.1.4. Prelude to the rainfall technique developed

The satellite rainfall technique developed for the SIMAR project is a multi-spectral and indirect rainfall estimation method. Active rain-cloud identification is accomplished by the discrimination of high level cloud characteristics, associated with the rain/no rain classes. Cloud textural patterns, intensity and high-level vapour content are used in this recognition process. The basis of this process is a simplified linear discriminant function, modelled on instantaneous radar spatial reflectivity fields. In addition to the satellite information, surface characteristic information is used for identifying possible warm orographic rainfall, which may be neglected by the satellite data alone.

The delay of the coming of age of the first user-operational data stream from MSG, necessitated the optimal utilization of the data sources from the current Meteosat-7 system. All three channels of data are utilized in this switch-based rain area recognition rainfall estimation technique. Only the IR channel data are used for the actual estimation of surface rainfall values, though. The IR information is divided in three classes for improving quantitative rainfall estimation for cold, convective clouds, middle layer and warm coastal clouds.

4.1.5 Data sets

The geostationary Meteosat-7 satellite covers the South African region and utilized as source for geostationary IR, WV and VIS data for SIMAR in preparation for the MSG series of satellites, being the most advanced meteorological satellites to date. The delays of the launch of MSG-1 left Meteosat-7 as the sole source of satellite information for SIMAR.

The Meteosat space segment consists of a spin-stabilized satellite located in geostationary orbit 35800km above the earth's surface. It normally remains within half a degree of latitude and one degree of longitude of the nominal position over the equator, at zero degrees of latitude and zero degrees of longitude (EUMETSAT, 1988). The satellite rotates around an axis that allows the satellite to remain stable. With every revolution one image line is scanned in the East-West direction by the radiometer. During the next revolution the radiometer is tilted so that a scan further north comes into view. Following this procedure it takes the radiometer 25 minutes to complete a full-Earth image. At the end of the cycle the radiometer is brought back to its original position and stabilized. This take a further 5 minutes and therefore a full image is produces every half-hour (Grimes, 1999).

Meteosat-7's primary mission is to observe the evolution of cloud systems. To do this it generates images in three different spectral channels each thirty minutes. The Meteosat spin scan radiometer operates in three spectral bands:

0.5 - 0.9 µm (visible band)
5.7 - 7.1 µm (infra-red water vapour absorption band)
10.5 - 12.5 µm (thermal infra-red band)

4.1.5.1 *Visible (VIS)*

The visible image is composed of 5000 lines of 5000 pixels giving a pixel resolution of about 2.5km at the sub-satellite point. In the visible spectrum the solar radiation reflected from the earth's surface i.e. sea, land and clouds is measured. This directly relates to the albedo of an object. For cloud systems the albedo is dependent on the optical depth of the cloud, which in turn relates to the droplet concentration. This allows for the distinction between different types of cloud.

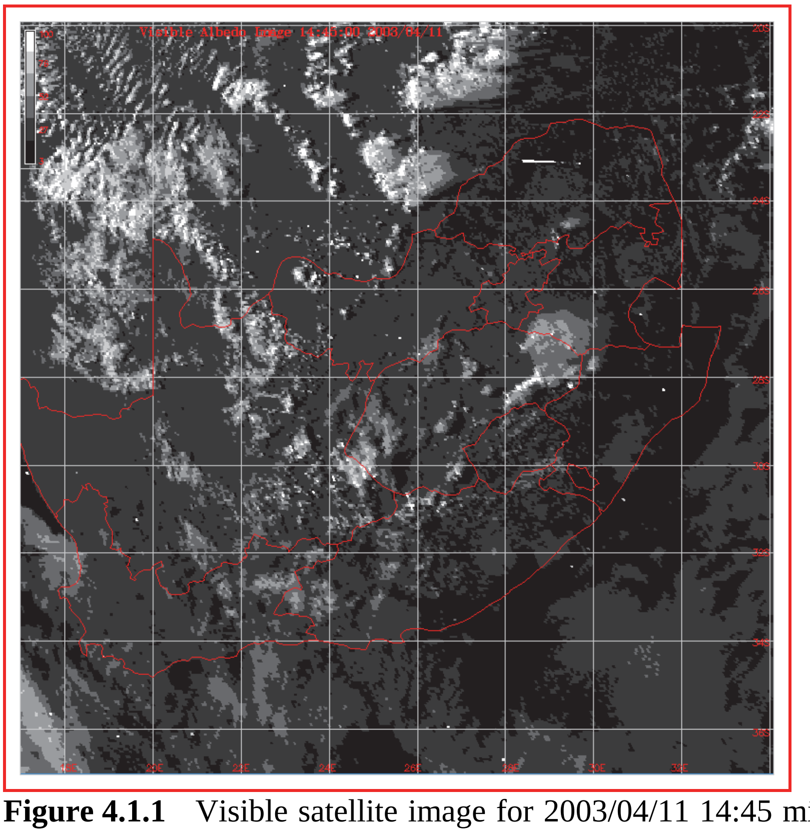

Figure 4.1.1 Visible satellite image for 2003/04/11 14:45 mid scan time. The structure of the different cloud systems is easily discernible, with the white areas corresponding to cloud of significant optical depth.

During daylight hours visible imagery is recorded at half-hourly intervals, with one High Resolution Visible (HRV) measurement at 11:30 GMT daily. Although the optical images have greater spatial resolution than infrared images and are useful for visually identifying deep convection, their temporal availability is limited to daylight hours. Infrared imagery is preferred for precipitation estimation due to its continual temporal availability during 24-hours. Bi-spectral combinations of the IR and VIS channels for rainfall area masking are acceptable, though (Lovejoy and Austin, 1979; Tsonis and Isaac, 1985; Bellon and Austin, 1986), and form the foundation for the cloud classification scheme for SIMAR.

4.1.5.2 *Water Vapour (WV)*

The water vapour images are composed of 2500 scan lines containing 2500 picture elements, each with a resolution of approximately 5km at the sub-satellite point. The thermal radiation emitted principally by atmospheric water vapour in the middle troposphere, is measured in this absorption band. The surface cannot be observed, but information on the cloud tops and the distribution of water vapour in the clear air is gathered.

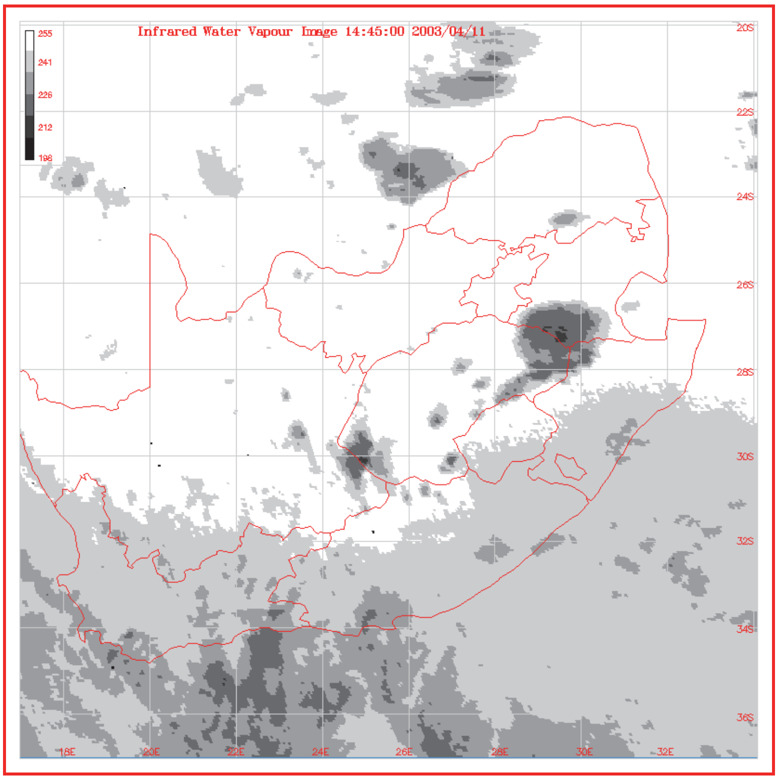

Figure 4.1.2 Infrared water vapour image for 2003/04/11 14:45 mid scan time. The darker gray areas correspond with high moisture at middle or high levels.

A part of the radiation emitted from the earth's surface and atmosphere is absorbed and re-radiated by water vapour into the atmosphere above the cloud tops or earth's surface. If little or no water vapour exists above the clouds, the brightness temperature measured by the satellite will be representative of the cloud top or surface. If water vapour is present above the clouds this absorption will lead to lower radiances measured by the satellite. Since the air temperature varies significantly in the vertical, the re-radiation by the water vapour is at different energy levels than the radiation emitted from below. Generally, the water vapour above the clouds or earth's surface is colder due to its altitude above ground. This leads to the moisture re-radiating at lower energy than that arriving from below. This causes the net intensity of radiation measured by the satellite to be reduced by the re-radiation by water vapour in the path. It is this reduction that enables the detection of the presence of water vapour in the atmospheric column.

The amount of absorption of radiation by water vapour is dependent on the amount of moisture in the radiation's path and the wavelength of the radiation. Increased amounts of moisture, or water content, in the radiation's path lead to more absorption of the radiation emitted from lower layers. Therefore, if the air temperature decreases with height, higher moisture content results in colder brightness temperature. On a 6.7µm image the coldest temperatures correspond to high cloud tops, whilst the warmest are observed over lower altitude areas when the air is very dry through a deep layer in the atmosphere. For the 6.7µm water vapour channel, the radiation values may also be converted to brightness temperatures. A difference exists between 6.7m brightness temperature and that of standard infrared (10.5-12µm) channel. This is attributed to the absorption and re-radiation by water vapour above the earth's surface or clouds. It is this difference that allows for distinguishing between Cirrus and moist updraft regions.

Unfortunately, WV imagery is not available at the same temporal frequency as the 11mm infrared channel data. It is available at half-hourly frequencies during late evening and early morning (22:00 - 05:30 UTC), hourly for early evening (19:00 - 21:30) and three hourly during the course of the day (06:00-18:00). The load on data flow decreases during the evening when the demand for data decreases, thereby allowing WV to be available at the highest sampling frequency available.

4.1.5.3 *Thermal infrared (TIR)*

As with the WV images, the thermal infrared data is collected as a 2500 by 2500 matrix of radiances at a sub-satellite point resolution of 5km.

The thermal infrared (TIR) channel directly measures the intensity of energy radiance from the surface and cloud tops and indirectly surface- and cloud top temperature (Grimes, 1999; Cresswell, 1998). The IR data fields contain the radiance counts, as measured by the radiometer. Since the radiation intensity in the infrared is highly correlated to the temperature of the emitting object (Stephan-Boltzman law), the radiation measurements can be converted to brightness temperatures. These temperatures are essentially the temperature that an object would have if it were radiating near black body characteristics and if no significant absorption of the radiation took place.

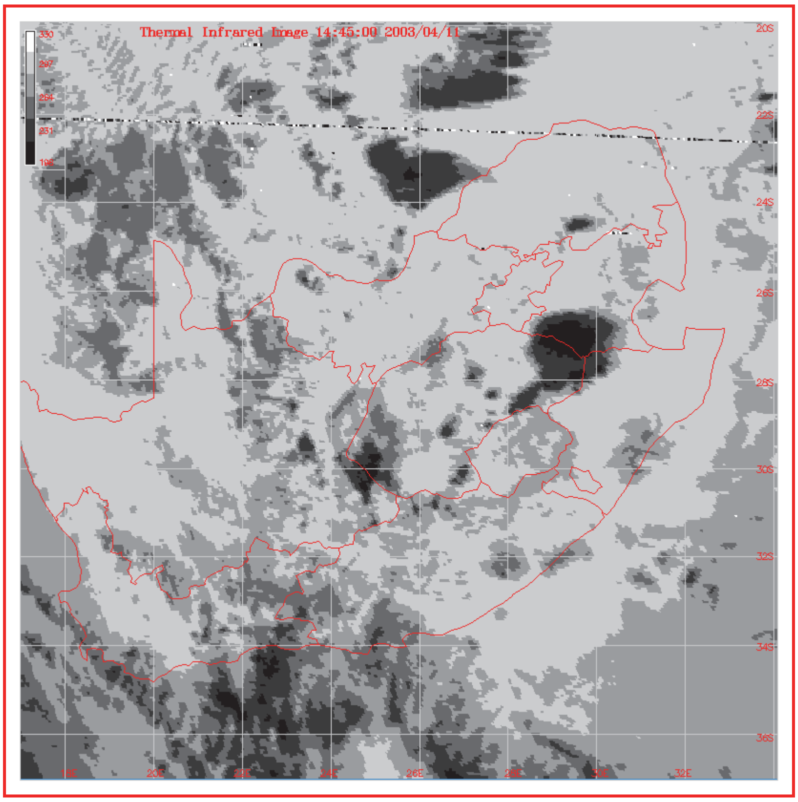

Figure 4.1.3 Thermal infrared image for 2003/04/01 14:45 mid scan time. The darker areas correspond to colder (higher) cloud features.

A statistical relationship exists between cloud top temperature and surface rainfall (Arkin, 1979; Arkin and Meisner, 1987) and therefore analysis of cloud top temperature is used to estimate the rainfall falling at the surface. The thermal infrared data from Meteosat-7 channel 2 are received every half-hour. This is another reason why IR data is preferred for rainfall estimation.

All these data sets are received with the Tecnavia satellite data processing system in Pretoria, with an approximate lag-time of 15-30 minutes from end scanning time. Since the satellite is not fixed absolutely in its orbit relative to the Earth the image needs to be standardized by EUMETSAT ground station in Darmstadt before relaying it to the user via Meteosat-7, thus causing the delay.

4.1.6 The Future in progress: Meteosat Second Generation (MSG)

The advances made in the field of science and in the accuracy of numerical weather prediction necessitate more frequent and comprehensive data from space. This has lead EUMETSAT to develop a new generation of Meteosat satellites called MSG. MSG has been designed in response to user requirements in the fields of now-casting, numerical prediction, climatology and will be a significantly enhanced follow-on system to the current Meteosat satellite (Grimes, 1999; EUMETSAT, 1999).

MSG-1, launched during September 2002, is the first of second-generation satellite and is currently undergoing vigorous testing. After the successful launch of MSG-1 and its injection in transfer orbit by Arianespace, the European Space Operations Center (ESOC) controlled MSG-1, and through several motor firings placed it into geosynchronous orbit and controlled it until handover to EUMETSAT on 25 September 2002, at which time

commissioning began. EUMETSAT has made the MSG first images available via the Website and will continue to provide raw SEVIRI images in the same way. The first test images were received and processed by EUMETSAT on the 28 November 2002. The first trials of rectified images (level 1.5 data) were made available via the web site during mid February 2003.
The following activities will need to be completed during the commissioning phase (EUMETSAT 2003):

- To determine the functionality and performance of the MSG System (including satellite) after launch
- To verify the MSG-1 satellite requirements
- To verify the MSG-1 system requirements
- To determine the calibration factors and operating parameters
- To tune algorithms for image and meteorological product processing
- To validate the end user requirements
- To prepare the system for routine operations

The commissioning phase should be completed by end 2003, when the routine operations should commence.

The main payload of MSG is a new radiometer, the Spinning Enhanced Visible and Infrared Imager (SEVIRI) that will have twelve spectral channels (EUMETSAT, 1999). These twelve spectral channels with their respective applications are as shown in Table 4.1.1 (SEVIRI Science Plan, 2000; EUMETSAT, 1999).

Table 4.1.1 Spectral characteristics and applications for 12-channel MSG radiometer

Three visible (VIS) and One near-infra-red (NIR) channels

Channel with spectral characteristics	*Application*
VIS0.6 (0.56 - 0.71)	Cloud detection and tracking, aerosol- and vegetation monitoring.
VIS0.8 (0.74 - 0.88)	Cloud detection and tracking, aerosol- and vegetation monitoring.
High Resolution Visible (HRV) (0.6 - 0.9)	High-resolution cloud detection and scene analysis.
IR1.6 (1.50 - 1.78)	Discriminates between snow and cloud, ice and water clouds. Give information on aerosols.

Five infrared (IR) channels

IR3.9 (3.48 - 4.36)	Low cloud and fog detection. Measurement of land and sea surface temperature at night.
IR8.7 (8.30 - 9.10)	Quantitative information of thin cirrus clouds and discriminates between ice and water clouds.
IR9.7 (ozone absorption 9.38 - 9.94)	Produce ozone radiances used input to eather Prediction (NWP) models. Experimental channel used for tracking ozone patterns representative of wind motion in the lower stratosphere and monitoring of evolution of total ozone field.
IR10.8 (thermal infra-red 9.80 - 11.80)	Used together with IR12.0 for measurement of earth surface and cloud top temperatures. Detection of cirrus and inference of total precipitable water vapour over sea.
IR12.0 (thermal infra-red 11.00 - 13.00)	Used as IR10.8
IR13.4 (carbon dioxide 12.40 - 14.40)	Height determination of transmissive cirrus clouds and temperature information from lower troposphere (cloud free areas) for instability assessment.

Two infrared water vapour channels

WV6.2 (5.35 - 7.15)	Used together with WV7.3 for upper- and mid-tropospheric water vapour measurements. Cloud and water vapour tracking and height allocation of semitransparent clouds.
WV7.3 (6.85 - 7.85)	Utilized as WV6.2, but used specifically for mid-tropospheric water vapour measurements.

METEOSAT SECOND GENERATION

EUMETSAT esa

MSG-1 First Images

Below are images that represent the 12 channels of the MSG satellites. Click on each image to get a slightly higher resolution view of that image.

The images are raw unrectified images with preliminary instrument settings. Note: users are requested not to request any images from the EUMETSAT archive until its readiness is announced.

The Multi-channel viewer can be used to view other MSG-1 images in a higher resolution!

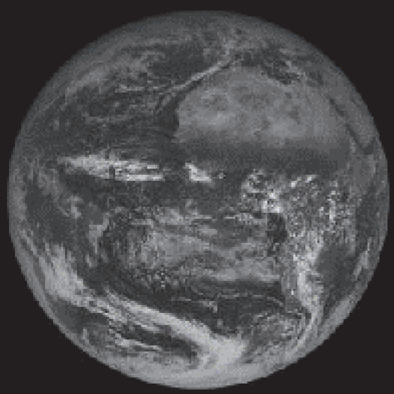

Visible 0.6

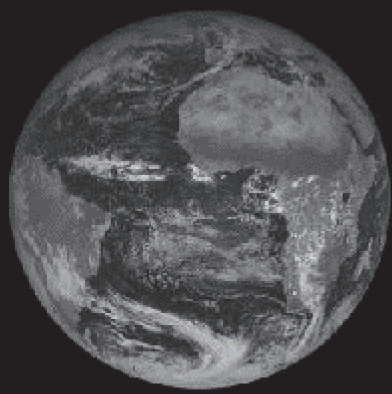

Visible 0.8

These channels are essential for cloud detection, cloud tracking, scene identification and the monitoring of land surfaces and aerosols. They can be used together to generate vegetation indices.

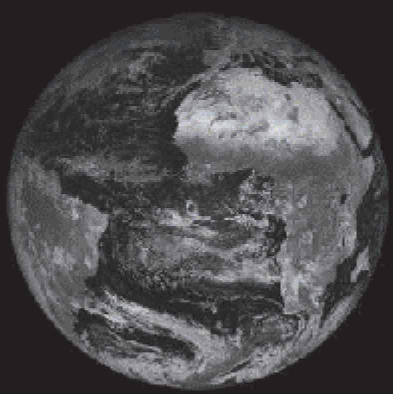

Near Infrared 1.6

Helps to discriminate between snow and cloud,

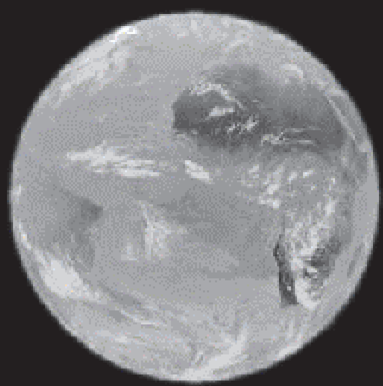

Infrared 3.9

Primarily for detection of low cloud and fog

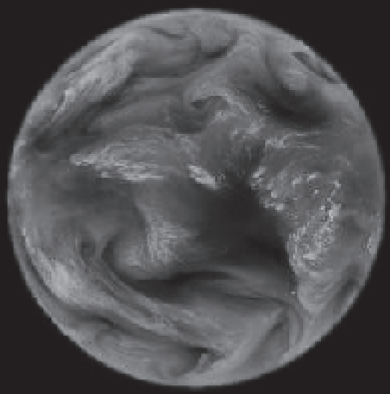

Water Vapour 6.2

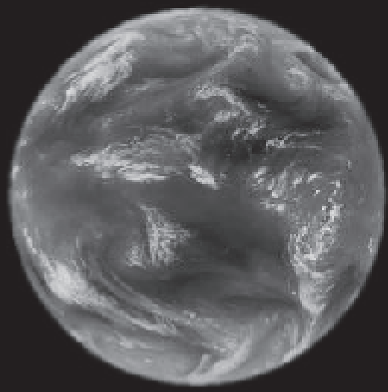

Water Vapour 7.3

Continues the Meteosat broadband Water Vapour Channel to measure mid-atmospheric Water Vapour and provide tracers for atmospheric winds. Also supports height assignment for semi-transparent clouds. Two separate channels representing different atmospheric layers instead of the single channel on Meteosat.

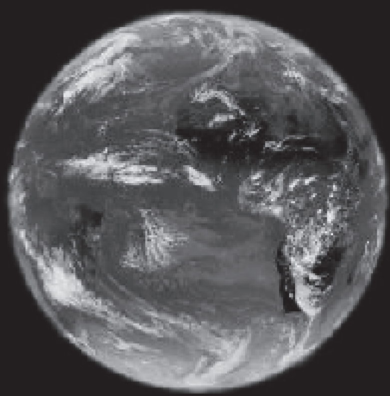

Infrared 8.7

Used mainly to provide quantitative information on thin cirrus clouds and to support the discrimination between ice and water clouds.

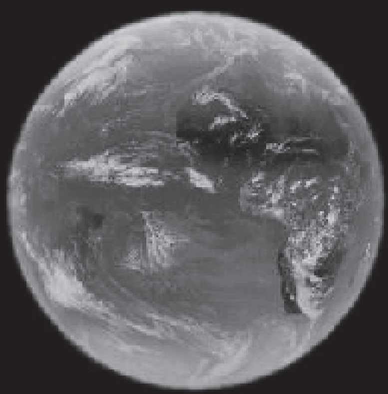

Infrared 9.7

Responsive to ozone concentration in the lower stratosphere. It will be used to monitor total ozone and assess diurnal variability. Potential for tracking ozone patterns as an indicator of wind fields at that level.

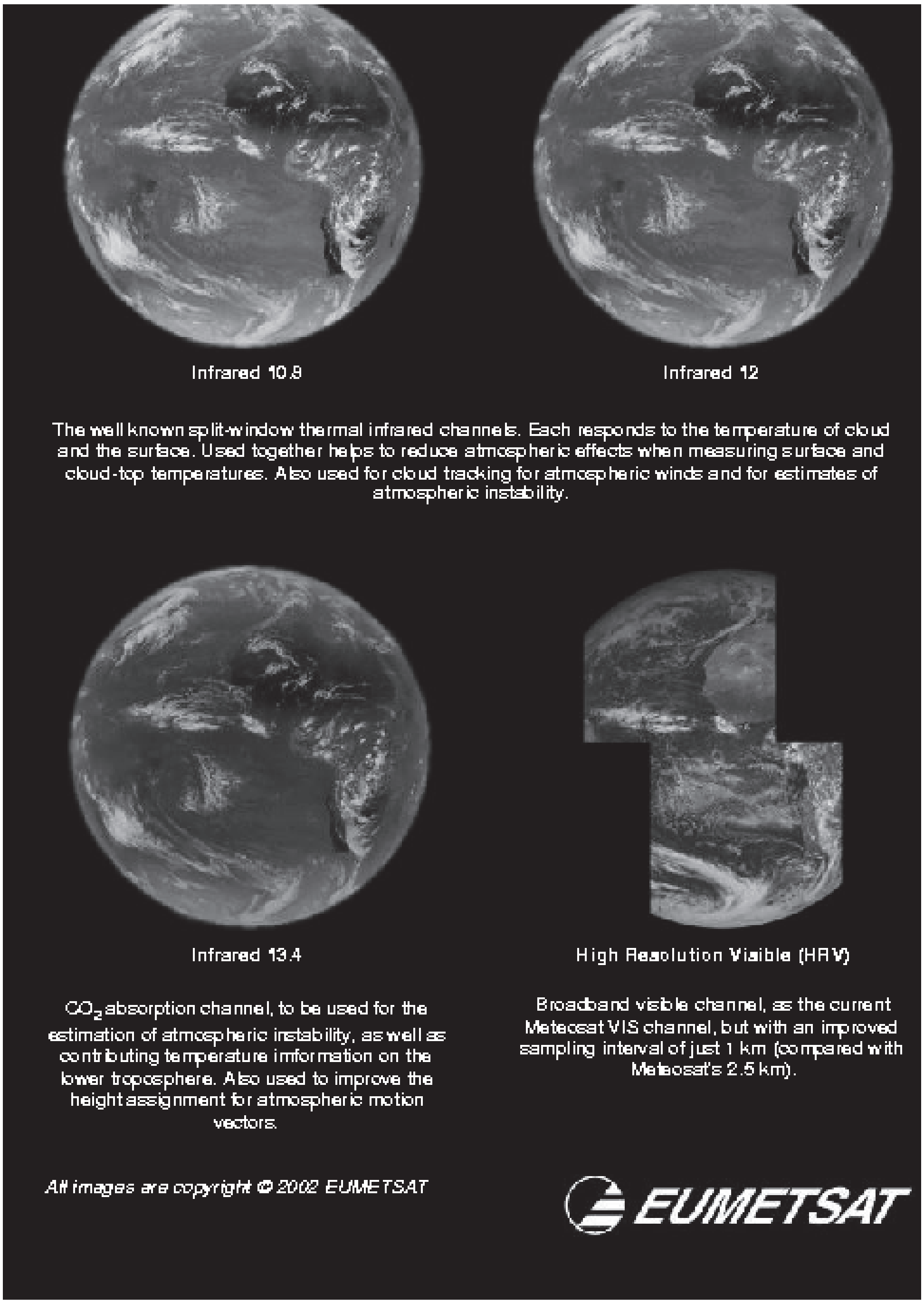

Figure 4.1.4 Graphical examples of the 12 SEVIRI spectral channels (EUMETSAT®2003)

The MSG Application Ground Segment processing facility in Darmstadt will produce a range of meteorological products (SEVIRI Science Plan, 2000; EUMETSAT, 1999; Tjemkes et. al. 1999) derived from satellite data. These products include:

- Atmospheric motion vectors (AMV)
- Air mass classification
- Cloud analysis (CLA) at synoptic scale
- Cloud top height (CTH)
- Automatic satellite image interpretation
- Cloud mask and cloud amount
- Cloud type
- Rapid developing thunderstorms
- Tropospheric humidity
- Convective rainfall rate
- Layer precipitable water
- Precipitating clouds
- Total precipitable water in clear areas
- Global instability (GI).

These MSG products will be delivered to the meteorological community in near-real time via the Global Telecommunication System (GTS) of the World Meteorological Organization (WMO) in standard WMO BUFR format or via the satellite communication channel (EUMETSAT, 1999)

The implications that these derived products will have in the field of meteorology and in related sciences will be greatly advantageous, i.e. they will:

- contribute to the vast improvement of real-time observations used for forecasting and NWP
- greatly improve the ability to identify precipitating clouds for use in rainfall estimation
- be greatly beneficial in it applications for severe weather watch.

With the improvements of the SEVIRI lenses and underlying electronics the nominal resolution of MSG will be an improvement on the current Meteosat series. The sampling distance is the distance between centres of adjacent instantaneous fields of view at the sub-satellite point. For all the channels the sampling distance will improve to 3 km, except for the broadband HRV for which the sampling distance will be 1 km. The temporal resolution, defined as the image repeat-cycle, will improve significantly from 30 minutes for Meteosat-7 to 15 minutes. (SEVIRI Science Plan, 2000; EUMETSAT, 1999). With MSG the radiometric resolution will improve from 0.4 K of the current Meteosat-7 to 0.25 K (SEVIRI Science Plan, 2000). The radiometric resolution is the smallest radiance difference that can be resolved by the SEVIRI radiometer. These improvements in the spatial and temporal sampling frequency will bring vast improvements in the identification and observation of smaller scale features of weather systems. These include:

- the detection of low clouds and fog
- the distinction of water and ice in the atmosphere
- improved identification of cirrus clouds
- improved atmospheric soundings with improved vertical resolution on more levels

- improved detection of humidity on more levels
- increased accuracy of radiance and derived temperature measurements (EUMETSAT, 1999).

This progress will stimulate immense advances in the fields of mesoscale meteorology, precipitation estimation from satellite, nowcasting, identification and prediction of severe weather such as thunderstorms, heavy rain, -snow or -fog and initialisation of NWP models.

4.2. Producing a satellite rainfall map for southern Africa

Objectives addressed in this section are the following:

- Provide history of the development of the satellite rainfall scheme
- Revisit the ITR technique
- Revisit the BSRR technique
- Provide an overview of the MSRR technique
- Provide a flow diagram of the MSRR algorithm layout
- Explain each component of the MSRR algorithm
- Entertain the improvements made.

4.2.1 Satellite rainfall algorithm implemented 2001

4.2.1.1 *The core of the Infra-red Threshold Rainfall (ITR) technique*

Various single channel infrared techniques were investigated for estimating surface rainfall for the Southern Africa region using geostationary Meteosat-7 satellite data. This was done during the period Oct. 2000 - May 2001. Special attention was given to the following techniques: GOES precipitation index (Arkin and Meisner, 1987), Negri-Adler-Wetzel Technique (Negri et al., 1984), NESDIS Auto Estimator (Vicente et al, 1998) and infra-red Power law Rain rate (IPR) technique of Goodman (Goodman et al. 1993). Ebert and Le Marshall (Ebert and Le Marshall, 1995) successfully implemented and evaluated the GPI, IPR and NAWT technique for rainfall estimation in Australia. They found these techniques to perform reasonably well with good correspondence of their individual results with real observations. This acted as testimony for these techniques.

Further investigation led to the development of the infrared Threshold Rainfall (ITR) technique. The ITR is a fusion of the above-mentioned techniques. It is widely accepted that a specific satellite rainfall technique is not necessarily transferable to another climatic region (Adler and Negri, 1988), since dynamic rain processes differ from region to region. This was overcome by combining existing techniques. Evaluation studies have indicated that the technique suited our climate regimes reasonable well as a first guess field.

The ITR is an indirect infrared temperature based method. Precipitating areas are delineated by assuming all clouds colder than 253K to be active convection. This threshold signals a compromise between extensive overestimation and less significant underestimation (neglecting warm coastal rain) of spatial rainfall fields. It was found that even increasing the threshold to 263K led to extensive overestimation of rainfall, unless a more sophisticated cloud identification technique is used. The 253K threshold has been found to be optimal for cold cloud filtering, i.e. cold convective and frontal systems producing most of the rainfall in our region. Also, Negri et al.(1984), Goodman et al.(1993) and Porcu et al.(1999) have found this threshold to be useful for identifying convective rainfall in the tropics.

The cloud mask is set up as follows:

$$IR_{mask} = 1 \;\}\; IRB \leq 253K \qquad \textbf{(1a)}$$
$$IR_{mask} = 0 \;\}\; IRB > 253K \qquad \textbf{(1b)}$$

The Infrared Power Law Rain rate (IPR) technique of Goodman et al.(1993) is applied to the remaining cloud filtered pixels, for estimating a half hourly rain rate. The IPR technique was originally developed for the Amazonian basin. IPR rain rate techniques (Goodman et al., 1993) are used to estimate three-hourly rainfall rates in the tropics by applying a power law relationship of surface rainfall and IR temperatures on the delineated precipitating pixels. This power law relationship was derived from a statistical non-linear regression of co-located surface rain gauges and 11.2 μm infrared cloud top temperatures from GOES imagery. This technique estimates rain as a continuous function of cloud brightness temperature and can therefore reproduce the scale of features observed in the satellite imagery (Ebert and Le Marshall, 1995). By adapting the offset values it was found that the IPR technique led to promising and acceptable rainfall estimations for our region on half-hourly intervals.

This adapted IPR equation is given by:

$$R_s\,(mm.h^{-1}) = 0.00373(267-TB)^{1.75} \qquad \textbf{(2)}$$

The ITR technique served as basis for further development and improvement of a satellite rainfall technique for the SA region. The ITR technique has been in operational use since February 2001.

4.2.1.2 *Additional spatial filters*

In addition to the basic ITR technique spatial filters were developed for improving the spatial fields. A growth filter was added to identify those storms that were actively growing. This filters storms with stationary growth or decay. This technique does not take advection effects into account (a limiting factor) and is based on the observed life cycle of convective clouds. The growth filter decreases the contamination of non-precipitating clouds, but is limited. Turbulent, thick cirrus downwind from thunderstorms may still go undetected by this filter.

$$IR_{t2} \geq IR_{t1} \;\}\; RFE=0 \qquad \textbf{(3a)}$$
$$IR_{t2} < IR_{t1} \;\}\; RFE=R_s \qquad \textbf{(3b)}$$

Additionally, a spatial IR temperature slope filter, developed by Negri (Negri et al., 1984), was implemented for improving spatial fields. This technique is founded on the idea that convective domes (updraft) have steep IR temperature slopes in a specified neighbourhood. Firstly it is tested if the central pixel is the minimum in a 3x3 pixel neighbourhood. If it is thought to be a local depression (dome), the deviation of the central pixel to the average slope of the neighbourhood is calculated.

$$T_{slope} = 0.568(T_{min} - 217.0) \qquad \textbf{(4)}$$

The local minimums are taken to be cirrus if the surrounding slope is less than this threshold slope. Otherwise, the local temperature depressions are taken to be an overshoot top. The linear discriminant function developed by Negri (Negri et al., 1984) (4) is used to distinguish between cold steep domes and cold flat cirrus. Only the areas thought to be convective domes are retained. This filter proved extremely useful for tropical convection, less useful for isolated storms and not usable at all for flat frontal (widespread) rain systems.

4.2.1.3 *Limitations of basic ITR technique*

Evaluation of the ITR technique on daily, monthly and seasonal rain gauge data indicated the limitations of this technique. These include:

- Warm coastal and orographic rain tends to go undetected. This is fundamentally due to the 253K threshold
- The spatial extent of convective rainfall due to cirrus contamination is overestimated
- Severe convective rainfall is quantitatively underestimated. This indirect method cannot intelligently identify the true extent of convective dynamics
- Frontal rain systems are generally underestimated. Again the method cannot identify the underlying dynamics, relating to the rain process
- The spatial filters are limited, yet useful.

This technique suffers from the inherent limitations of a single-channel IR-based technique. The main reason for the errors in an IR-based RFE scheme relates to the fundamental assumption that precipitation at the surface is a function of cloud-top temperature. If this assumption is violated, errors in rainfall detection occur. Even if the clouds are correctly identified as precipitating, the estimated rain amounts may contain a large amount of random error, due to the different dynamical processing occurring inside the clouds.

These limitations warranted the redesign of the satellite rainfall technique, leading to the continual evolution of the SIMAR satellite rainfall technique. The intermediate step of development was the experimental Bi-Spectral Rain Rate technique.

4.2.2. Overview of the progression of the Multi Spectral Rain Rate (MSRR) technique

The methodology of the Bi-Spectral Rain Rate (BSRR) technique, being the experimental predecessor, laid the foundations used in the MSRR technique. The BSRR technique was purely an experimental one, embedded within a GIS controlled by scripts. Its limitations and the necessitated technique optimisation during its operational implementation, contributed to the fusion of the MSRR technique.

The aim of the BSRR technique was to improve the ability to recognize the instantaneous rainfall areas and to refine the rainfall estimation from IR data. This was accomplished by utilizing:

1. WV information to improve the ability to identify no-rain cirrus conditions (4.2.2.1)
2. Image processing techniques, such as median filtering and edge detection schemes for filtering non-relevant cloud characteristics and cleaning up images (4.2.2.2)
3. Morphometric cloud analysis for identifying the planar areas of overshoot tops, which was found to correspond best to the cloud area related to surface rainfall (4.2.2.3)
4. Wind flow and topograhic information for orographic cloud detection (4.2.2.4)

The spatial rainfall fields as observed by the radar were used as a typecast model, as ground truth and as rainfall area template. The aim of using the radar data as role model and utilizing the added intelligence was to diminish the consistent bias evident in the ITR technique.

4.2.2.1 *WV*

Water vapour was incorporated as additional information on the cold cloud top temperature areas that was possible causing rain at the surface. Water vapour is a source of information on the available moisture in the vertical atmosphere, a dynamic characteristic of the surrounding cloud area that can assist in cloud identification. Despite the limitations of this data set, its contribution in rainfall estimation is significant.

The main culprit for spatial overestimation of rainfall derived from IR data is the contamination of cirrus-induced rainfall. Various applications of WV data as cirrus filter were investigated, but a novel and simple principle was found to produce the best results. The IR and WV spectral brightness temperatures are used to calculate the Infrared Water Vapour Spectral Mask (IWSM), which correspond to cold convective rainfall areas. This technique will be discussed in detail under heading 4.2.3

4.2.2.2 *Image processing techniques*

a) Median filtering

Feature enhancement entails increasing the contrast of specific features, such as edges, at the expense of other object in the image (Engelmann et al. 2001). There are various methods for feature enhancement. Rank filtering entails the ordering of the pixels, in some neighbourhood, in sequence from minimum to maximum. The result of the pre-processing is that the center pixel of the neighbourhood is replaced by some statistics of this sequence or a value in this sequence.

Median smoothing is a special kind of the more general rank filtering techniques (Rosenfeld et al. 1982,Yaroslavskiilp, 1987). Median filtering is a non-linear smoothing method that reduces the blurring of edges (Tan, 1981,Sutter 2001). Individual noise spikes do not affect the median of the brightness temperatures in the neighbourhood. Therefore, median smoothing is able to eliminate random spot noise on the infrared images. The very nature of the image capturing process produces noise in an image (McCain 2002). Mostly this noise is associated with interference on the radiometer caused by the sun during an active sunspot period.

b) Edge detection

Most edge detectors are based on the principle of measuring the change of intensity or intensity gradient at a certain point in the image (Morse, 2000). One generic approach to edge detection is to calculate a first derivative operator, that gives an indication of the local magnitude and orientation of gradient. Edges are observed as local extrema, that is where maximum change in intensity occurs. In order to establish the significance of an edge, it needs to be compared with a pre-defined threshold value. This process is called thresholding (McCain 2002). This threshold will differ from applications and contents of images.

The Sobel edge detection filter is a first-derivative based method. The Sobel kernel relies on the technique of central differences for detecting edges and is a non-linear edge detection method (Engelmann et al. 2001). The Sobel kernels are defined as (Sonka et al. 1993):

-1	0	1
-2	0	2
-1	0	1

$\partial/\partial x$

-1	-2	-1
0	0	0
1	2	1

$\partial/\partial y$ **(6)**

The magnitude of the gradient is given by,

$$S_B = \sqrt{\left(\frac{\partial}{\partial x}\right)^2 + \left(\frac{\partial}{\partial y}\right)^2}, \qquad \textbf{(7)}$$

and the direction is given by, $\tan^{-1}\left[\frac{\partial/\partial x}{\partial/\partial y}\right]$.

The Sobel kernels can be thought of as a 3x3 approximation to the first derivative of a Gaussian operator(Morse, 2000). This means that the Sobel operator is equivalent to first blurring the image using a 3x3 approximation to a Gaussian and then calculating the first derivative, one reason why the Sobel kernels are so effective.

Edges are difficult to extract using gradient magnitude alone, since the local maximums are not always significant. Thresholding is applied for identifying significant Sobel edges, in conjunction with a method for describing the textural information of the edges. One way to describe textures is through their statistical properties (Morse, 2000). Variance describes how similar the intensities are within a region and is done by spatial convolution. High variance values indicate heterogeneity and an area where the gradient magnitude changes abruptly. These strong edges are taken to be significant. It was found that a 3x3 Sobel variance filter proved the most useful. Coefficient of variation is calculated as follows:

$$V_s = \left[\sqrt{\sum_N S_{Bi} S_{Bj} - \frac{\sum_N S_{Bi} \sum_N S_{Bj}}{N}}\right] / \left[\frac{\sum_N S_{Bi}}{N}\right] \qquad \textbf{(8)}$$

$V_s > 1\ S_B > 1\ \}\ IR_{EDGE} = 1$ **(9a)**

$V_s \leq 1\ S_B \leq 1\ \}\ IR_{EDGE} = 0$ **(9b)**

4.2.2.3. *Morphometric feature analysis*

Morphometric parameters are combined to give a classification of features in the infrared image. These features are related to the shape of the features on the infrared field and are not in the same context as the GLCM features, which are categorized as statistical texture features. Morphometric features are characteristic of any surface (Wood, 1996) and relevant to an infrared cloud top image, as continuous surface.

The most widely used set of morphometric characteristics is the subdivision of all points on a surface into one of the following classifications: pits, peaks, channels, ridges, passes and planes. The names of these features suggest a geomorphological interpretation, but they may be unambiguously described in terms of rates of change of three orthogonal components.

These subdivisions of morphometric characteristics are described by second derivatives and given by (Wood, 1996):

$$\text{Peak: } \frac{\partial^2 z}{\partial x^2} \rangle 0 \quad \text{and} \quad \frac{\partial^2 z}{\partial y^2} \rangle 0 \qquad \textbf{(10a)}$$

$$\text{Ridge: } \frac{\partial^2 z}{\partial x^2} \rangle 0 \quad \text{and} \quad \frac{\partial^2 z}{\partial y^2} = 0 \qquad \textbf{(10b)}$$

$$\text{Pass: } \frac{\partial^2 z}{\partial x^2} \rangle 0 \quad \text{and} \quad \frac{\partial^2 z}{\partial y^2} \langle 0 \qquad \textbf{(10c)}$$

$$\text{Plane: } \frac{\partial^2 z}{\partial x^2} = 0 \quad \text{and} \quad \frac{\partial^2 z}{\partial y^2} = 0 \qquad \textbf{(10d)}$$

$$\text{Channel: } \frac{\partial^2 z}{\partial x^2} \langle 0 \quad \text{and} \quad \frac{\partial^2 z}{\partial y^2} = 0 \qquad \textbf{(10e)}$$

$$\text{Pit: } \frac{\partial^2 z}{\partial x^2} \langle 0 \quad \text{and} \quad \frac{\partial^2 z}{\partial y^2} \langle 0 \qquad \textbf{(10f)}$$

The x is the column coordinate, y the row coordinate of the image and z is functional value at (x,y) , i.e. the infra-red temperature value.

The standard method of identifying morphometric features is to pass a local (usually 3 x 3) window over the infrared images and examine the relationships between a central cell and its neighbours (Peucker and Douglas, 1974, Evans, 1979). By comparison with radar reflectivity fields, it was generally found that the areas identified as planes corresponded the best to the storm structures it was found, though, that channels and ridges might correspond to a radar echo. This may be attributed to high cloud or transitional areas between storms, obscuring the low-level radar echo structure. It was found that the plane feature corresponded to individual domes (convective), undulations or other elements in the clouds, which is for cold convective clouds and warm stratiform clouds. This process will not filter all non-precipitating clouds. Only the undulations in the cloud top field will be retained, but this may cause a significant amount of cirrus to go undetected. Generally, the results signal a drastic improvement in removing non-precipitating areas, especially when combined with edge detection technique. The areas identified as planes, but corresponding to an edge, will not be accepted. Speckled noise occurs as residual of the technique and is removed by image smoothing.

4.2.2.4. *Warm orographic scheme*

To address this issue an investigation was conducted on the areas prone to the effect of orographic rain. This is generally where the ITR technique fails. Instantaneous radar, IR and WV was used for identifying these areas and conditions of orographic rainfall. Even the radar failed at times and cloud data was used to supplement the information. Investigation indicated that the W Cape coast (especially the winter rainfall area) is the prime area where the ITR underestimated warm coastal and orographic rain. These clouds were generally found to be in the warm temperature range of 267 - 278K. Underestimation was also evident along the E-Cape and Kwa-Zulu Natal coastlines and coastal escarpments, but these were less frequent observed than in the W-Cape coastal regions. The use of 3-hourly synop wind direction and speed data in conjunction with a DEM, slope and aspect field were investigated for identifying orographic rainfall.

This technique entailed:

- Interpolating the wind direction and speed data to raster grid (forced linearly, not the most appropriate technique)
- Using a 45-degree window of direction for determining if wind direction is orthogonal to aspect hills
- Wind speed data and Pythagoras law are used to calculate a vertical motion weight
- Threshold this weight and use a 3x3 average smoothing to spread information
- The slope fields must be higher than threshold and the DEM field must correspond to low lying coastal areas; $IR_{slope} > 6^0$ and $H_{elev} < 1000$ m
- This produces a warm coastal mask, $T_{HC.}$

A spatial mismatch was found to exist down-wind from the actual rainfall field. Only directional hills perpendicular to the wind direction were considered as receiving precipitation, but it was found that rainfall might occur on hills that do not face toward the general wind flow. This is due to the complexities of topographic-induced wind flow dynamics. This, and the fact that the wind data are interpolated linearly, without some meteorological weight factor, such as isobars, limited the use of this technique. For these reasons this technique remained experimental, but proved useful in identifying the areas where additional information is needed for accurately estimating warm rainfall.

4.2.2.5 *Producing the improved rainfall mask*

The rainfall mask is produced by:

A	WV & IR	B	IR (No WV)
1	IWSD = 1 for IR $\leq$ 218K		
2	IR_{EDGE} = 0 for IR > 218K	1	IR_{EDGE} = 0 for IR>190K
3	$\partial^2 z/\partial x^2=0$ & $\partial^2 z/\partial y^2=0$ for IR>218K	2	$\partial^2 z/\partial x^2=0$ & $\partial^2 z/\partial y^2=0$ for IR>190K
4	T_{HC} = 1 for IR < 267K	3	T_{HC} = 1 for IR < 267K

4.2.3 The Multi-Spectral Rain Rate (MSRR) technique: overview

The MSRR rainfall technique came into existence during the operational implementation of the BSRR technique. The BSRR set the necessary foundations in place for improving estimations of rainfall. The evolution from BSRR to MSRR is as follows:

	BSRR	**MSRR**
A. IR/WV spectral mask	Experimental	Inherited
B. Image pre-processing: median filter	Experimental	Inherited, but adapted
C. Image pre-processing: Edge detection	Experimental	Partly inherited
D. Morphometric feature analysis	Experimental	Replaced with GLCM texture DF
E. Orographic cloud detection scheme	Experimental	Omitted/ Replaced
1. GLCM IR texture DF	N/A	Replaced D.
2. VIS utilization for warm/cold rain	N/A	Replaced E.
3. WAR speckle filter	N/A	EnhancedA-C.

4.2.4. The Multi-Spectral Rain Rate (MSRR) technique: the layout

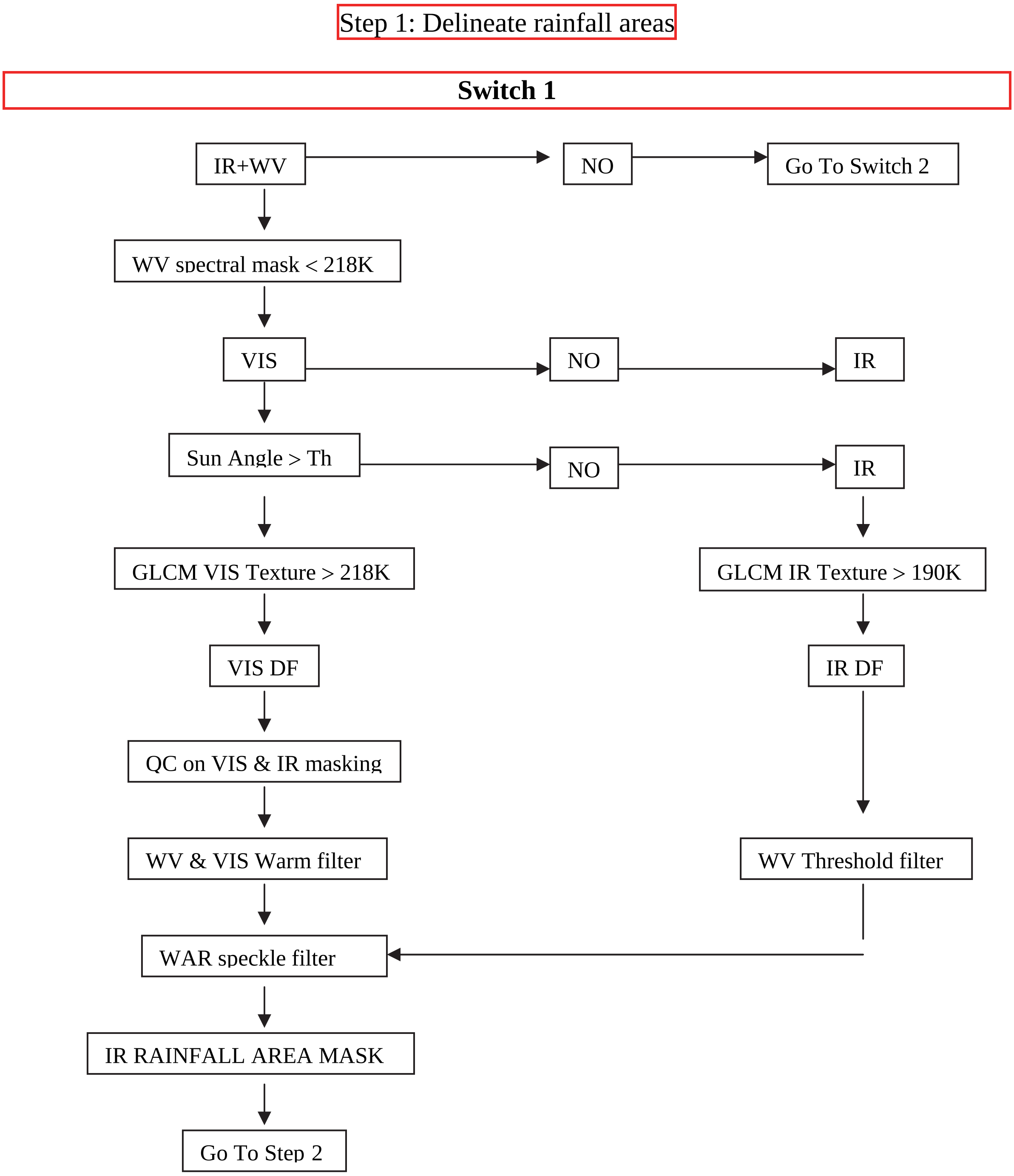

Switch 2

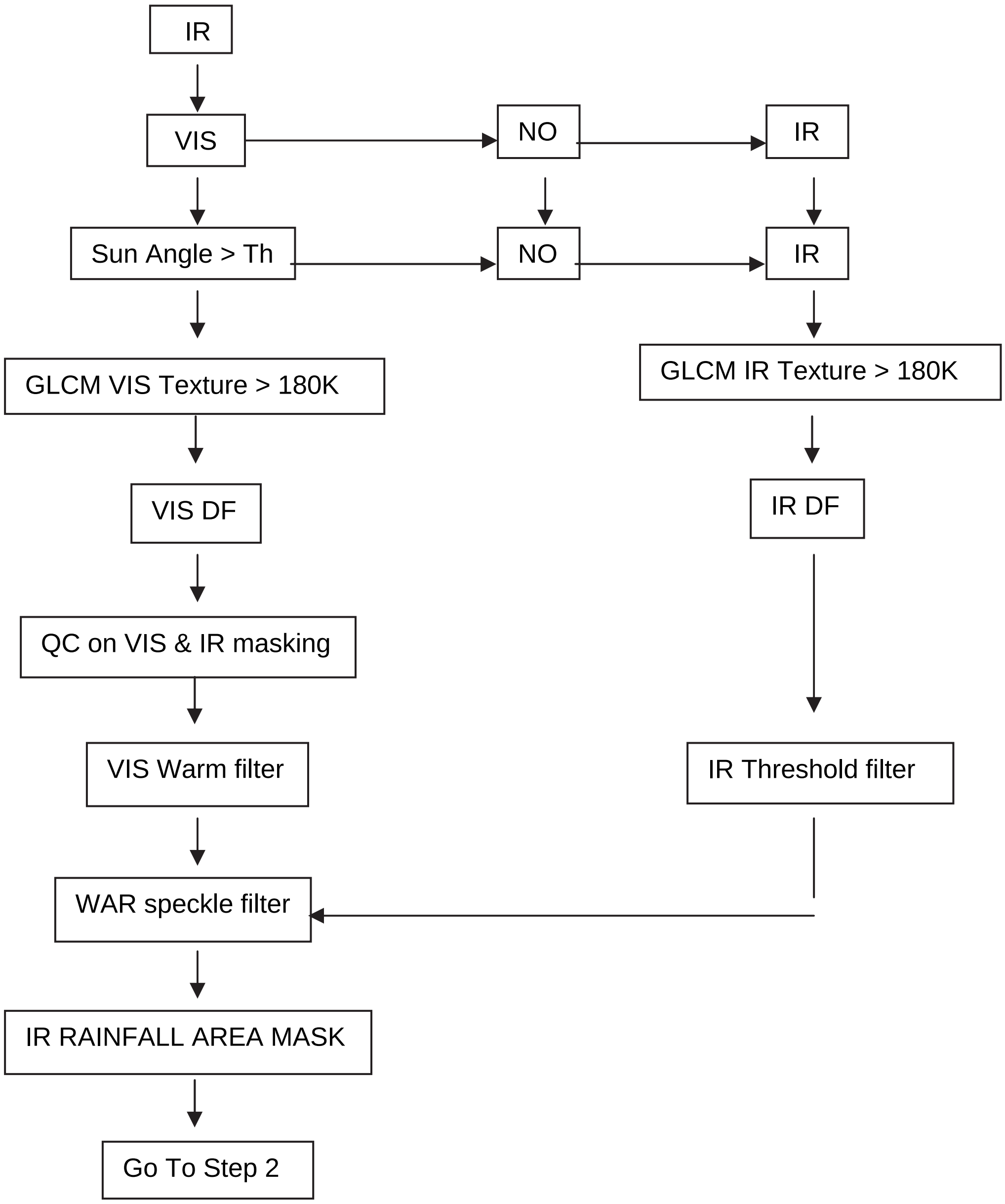
IR
VIS
NO
IR
Sun Angle > Th
NO
IR
GLCM VIS Texture > 180K
GLCM IR Texture > 180K
VIS DF
IR DF
QC on VIS & IR masking
VIS Warm filter
IR Threshold filter
WAR speckle filter
IR RAINFALL AREA MASK
Go To Step 2

Step 2: Determine rainfall from IR masked field

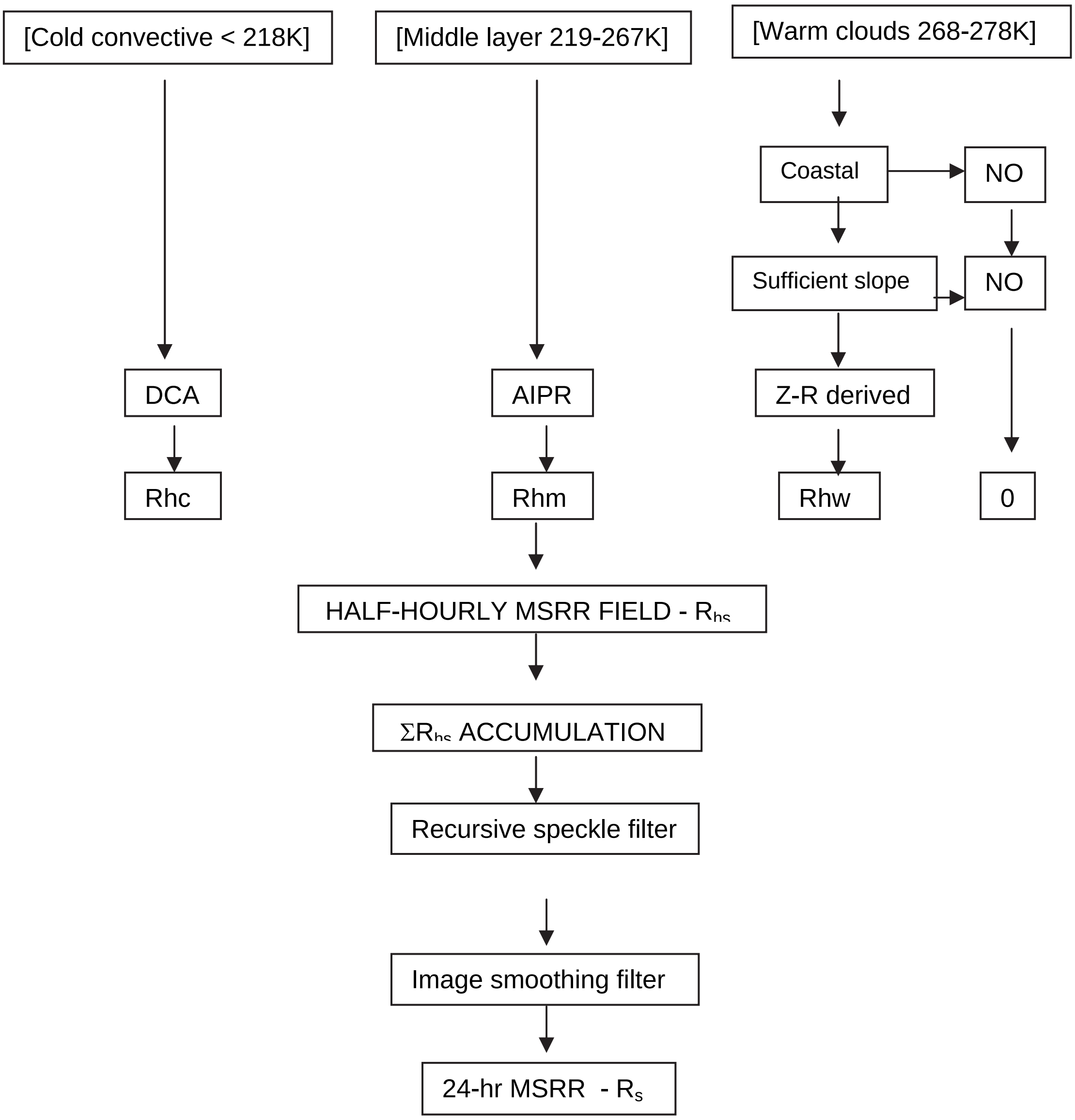

Description of Step 1

Switch 1 (WV - YES)

1. The WV field is used to calculate the Infrared Water Vapour Spectral Mask (IWSM), by subtracting the IR brightness temperature. The potential of using water vapour data is indicated by the observation of relatively warm water vapour pixels over deep convective clouds (Tjemkes et al. 1997). The negative response of this spectral field relates to the high, moist convective cloud tops, which should produce the highest intensity of surface rainfall. This specifically masks the cold clouds (≤ 218K), where the WV information is more reliable in the vertical.
2. For the remainder of the cloud field (>218K) the textural features of the clouds, as derived from the GLCM, is used to distinguish between the rain and no-rain classes. A discriminant function (DF), trained with the aid of radar data, is used for this classification process. The thermal IR is used as baseline data set for the

classification of cloud textures. During the day and when the sun angle is sufficient and the albedo data reliable, VIS images are preferred above IR. VIS data is obtained at higher resolution than the IRs and the albedo relates to the optical depth of a cloud, which is a more direct measure of the clouds efficiency in producing rain. These allow for the VIS to produce higher quality texture images, than the IR. For warm orographic rainfall the results of King et. al. (1995) showed that incorporating VIS data with IR produced higher correlation with ground truth data, than using IR data alone. For cold, bright thunderstorm clouds King et. al. (1995) found the correlation to be similar. These reasons contribute to why VIS data is utilised when possible. A unique DF is used for each data set, for IR and VIS. When VIS is available the VIS texture mask is used to mask the IR field. This mask is used for rainfall estimation by empirical relationships between cloud top temperature and surface rainfall.

3. Since the DF is a simplified linear approximation to the classification process, post filtering must be applied for improving the resultant mask. The post processing of the images entail two stages. Firstly, empirically derived WV and VIS thresholds are used to ensure that non-precipitating clouds, that is clouds with low mid/high atmospheric moisture and low albedos (low droplet concentrations), which have been incorrectly classified by the DF, are filtered.
4. Secondly, a convolution with a Wetted Area Ratio (WAR) speckle filter diminishes the effect of small-scale rainfall areas. These outliers in the mask are due to edges being classified as cloud areas and as residual of the DF classification routine.
5. These produce the masked IR rainfall area mask. This mask is used for the rainfall estimation (Step 2).

Switch 2 (WV – N/A)

1. Similar to Switch 1.2. The only difference is that the whole range of the IR or VIS field is used for the GLCM texture classification, and not only the mid to warm range.
2. Post-processing filter similar to Switch 1.3. An empirically derived VIS threshold filter removes possible false alarms that have been incorrectly classified.
3. Post-processing WAR filter (same as Switch 1.4).
4. These produce the masked IR rainfall area mask. This mask is used for the rainfall estimation (Step 2).

Description of Step 2

Part A - Rainfall estimation

Switch 1 (IR ≤ 218K)

1. Identify possible cold convective cloud tops with empirically derived threshold. It is assumed that the cold rainfall areas classified by Step 1's WV and GLCM DF are associated with convection.
2. This cloud type produces the highest rainfall rates over SA and the Deep Convective Activity (DCA) index is used for estimating this type of rainfall. The DCA is a linear difference based method and suitable for convective rainfall.
3. The DCA produces the half-hourly rainfall field, Rhcs.

Switch 2 (218 < IR ≤ 267K)

1. Identify possible precipitating middle clouds, such as Nimbostratus or Altostratus. Rain from these types of clouds tends to persist at a low rate and for extended periods of time. A low rainfall generating technique is used for this class.
2. The Adapted infrared Power law Rain rate (AIPR) technique handles this type of rainfall and produces the half-hourly rainfall field, Rhms.

Switch 3 (267 < IR ≤ 278K)

1. Aim to identify the rainfall from warm clouds, such as Stratocumulus.
2. Topographic information is used to constrain this technique to the coastal areas, where these clouds usually produce rainfall.
3. The slope of the surface features is utilized for finding possible orographic rainfall along this coastal plain.
4. A rainfall technique, Warm Stratiform Rain Rate (WSRR), was developed specifically for the coastal plains with the aid of radar reflectivity fields. This Z-R derived technique produces the half-hourly rainfall field, Rhws.

Part B - Accumulation and post-processing

1. Combine the instantaneous cloud type rainfall fields Rhcs, Rhms, Rhws to produce the half-hourly satellite rainfall field Rhs.
2. Accumulate these instantaneous rainfall fields $R_{hs}^{i=0}$….$R_{hs}^{i=7}$ to produce the 24-hourly MSRR field R_s.
3. As post-processing an iterative WAR filter similar to Step 1 - Switch 1.4, but with less stringent areal threshold, and Image smoothing filter is used to clean up the image, enhancing rainfall features and removing small scale fluctuations.

4.2.5 The MSRR components

The various components of the MSRR technique, as mentioned in 4.2.2.1, will now be discussed individually, in more detail.

4.2.5.1. *Infra-red Water Vapour Spectral Mask (IWSM)*

Szejwach (1982) pursued a bi-spectral method to infer the cirrus cloud-top temperature. This technique relied on 6.5µm water vapour and 11.5µm standard infrared channel data. A bi-dimensional histogram, frequency analysis of grey level adjacency occurrence and determining the principal axis of the histogram formed part of the technique for identifying cirrus cloud. This technique indicates the use of a bi-spectral method in identifying cirrus. Inoue (1987) showed that it was feasible using a split window channel IR data, e.g. 11µm and 12µm for cirrus detection. Kurino (1996) applied this technique and found that an 11µm and 12µm spectral difference of larger than 3K corresponded well with Cirrus, which is not associated with precipitation. In the use of the 6.7µm IR water vapour channel data Kurino (1996) found that the areas with an 11µm and 6.7µm spectral difference less or equal to 0K corresponded to deep convection. The same principle is applied for the IWSM.

Generally the 6.7µm channel is colder than 11µm due the absorption and re-emission of energy, causing a net reduction in radiation. If the 6.7µm channel is warmer than 11µm, a deep layer of moisture must exist, either at cloud top or below, in order to achieve high emission rates, so as to be warmer than 11µm. This proves useful for identifying areas of deep convection, thus removing cirrus by ignoring those pixels. This is the philosophy behind the infrared and Water Vapour Spectral Difference (IWSM) mask. The negative response of this mask has been found to correspond to significant convective echoes as observed by radar (Figure 5). For these purpose significant echoes refers to those echoes with a reflectivity higher than 30dBZ. A 3-month test data set comprising of 5-min radar data, 30-min satellite IR and WV fields, rain gauge and cloud type information; was used to define empirical thresholds for optimally masking cloud tops corresponding to surface rainfall.

The objective was for the IWSM mask to resemble the structure of storms on instantaneous radar field as closely as possible (Figure 5). The radar fields were used as ground truth for the spatial extent of precipitating areas; taking into accounts all of the limitations of radar (e.g. range effects, contamination, etc.). The cloud and rainfall data were used as an additional ground truth for refining the non-precipitating area mask. Attention was given to regional and mesoscale comparisons, but without loosing scope of the national picture. A definite contrast was observed along the coastal regions and NE inland regions. In tropical convective systems associated with a surface and upper air trough, it was found that the mask threshold had to be lowered to counteract the spatial overestimation of rainfall over coastal and ocean areas. A higher threshold is used over the inland regions:

$$WV - IR < -3^{\circ} \,\&\&\, DEM > 1000\ m \,\}\ IRm = 1 \qquad \textbf{(11a)}$$

$$WV - IR < -5^{\circ} \,\&\&\, DEM < 1000\ m \,\}\ IRm = 1 \qquad \textbf{(11b)}$$

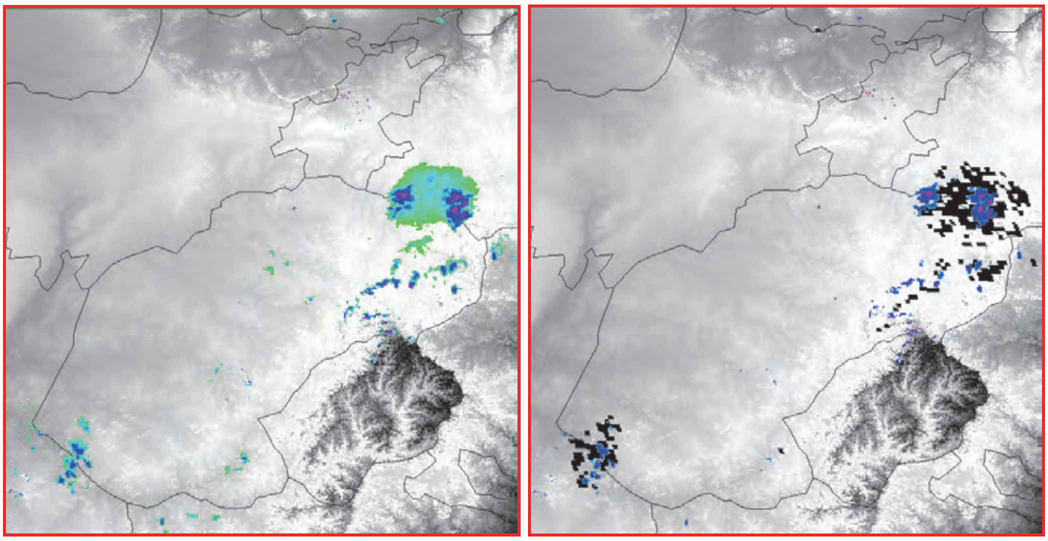

Figure 4.2.1 2003/04/11 14:45UTC a). The significant radar echoes > 20dBZ; b). IWSM in black with the radar echoes > 30dBZ overlaid. The areas masked as precipitating on b). correspond spatially with the radar echoes of a). (±1 mm/h areal distinction). The IR masked area consists of values < 210K.

This technique has proved to be useful for identifying areas of active cold convection and therefore indirectly acts to actively filter cirrus. It was found that this technique was useful for cirrus removal at temperatures colder than 218K. Another means of identifying warmer (>218K and < 267K) convection and warm coastal (> 267K) rainfall need to augment this technique. One such a technique, utilizing textural analysis (4.2.5.3) will be discussed next. Also, if a WV image is not available, this technique is used to estimate rainfall through the full range of Kelvin values.

4.2.5.2. *The image processing components*

In computer vision two levels of processing are distinguished: low-level image processing and high-level image understanding (Sonka et al. 1993). Low-level methods do not necessarily have any knowledge of the contents of the image, whilst high level processing tries to mimic human cognition and the ability to make decisions according to image content. Low-level image processing includes pre-processing methods of filtering, image sharpening and edge detection (Sonka et al. 1993). Some of these low-level processing techniques proved useful in improving image quality and extracting image features. The high-level processing is the aim of the texture based cloud recognition scheme, discussed under heading 4.2.5.3

Image processing is useful in a variety of situations. It suppresses information that is not relevant to the specific image processing or analysis task, enhance the image content and assist in identifying certain spatial features. The processing methods used here are based on the spatial convolution of a small neighborhood centered on a pixel. Convolution is the process of implementing linear operations in images using a user-defined kernel (Engelmann et al. 2001). Convolution will produce a new brightness value in the output image by deriving the center value from some function of the neighborhood values. This type of processing operations is referred to as image filtering (Sonka et al. 1993). As image filter for cleaning up image content, an average convolution is used, given by:

$$R_f(i,j) = \frac{1}{\sum_{K=0}^{N} e^{\frac{-r^2}{2\sigma^2}}} \sum e^{\frac{-r^2}{2\sigma^2}} R_s(i,j) \qquad \textbf{(12)}$$

Where r is the radial distance of $\sqrt{i^2 + j^2}$ and σ the standard deviation of a Gaussian weight matrix. This function has a non-negative impulse response to smooth noisy data. In addition, the Gaussian weight has the effect of a weak high pass filter that enhances the objects within the image.

4.2.5.3. *The texture analysis component*

A common characteristic of images is that neighbouring pixels are related and highly correlated. Infrared images of 11µm are no different and contain vast amounts of information on various spatial scales of cloud and surface features. One of the aims of pattern classification is to classify a pattern using its texture characteristics (Pican et al. 1998). Texture is one of the most important defining characteristics of an image (Dulyyakarn et al. 2000). It is characterized by the spatial distribution of grey levels in a neighbourhood (Jain et al. 1985). For infrared images the classification problem pertains to extracting or discriminating textural features of clouds that are associated with significant surface precipitation.

Textures may be random, but with certain consistent properties, and can be described by their statistical properties. These include the mean intensity, variance, skew ness and kurtosis computed from 1-D histogram (Morse, 2000). In order to capture the spatial dependence of grey-level values, which contribute to the perception of texture, some well know techniques exist, e.g. Markov Random Fields, Grey Level Co-occurrence Matrix (GLCM), self-organizing maps(SOMS), fractal components and 2-dimensional FFT (Pecan et al. 1998,Morse, 2000,Dulyyakarn et al. 2000,Chan et al. 2000). The choice of a suitable method depends on the constraints of the application in terms of the nature of the texture and computation time (Pican et al. 1998).

The GLCM is a well-known statistical technique for feature extraction (Dulyyakarn et al. 2000) and has been successfully applied for seabed classification (Pican et al. 1998), sea ice identification (Kaleschke and Bochert) and have been used widely for land cover classification ((Dulyyakarn et al. 2000), (Chan et al. 2000), (Smits and Annoni, 1999)). GLCM statistically samples the way certain grey-levels occur in relation to other grey-levels (Morse, 2000) and is based on the repeated occurrence of some grey-level configuration. Haralick (Haralick, 1979) defined the GLCM as Pd,r(i,j) such that Pij is the relative number of occurrences of a pair of grey level values (i,j) within a pixel distance d and along direction (angle) r. GLCM provide quantitative descriptions of the spatial and attribute relationship between cells within a gridded framework (Wood, 1996).

For the infrared images the decoded values are scaled and coded in grey-level before calculating the GLCM. The GLCM can be defined as the two-dimensional matrix Pd,r(i,j) that counts the number of times a pixel with grey-level i occurs at distance d and direction r from a pixel with grey-level j ((Doyle, 1997),(Sutter 2001), (Dulyyakarn et al. 2000)). The direction r is taken as 0^0, 45^0, 90^0, 135^0, 180^0, 225^0, 270^0, 315^0 from the central pixel. For infrared images SIMAR research has indicated that a distance of 3-4 pixels is sufficient in retaining most of the cloud characteristics useful for the feature classification. This relates to a neighbourhood matrix of approximately 9x9. This kernel approach to solving the GLCM, improves the computational efficiency of the technique so that it can be useful for real-time processing. The standard method of calculating the GLCM on the whole data domain makes it virtually too cumbersome for real-time applications.

All occurrences of a certain pair of grey-level values are accumulated, whilst stepping through the possible scaled values in the image. The occurrence count matrix is normalized according to the total amount of grey-level pairs, giving the probabilities of the occurrence of each pair of values, called the GLCM. The textural features are derived from the GLCM and include contrast, dissimilarity, mean, variance, entropy, energy, angular second moment (ASM), correlation, asymmetry and inverse distance moment (IDM). The ASM feature (Figure 4.2.2a) produced the best texture fields for IR and VIS imagery and is calculated by:

$$ASM = \Sigma_i \Sigma_j P_{d,r}(i,j)^2 \qquad \textbf{(13)}$$

Chan et al. (2000) used the GLCM for land cover classification using simulated high resolution MODIS data. They found that no additional information could be gained from the GLCM texture features if the kernel size was made larger than 11x11. For IR and VIS images a 9x9 matrix contain sufficient information for accurate description of cloud texture and provides a good trade off on computational efficiency.

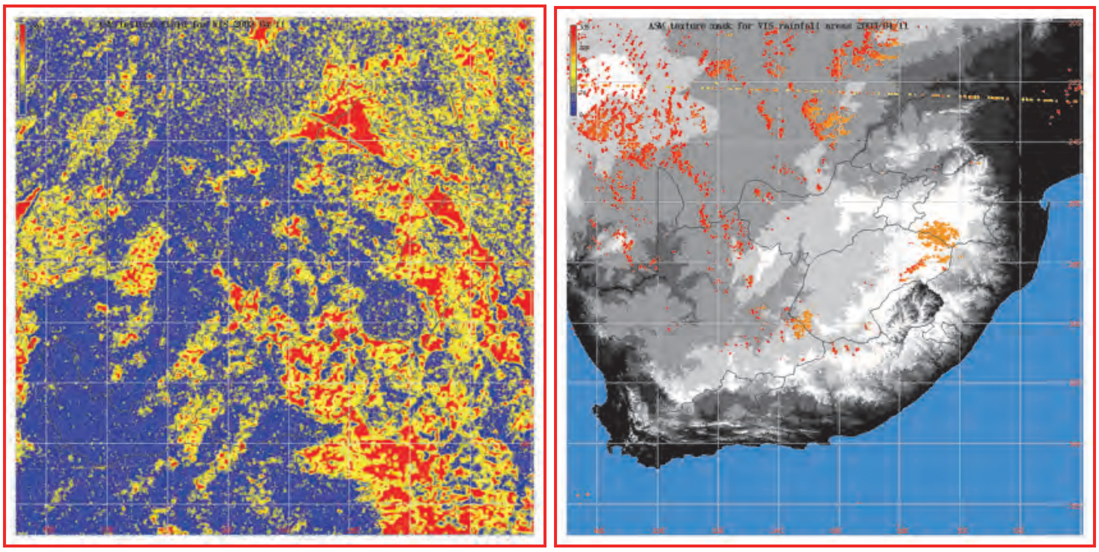

Figure 4.2.2 GLCM ASM texture field for 2003/04/11 14:45 Visible Image (Figure 1); b). DF classified rainfall Infrared areas from Figure 1 and a).

For the classification of the cloud textural features in the rain and no-rain classes a linear discriminant analysis (LDA) was performed to produce a general Discriminant Function (DF). This is a simplified approach for this two-class identification problem. A unique LDA was performed for each data set, IR and VIS, used for texture analysis. The LDA was trained on matching instantaneous radar reflectivity data and IR or VIS satellite images, pixel-wise. The radar data was preprocessed for quality purposes, removing ground clutter or other contamination and averaging the radar data to a coarser grid corresponding with the satellite. This was done to remove any biases, which may affect the LDA coefficients negatively. This training produced a DF for IR and VIS, respectively, and is given by:

$$IR_{(tex)} > -1.495(-115-IR)\ \}\ IR(mask)=1 \qquad \textbf{(14a)}$$
$$VIS_{(tex)} < 6.08(VIS-42)\ \}\ IR(mask)=1 \qquad \textbf{(14b)}$$

These data sets spanned a period of three months and a DF was generated to handle the general trend, to act as a climatological classification routine. Individual cloud systems may differ widely from this 3-month climatology and false alarms may occur. This is the reason for the post processing done utilising threshold and WAR filters. These will be dealt with next.

4.2.5.4 *DF classification false alarm filters*

It was found that overestimation in the warm spatial rainfall fields occurred due to the incorrect classification of the DF. The DF is a simplified linear approach to classification and under different weather conditions, may fail with warm clouds. As post image-processing filter WV and/or VIS thresholds are used to correct the possible misclassification of warm clouds (267-278K).

Upper air moisture plays an important role in the sustaining of weather systems. If there is not sufficient moisture in the mid to high levels, the changes are that the atmosphere will not be able to sustain rainfall at the surface. A WV threshold filter is used, when available, to ensure that the cloud areas identified by the DF has sufficient moisture. A threshold of 253K has been empirically determined for removing areas with low water vapor content (Figure 4.2.3).

VIS data is collected at higher resolution than the infrared channels and the intensity of the image relates to the droplet concentration in the cloud top. The RAINSAT technique (Lovejoy and Austin 1979; Bellon et al. 1980) screens out cold but not highly reflective clouds or those that are highly reflective but have a relative warm cloud top. This process reduced the number of false alarms of the IR technique (Levizzani). The same principle is applied here by masking warm clouds with a low albedo to reduce the false alarms of the GLCM DF. A threshold albedo of 42 is used for this purpose and was determined empirically with the aid of radar information (Figure 4.2.3).

Thermal IR data is not especially sensitive to low level clouds and it is difficult to distinguish warm cloud areas from the background surface features if the cloud tops are sufficiently warm (>273K). Relatively cold surface features (273-278), such as mountain ranges, may be recognized as cloud areas by the GLCM DF due to their course texture. This problem worsens during the winter months, when the surface can cool down to below 273K. This incorrectly assigns rain to areas where there are no warm clouds. It is preferred to rather ignore warm cloud, when IR is the only data set available for rain area masking.

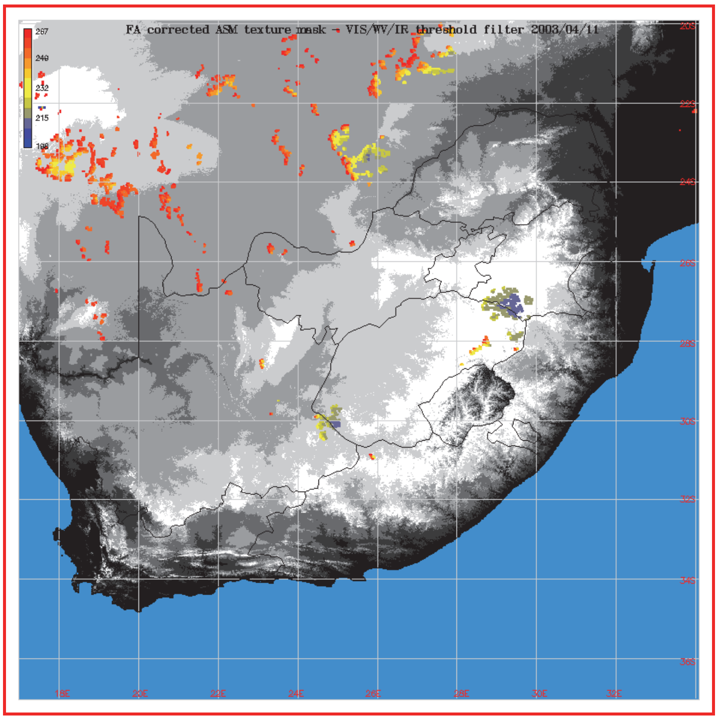

Figure 4.2.3 WV/VIS/IR threshold FA filter applied to Figure 4.2.2

4.2.5.5 *WAR speckle filter*

The reason for a speckle filter is to remove any redundant cloud features, which may have passed the classification process erroneously. It can be considered to be a false alarm (FA) correction filter at a post processing level. A Wetted Area Ratio (WAR) based technique was developed in response to the false alarms of the classification process (Figure 4.2.4). The technique is given by:

$$C_p = \Sigma_{i=0}\Sigma_{j=0}\ IRmij > T \qquad \textbf{(15a)}$$
$$C_T = \Sigma_{i=0}\Sigma_{j=0}\ IR_{mij} \qquad \textbf{(15b)}$$
$$C_F = 100\ C_p/C_T \qquad \textbf{(15c)}$$
$$C_F < WAR_T \quad \}\ IR_m = 0 \qquad \textbf{(15d)}$$
$$C_F \geq WAR_T \quad \}\ IR_m = 1 \qquad \textbf{(15e)}$$

where Cp is the partial count of the pixels with a value greater than a threshold T, 278K and masked as raining, CT is all the pixels masked or not and CF is the fraction of masked "wet" IR data. CF is referred to as the Wetted Area Ratio (WAR). A WAR threshold for reducing FA of the rain area classification was determined as 33%.

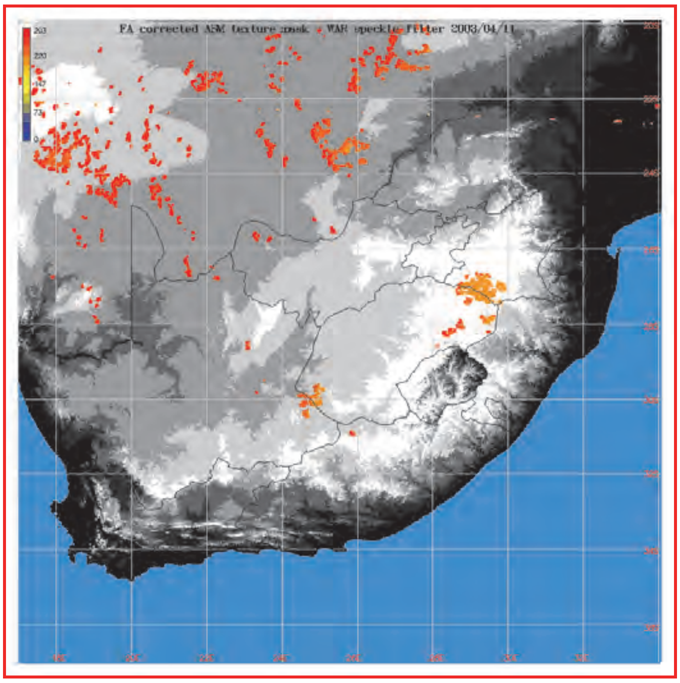

Figure 4.2.4 WAR speckle filter applied to masked rainfall areas (Figure 4.2.2)

The WAR filter has the same effect as a speckle-removing filter in that non-significant rain areas are removed (Figures 4.2.2 and 4.2.4). The filter has the added effect of object enhancement, by accentuating image edges and main features.

4.2.4.6 *Estimating rainfall from cloud top temperatures*

The estimation of rainfall depends on both the delineation of raining areas and the accurate determination of instantaneous rainfall rates for every pixel ((Vicente et al, 1998), (Lovejoy and Austin, 1979)). The IWSM, image processing techniques and GLCM DF classification mentioned above, dealt with identifying areas where rainfall occurs. Next we have to relate these delineated IR areas to surface rainfall.

Investigation of instantaneous IR and radar fields and daily gauge data indicated that three distinct cloud top temperature groups could be distinguished and associated with a certain category of rainfall type. The infra-red field are divided in three temperature categories: cold convection or frontal cloud colder than 218K, mid range convection and stratiform middle cloud (Nimbostratus, Altostratus) from 218 to 267K and warm coastal cloud from 267 to 278K. The performance of the satellite-rainfall technique is increased drastically by the effort made to delineate the raining areas and by dealing with these areas as if they could be classified according to their IR temperature. This is done to minimize the effect of varying seasonal and weather regimes in the satellite-rainfall technique.

Each of these categories is associated with a unique IR rainfall estimation technique:

Infra-red temperature range	**Rainfall estimation technique**	**Areas**
< 218K (cold)	Deep Convective Activity	SA and ocean areas
218 - 267K (mid range)	Infra-red Power Law Rain Rate	SA and ocean areas
267 - 278K (warm)	Z-R Derived	SA coastal regions

a) The Deep Convective Activity (DCA) index:
The IWSM mask has been found to successfully identify areas of cold convection. The DCA index produces more reliable rainfall estimations for cold convection compared to the ITR technique. It produces higher rainfall rates with an upper bound of ~18 mm/h at 190K, which was found to be a more acceptable approximation of general convective rain rates. It should be noted that higher rain rates (> 18 mm/h) could be produced by strong convection. The main advantage of this technique is that it gives more weight to colder cloud tops, since a difference technique is used (Pullen and Butterworth, 2001). The DCA index was developed by Hendon and Woodberry (1993), based on the work of Fu et al. 1990. The definition of DCA is given by:

$$R_{hcs} = \alpha(230-T_B) \qquad \textbf{(16)}$$

α = 0.45 $mm^{-h}K^{-1}$ and T_B is the infrared brightness temperature. The coefficient α was adapted to produce more reliable convective rainfall for South African storms.

b) The Adapted Infra-red Power Law Rain Rate (AIPR) technique:
The IPR technique (Goodman et al. 1993) was used as the only rainfall estimation scheme of the ITR technique with a temperature threshold of 253K. The offset value of the IPR technique was removed, resulting in increased sensitivity to warmer clouds. By doing so the IR threshold was increased to 267K. The performance of this technique is dependent on the correct delineation of raining clouds. With the ITR technique, the IPR estimations performed the best for the mid range (218 - 267K) values in an infrared images. These values relate to moderate and fairly warm convection, stratiform middle cloud (Nimbostratus) and even significant low-level cloud (Stratocumulus). The adapted IPR technique is as follows:

$$R_{hms} = b(267-T_B)^{1.85} \qquad \textbf{(17)}$$

b = 0.00303 and T_B is the brightness temperature. The original coefficients, developed for the Amazonia (Goodman et al. 1993), have been adapted to suit our climate region, but its empirical nature of estimating rainfall was retained.

c) The Warm Stratiform Rain Rate (WSRR) technique:
Investigation on the instantaneous IR, WV, radar and cloud data for a 3-month evaluation period, showed that significant amounts of rainfall originated from extremely warm

stratiform clouds along the low lying regions of SA, especially along the Western Cape. The temperature of these clouds was found to be in the range 267 to 278K. The IPR technique is not sensitive enough to identify such warm clouds. This warranted another technique to be used, which was developed locally due to the low thresholds that had to be used. The warm stratiform rain rate (WSRR) estimation technique was developed by linear regression of co-located IR and radar reflectivity values along the coastal region of SA for Spring/Summer 2001. This was done to instill some kind of memory of varying conditions (regional and synoptic related) that could produce warm rainfall. It is hoped that this technique will serve as a general estimation for warm rainfall, along the SA coastal region.

The WSRR estimation technique is given by:

$$R_{hws} = \left[\left(\frac{\log^{-1}(73.32 - 0.1726 T_B}{10} \right) / 200 \right]^{0.625} \quad \textbf{(18)}$$

Low lying areas are considered to be those below 1000 m above sea level. As an additional filter, all surface areas below a threshold elevation slope of 6 degrees are filtered. This is done to counteract any spatial overestimation that may occur and to incorporate possible orographic effects.

4.3 Validation of satellite rainfall fields

The rainfall fields produced by the MSRR technique are validated against the point measurements of rainfall observed by the daily rain gauge network of South Africa. Each value of a rain gauge is assumed to be representative of the rainfall across the pixel, which correspond to its position. This limits the amount of rain gauge pixels used for evaluation purposes to approximately 250. To increase the amount of data points used, in order to get a better idea of areal rainfall; the 9-pixel neighbourhood of each rain gauge is used as validation area. The interpolated rain gauge rainfall field produced by the kriging routine developed under the auspices of SIMAR (discussed in 5.2.3) are used as data source validating the satellite rainfall values over the rain gauge neighbourhood. According to the explained variance of the kriged rain gauge field, the interpolated values are still reliable and accepted as ground truth.

Monthly data sets of satellite rainfall, corresponding to the rain gauge neighbourhood area, are used to evaluate the MSRR technique’s ability to quantitatively estimate surface rainfall. The data sets for the months December 2002 – February 2003 was chosen as evaluation period for these months contributed the largest component of rainfall during the summer 2002/2003 period. The distribution of the satellite values relative to that of the rain gauges are shown in figures 4.3.1a - 4.3.3a for each month during the validation period, respectively. The distribution of the relative bias of each satellite measurement, compared to their gauge counterpart, with elevation is shown in figures 4.3.1b - 4.3.3b. This indicates the consistency, or lack thereof, of the bias of the MSRR technique with height. If the bias is consistent it signals that the MSRR technique has the ability to observe different rainfall regimes; i.e. coastal, orographic, interior, convective, frontal, etc.; equally well or bad. This would mean that the MSRR has the ability to cater for all types of rainfall systems, without a systematic bias. The same evaluation fields are given for the corresponding quality controlled radar rainfall fields (Figure 4.3.1c - 4.3.3c and 4.3.1d - 4.3.3d) and used as comparative fields.

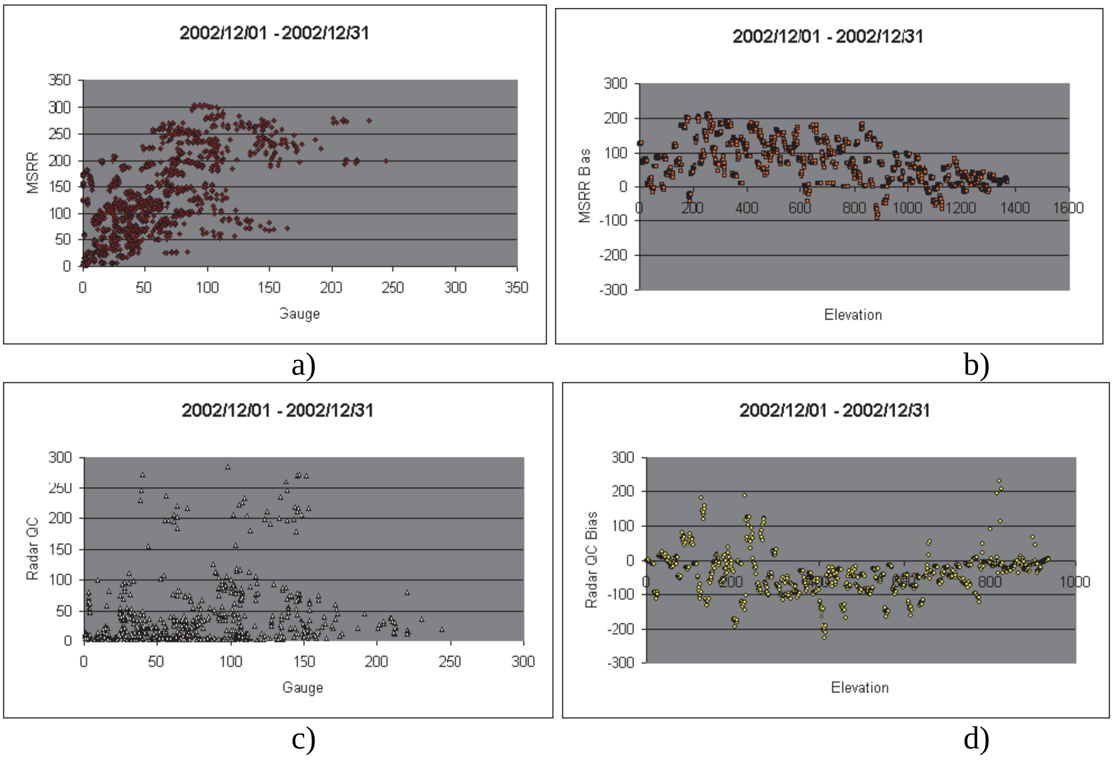

Figure 4.3.1 Validation of MSRR and Radar rainfall fields for December 2002. a). Monthly MSRR satellite rainfall, in mm, compared with rain gauge values; b). The bias, in mm, of the MSRR field relative to the rain gauges in relation to height; c). the monthly quality processed radar rainfall field; and d). the distribution of the radar's bias relative to height.

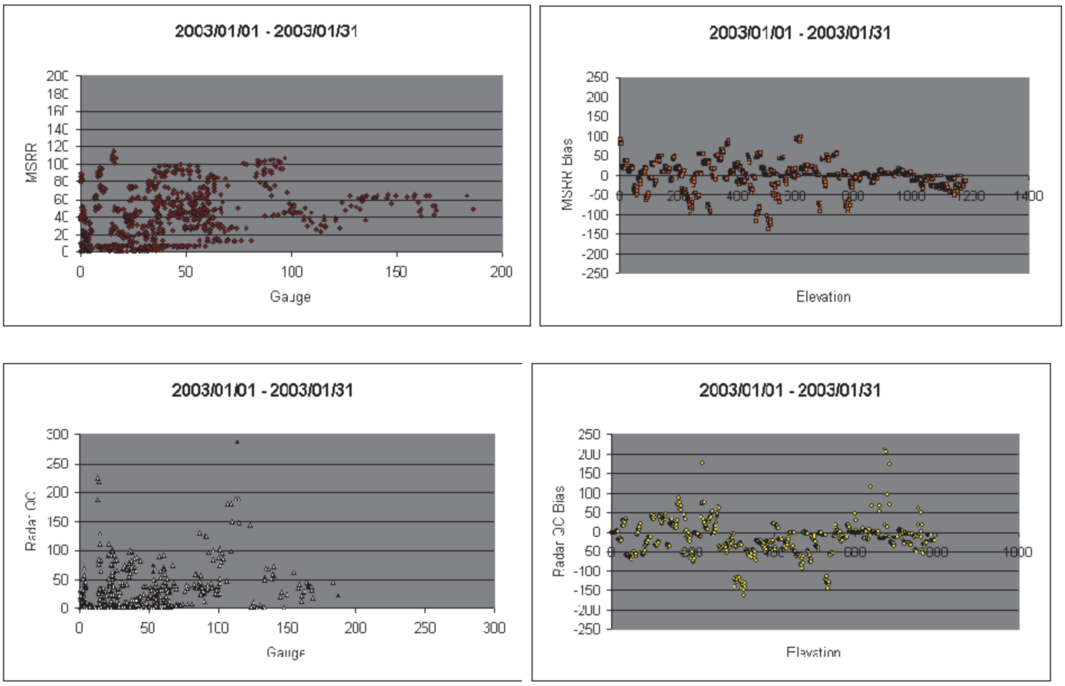

Figure 4.3.2 Validation of MSRR and quality processed radar rainfall fields for January 2003 a). – d). same in Figure 4.3.1.

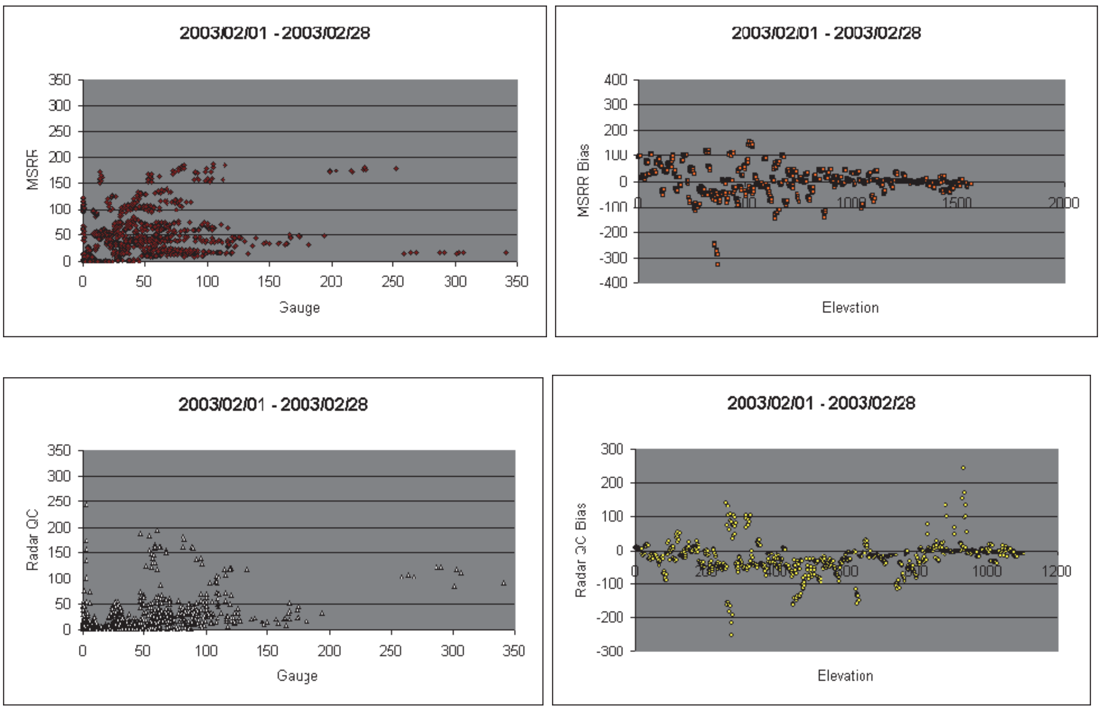

Figure 4.3.3 Validation of MSRR and quality processed radar rainfall fields for February 2003 a). – d). same in Figure 4.3.1.

Table 4.3.1 Evaluation statistics corresponding to Figures 4.3.1 – Figure 4.3.3

Gauge	Satellite	Dec 2002
243.94	303.12	**Max**
0	0.55	**Min**
56.62	125.85	**Average**
47.35	114.8	**Median**
2132.62	6644.28	**Variance**
46.18	81.51	**Std Dev**
	0.67	**Correlation**
Gauge	**Satellite**	**Jan 2003**
186.54	114.78	**Max**
0.07	0	**Min**
32.46	31.59	**Average**
23.21	25.38	**Median**
1185.75	845.62	**Variance**
34.43	29.08	**Std Dev**
	0.47	**Correlation**
Gauge	**Satellite**	**Feb 2003**
341.05	186.74	**Max**
0	0	**Min**
39.91	40.53	**Average**
30.19	31.75	**Median**
1776.11	1717.12	**Variance**
42.14	41.43	**Std Dev**
	0.28	**Correlation**

In general the distribution of the satellite rainfall is quite consistent with regard to the rain gauge values. This is supported by the similar values of average and median for Jan and Feb 2003. The variance and standard deviation values for these two months indicate a similar infield fluctuation around the individual means, although the correlation values are quite low. The bias in the rainfall field for Dec 2002 is the greatest, with the distribution of values skewed towards the maximum. This can be seen from the shifted maximum, median and average, although the case, Dec 2002, has the highest correlation of ~ 0.7.

The biases in the satellite rainfall are fairly clustered relative to height, with the highest deviations from ground truth occurring mostly below 500-750m. This indicates that the satellite technique is able to produce reliable representations of surface rainfall across South Africa. A contrast does exist between the interior and coastal rainfall (Dec 2002 and Feb 2003), that indicates the greatest limitation of the MSRR technique is for coastal rain systems, either being orographic or warm-rainfall related. The bias distribution with height is similar for Jan and Feb 2003, with their statistics corresponding the best to that of the gauge (Table 4.3.1). The drastic difference in bias distribution of Dec 2002, signals a different type of cloud system. Dec 2002 was prone to tropical moisture and surface troughs, which are associated with extensive cirrus anvils and turbulent middle layer clouds. The texture of these high level clouds is quite similar to that of individual convective clouds, due to their undulated nature and cloud elements. This case proves to be difficult for the classification function and the false alarms lead to incorrect rainfall values and the subsequent quantitative overestimation.

From figures 4.3.1 – 4.3.3 it can be seen that the bias of the radar rainfall field is far more inconsistent with height than the satellite rainfall, especially along the coast. The radar almost always underestimates the low rainfall values. The consistent peaks of overestimation in Figures 4.3.1d – 4.3.3d around 900m are probably due to remnants of ground clutter effects.

For Dec 2002 – Feb 2003 a consistent feature is the false alarms of incorrect rainfall classification, varying between 0 – 150mm along the y-axis of figure 4.3.1a – 4.3.3a. This incorrect classification of clouds as precipitating, whilst actually not, is fundamental to the process involved in training the linear discriminant function on modus cloud textures. There will always be certain 'outlier' type rainfall systems, with regard to their textural shape, for which the classification process will fail.

4.4 Operational satellite data flow and products

The objective in this section of the report is to discuss:
- The data flow and processes involved
- Data processing
- Data quality issues

4.4.1 Data flow layout

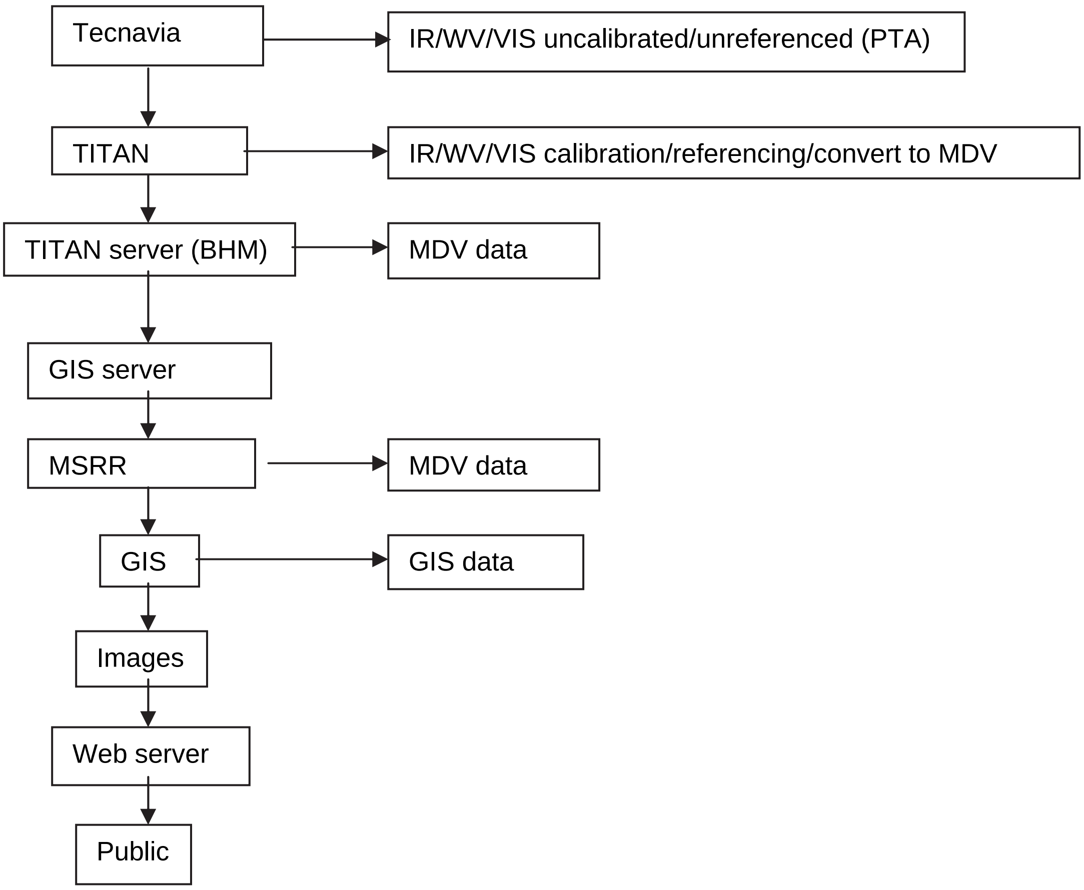

4.4.2 Raw satellite data processing

The raw satellite images are stored in a Tagged Image File Format (TIFF). A raw image is not georeferenced and is in the original satellite projection, that is a distorted, but standardized grid as seen from the viewpoint of the satellite. The image covers the whole field of view of the radiometer and is stored as a 2500 by 2500 block of data for the infrared channels and 5000 by 5000 for the visible. The satellite projection needs to be converted to a flat latitude/longitude representation of the image, to make it usable. From the 2500 by 2500 block only the appropriate block for South Africa is extracted, whilst the lower image resolution of the satellite is forced to the higher resolution of the standard 1024 by 1024 matrix used for the SIMAR merging process. The centre latitude/longitude position of each pixel of the 1024 by 1024 matrix positioned over Southern Africa from 17E to 3404'E and from 1956'S to 37S, is calculated. The original distorted satellite image is then searched to see within which original pixel this position falls. The value of this larger pixel is then taken to be representative of the smaller pixel in the 1024 by 1024 matrix. This may lead to a loss of data accuracy, as will be explained. The radiometer assigns an average radiance count over the whole larger pixel; this count is then in turn assigned to all of the smaller pixels whose centre positions fall somewhere within the larger pixel. This creates a fictitious data resolution, since the radiometer did not measure the average radiance count over the smaller pixels. Thus in reality there will be a discrepancy with the actual radiance count that would have been measured over the 1-minute pixel.

The calibration procedure for all infrared, thermal and water vapour, data is handled by the Tecnavia satellite data processing system. The data is decoded as grey scale, with a built-in lookup table in the TIFF header. When decoding, the brightness temperature is extracted by decoding the grey scale levels using the lookup table in the header. The lookup data consist of scaled values in the range of values existing in the image. The reference to this scaled value in the TIFF header is stored in the image itself, according to a grey level scale. For the VIS data set, the Aledo values range from 0 to 100 and are directly stored in the image array and do not need decoding.

4.4.3 Data flow, quality and reliability

The infra-red MDV data availability is monitored and controlled automatically so as to ensure that all the available satellite images on the satellite receiving system are incorporated in the satellite RFE scheme. It should be noted that there is always one IR image missing daily at 13:30 SAST due to the reception of the HRV image at this specific time (Figure 4.4.1). On average data availability is above 90% and the whenever the data flow was unreliable (<90%) this was due to technical difficulties with local communication.

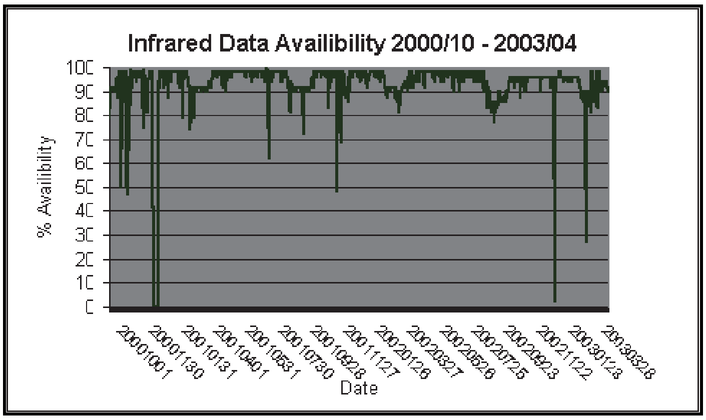

Figure 4.4.1 Infrared data quality during SIMAR project period

One important aspect affecting image quality is interference, usually solar induced. Instances of interference have been found to be either minimal, i.e. speckles of high intensity radiation or severe interference consisting of significant speckle areas or lines or arcs varying in width from a few to hundreds pixels. Minimal solar interference is easily diminished with the image preprocessing and the post-processing WAR speckle filter (Figures 4.1.3, 4.2.2, 4.2.3 and 4.2.4). The more severe interference is not so easily removed and such images are rather ignored. Minimal speckle interference occurs in ~ 10-20% of the images, whilst a mere 1% would contain the severe contamination.

5. PRODUCING THE SIMAR MERGED RAINFALL FIELD

In this chapter the following issues will be addressed:

- Rationale for merging rainfall fields
- Explain each data source briefly
- Explain the processes involved in merging the rainfall fields
- Discuss the feats of implementing these routines operationally.

5.1 Introduction

Water is one of the Earth's most precious resources. Being its source of replenishment at the surface, precipitation is essential for sustaining life on Earth. The spatial and temporal variable nature of precipitation makes its difficult to measure, though. This is the case even for ideal areas with good coverage by an observation network (Kidd, 1999). In reality, the spatial and temporal sampling of precipitation is limited by financial and logistic constraints. The existing rain gauge network of the South African Weather Service (SAWS), consisting of approximately 300 daily reporting stations, cannot provide the sampling required for sufficient monitoring of precipitation in our semi-arid country, which covers an area of approximately 1,27 million square kilometres. Of these daily-reporting gauges, 152 are manual standard rain gauges and 120 are automatic hourly reporting tipping bucket rain gauges.

The National Weather Radar Network (NWRN), consisting of 10 C-band radars and one dual-wavelength (S- and X-band) radar, greatly augments the spatial coverage of surface rainfall measurements in South Africa. This is accomplished by deriving a rainfall rate (R) from reflectivity data (Z) using an appropriate Z-R equation. Although the spatial sampling of rainfall by the NWRN supports that of the rain gauge network, it does not cover the whole country. Precipitation estimations derived from satellite measurements have the advantage of being spatially homogeneous over a large area (Bader et al., 1995) with a high temporal frequency. There is a recognized need for accurate estimates of rainfall on a variety of temporal and spatial scales (Ebert and Marshall, 1995). High spatial and temporal resolution of precipitation measurements is sought after by the hydrological and agricultural communities. Accurate and reliable rainfall fields are crucial for many socio-economic activities in South Africa.

The basis of the SIMAR system is the optimal integration of remotely sensed rainfall from weather radar and meteorological satellite with surface rainfall measurements. The philosophy underlying the merging of these multi-rainfall fields is to rely on the strength of each data source, filtering their weaknesses in order to produce one 'best estimate' rainfall field.

Each data source will be discussed briefly, highlighting their abilities and lack thereof. Thereafter the mathematical processes involved will be discussed and the merging process discussed in a stepwise fashion.

5.2 Rain gauge products

5.2.1 Strengths and weaknesses

Rain gauge measurements represent a simple, inexpensive method for point or areal rainfall estimations and are therefore extensively used as a surface precipitation-measuring device (Brandes and Wilson, 1987). However, gauge measurements are not representative of the areal precipitation and, therefore, ongoing investigation of alternative reliable methods of estimating areal precipitation is essential.

Inherent sampling errors of rain gauges are caused by adhesion or gauge funnel wetting, inclination of the gauge, splash into and out of gauge funnel, evaporation of water inside the gauge and airflow around the gauge (Brandes and Wilson, 1987). Dahlström (1973) showed that excluding airflow-induced errors, these amount to approximately 2% deficiency in catch, negligible in comparison to wind-induced errors. Mainly turbulence and increased wind speed in the vicinity of the gauge orifice contribute to the airflow-induced sampling errors. As the air rises to pass over the gauge, the precipitation particles that should have been sampled by the gauge are deflected and carried further downwind (Brandes and Wilson, 1987). These errors have been quantified (Sauvageout, 1992) as approximately 10% underestimation in sampling for a wind of 5 $m.s^{-1}$, 20% at 10 $m.s^{-1}$ and 20 - 40 % between 10 $m.s^{-1}$and 30 $m.s^{-1}$. These sampling errors of individual rain gauges and random sampling errors in areas of substantial spatial variance, contribute to the inherent errors in gauge estimates of area rainfall. These errors depend on the number and distribution of gauges, area size, length of the measurement period and the spatial variability of the rainfall event (Brandes and Wilson, 1987). Convective storms are short-lived with high spatial and temporal rainfall variability. Even a high rain gauge density will result in poor spatial sampling.

5.2.2 Gauge data processing

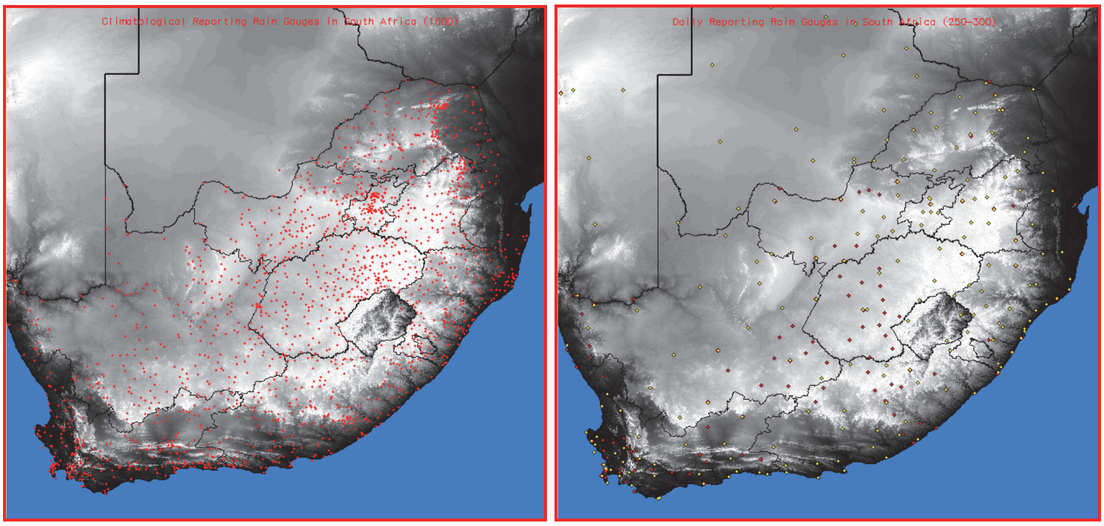

Figure 5.2.1 a) The distribution of climatological reporting rain gauges of SAWS, shown only for South Africa; b) The distribution of daily reporting rain gauges of SAWS, shown for the Southern Africa region. Yellow gauges correspond to synoptic stations (intermediate data set) and red/yellow represent the comprehensive set.

Daily surface rainfall data are extracted twice daily at 11:00 and 14:00 SAST from the database of the Climate Section of the SAWS. The data set consists of the entire daily reporting standard rain gauges, i.e. from synoptic and rain gauge stations, and automatic tipping bucket rain gauges, irregularly spaced over South Africa (Figure 5.2.1). These stations only amount to approximately 300 in number. Figure 5.2.1 shows the distribution of the daily reporting gauge network of the SAWS. Due to communication problems or the observer not being present over weekends, not all these stations are available for daily interrogation. Included in reports are accumulated rain, measured rain, rain not measured or no rain. No automatic quality control is done on the data and a manual inspection of the data is made at METSYS. Accumulated rainfall (typically over weekends) data or suspect values are identified and removed.

A main objective is to make the SIMAR rainfall field available in near real time. Since the rain gauge data form the most important link in producing this merged rainfall field, an intermediate data set is used to ensure that the real-time application of this data set is not lost. The intermediate data set is extracted from the Metgis forecasting workstation at Bethlehem and consists only of those stations reporting 3-hourly synops. These include all the automatic weather stations (~120) and first-order climate stations (~70) (Figure 5.2.1b). This data set is less comprehensive than the extracted data base report, but proves tremendously useful in producing a first guess merged rainfall field in near real-time. After a weekend, this rainfall data set is preferred as it contains no accumulated data, these stations having reported throughout the weekend.

The raingauge data set is required in a raster format for the SIMAR interpolation and merging routine. These point measurements of surface rainfall are converted to the standard SIMAR 1' latitude-longitude grid by using the nearest-neighbourhood method. The latitude and longitude of the rain gauges are used to locate its corresponding pixel in this 1024 by 1024 grid. The rain gauge value is taken to be representative of this one-minute pixel, which corresponds approximately to 1.3 by 1.8 km of sampling resolution.

If more than one rain gauge falls within the same pixel the average is taken of these measurements. The gridded rain gauge field is then converted to the standard SIMAR data format, the MDV file format.

5.2.3 Gauge data interpolation

The irregular raster rain gauge field is interpolated to produce a semi-continuous surface of rainfall. This surface is produced by the Kriging routine described in Volume 3 of this report. The pixel-based information is spread by the covariance information determined by analysis of historical radar data (Pegram 2001) in a Gaussian shape convolution. An iterative constrained deconvolution precedes the Kriging process, to ensure that the effect of the convolution is removed from the original data set. This will ensure that the original grid values will not be overestimated during the interpolation. Whilst producing a national kriged rain gauge field a rain gauge mask is produced, that is interpolated to the same regular grid. At a rain gauge position the value is assigned 100 and with distance the values decrease according to the covariance filter. This resembles the accuracy of the information in the rain gauge field as one move further away from the origin of the measurement. This field is referred to as explained variance and is useful as weight matrix for merging multi-data sets, since it signals the accuracy of the interpolated value.

Obviously, the role raingauges can play in the optimal merging of rainfields would be strengthened considerably if more raingauges, suitably located, could be deployed.

5.3 Radar information

5.3.1 Strengths and weaknesses

The most frequent quantitative application of radar is to derive precipitation fields from reflectivity data using an accepted Z-R relationship. Sauvageot (1991) named the advantages of radar, compared to a rain gauge network, as:

- having spatial continuity of observations
- giving improved information regarding the spatial and temporal variability of the precipitation
- observing the three-dimensional structure of the system generating the precipitation
- providing real-time surveillance over a wide area from a single observation point; and
- having the facility for in-situ data acquisition, storage and processing.

Weather radar is directly sensitive to precipitation elements and is hence a valuable tool in precipitation observation (Csiszar et al., 1997), but technical problems and limitations may seriously hamper its performance. These include:

- Attenuation of the radar signal by precipitation elements, clouds, gases or radome
- Non-uniform beam filling causing loss of data accuracy
- Side lobes detecting storms erroneously
- Presence of melting layer or ground clutter causing outliers
- The formation or evaporation of precipitation below the radar beam
- Violation of assumption that all hydrometeors are liquid
- Calibration difficulties (Sauvageout, 1992; Csiszar et al., 1997)

- Limitations relating to the assumption and implementation of the standard, reflectivity to rainfall rate, power law relationship (Batten, 1973; Doviak and Zrnic, 1984).

In South Africa the standard Marshall-Palmer formulae (Marshall et al., 1955) are used to relate reflectivity values to a rainfall rate. Merged rainfall fields are derived from the WRN data for various temporal scales at METSYS, Bethlehem. Recent and ongoing research and development (Terblanche et al., 2001) to improve weather radar measurements and derived rainfall over South Africa include:

- Filtering of permanent ground clutter and clutter caused by anomalous propagation;
- Bright band and hail filtering;
- Spatially and temporally modelling rain fields; and
- Applying techniques such as the WAR technique, to improve rain fields by calibration with gauge network.

5.3.2 Radar data processing

The 3-dimensional instantaneous (5-min) reflectivity fields of the 10 individual radars are converted from Cartesian space to a flat plane, where the fields are merged to form a complete radar field. During the same process this field is translated to a latitude/longitude grid of a coarser resolution of 1'. This MDV field is used for rainfall calculation by taking the maximum reflectivity in the vertical as representative of the intensity of rain falling at the surface. This composite reflectivity field produces rainfall according to the standard Marshall Palmer Z-R relationship. These instantaneous radar rainfall fields are accumulated to a variety of temporal scales and for SIMAR the 24-hour data set is used.

To improve the quality of the radar, limited post processing is applied to the 24-hour satellite rainfall field. This includes:

- Identification and removal of the effects of accumulated ground clutter-induced rainfall
- Limited infilling of gaps (missing areas) arising from clutter removal
- Areal average dilution
- Image processing.

a) Ground clutter filter

On-line historical ground clutter filtering is done for each instantaneous radar rainfall field, but ground clutter signals may vary considerable from day to day and can go undetected by a climatological filter. It is extremely difficult to accurately identify ground clutter on an accumulated rainfall map. Ground clutter signals may appear similar to convective rainfall areas and a compromise must be made between removing correct rainfall areas and ignoring clutter areas. This is a complex problem and impossible to properly solve on an accumulated field. Any improvements made will greatly improve the resultant kriged radar rainfall field, since ground clutter wreaks havoc if processed by the kriging routine. A simple approach is used for lessening the effects of ground clutter and is only efficient in removing the most severe contamination. On a rainless day this technique proves most useful.

The variance of a 3x3 neighbourhood is calculated and if greater than a predetermined threshold is flagged as erroneous. The variance is calculated as:

$$V(rad) = \left[\sqrt{\sum_N R_i^2 - \frac{\sum_N R_i \sum_N R_i}{N}} \right] / \left[\frac{\sum_N R_i}{N} \right] \qquad \textbf{(20a)}$$

$$V(rad) > T(var) \;\}\; Error(mask)=1 \qquad \textbf{(20b)}$$

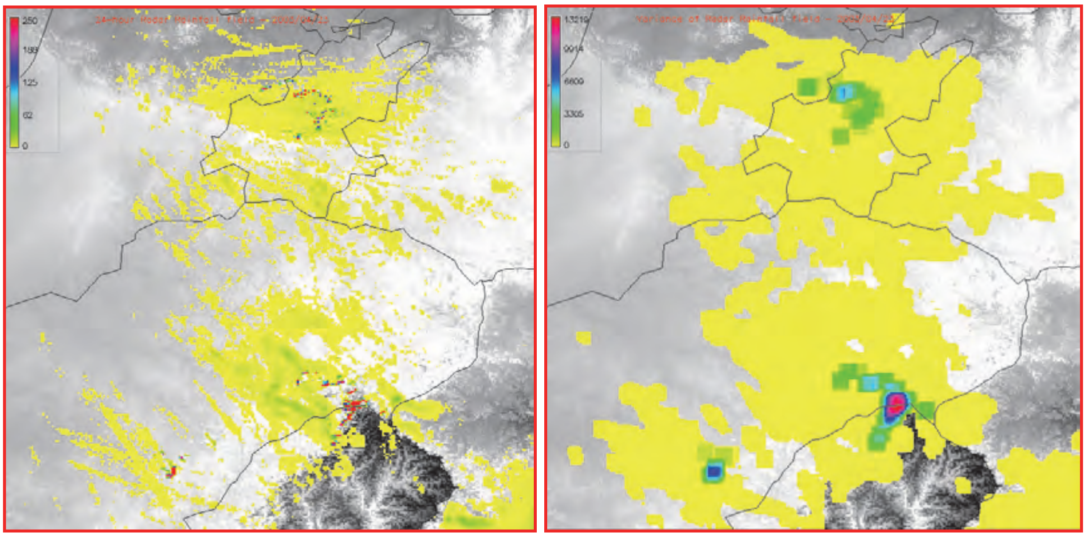

Figure 5.3.1 a) 24-hour raw Radar rainfall field for 2003/04/23 and b) corresponding variance field. High variance values correspond to areas of local heterogeneity and assumed to be ground clutter.

Low values signal little variation in the area surrounding the pixel in question, whilst high values correspond to heterogeneous areas (Figure 5.3.1). With such a small area corresponding to ~ 4 by 5.5km, the variation in rainfall fields, even convective, is not as intense as with ground clutter and is usually quite low. Daily accumulations of radar observed rainfall fields usually have little variance, in the order of 100's and not 1000's (Figure 5.3.1), which makes it possible to identify possible ground clutter-induced rainfall areas (Figure 5.3.2). A variance threshold filter of 1500 proved the most useful for identifying clutter rainfall areas (Figure 5.3.2).

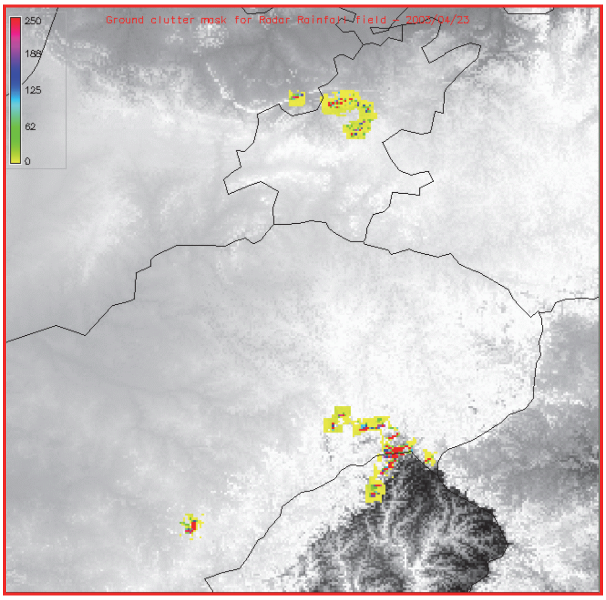

Figure 5.3.2 Masked radar echoes corresponding to ground clutter areas.

b) Infilling for flagged values

The radar rainfall values corresponding to the clutter mask are removed and need to be replaced with values which are some function of the values occurring in the immediate neighbourhood. This nearest neighbourhood infilling is done by considering the diagonal values, at angles 45^0, 135^0, 225^0 and 315^0 of the 9x9 neighbourhood surrounding the flagged pixel. The values are combined according to the covariance filter used in the Kriging interpolation, which signals the spread of information in a radar field and is given by:

$$G_{(i,j)} = e^{\frac{-r}{L}} \qquad \textbf{(21)}$$

Where $r = \sqrt{(i^2 + j^2)}$ and L the correlation length=12.3

$$R_n = \frac{\sum G_{(i,j)} R_{(i,j)}}{\sum G_{(i,j)}} \qquad \textbf{(22)}$$

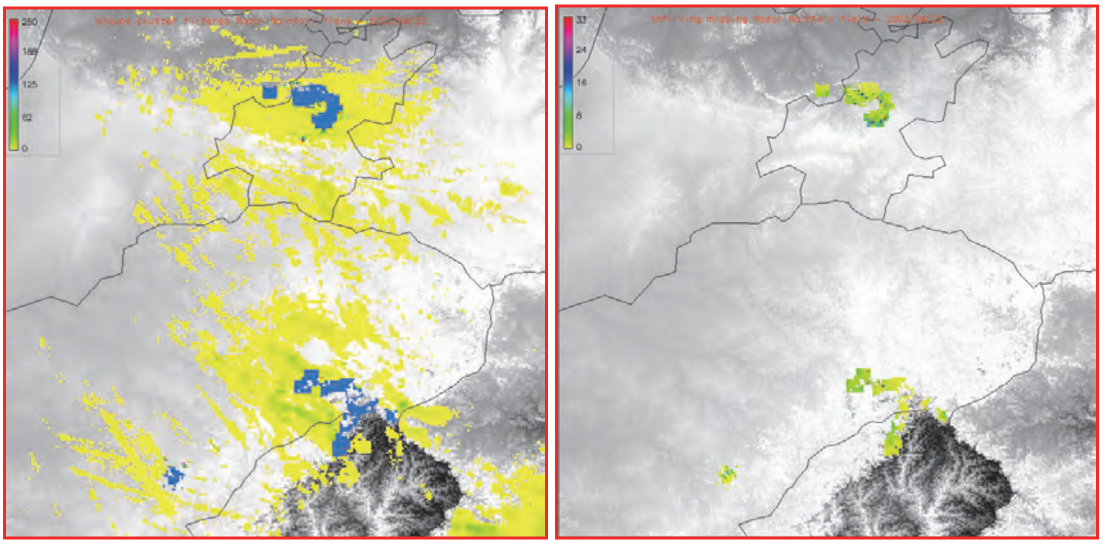

Figure 5.3.3 a) Radar rainfall for 2003/04/23 with areas of ground clutter masked in blue; b) In-filled rainfall for the masked blue (ground clutter) areas, based on information in the unmasked areas of a).

The effectiveness of this variance threshold based filter is limited in that it focuses on the strongest component of ground clutter. Smaller ground clutter areas can go undetected (Figure 5.3.3a, Figure 5.3.4b), but the majority of the clutter is removed when compared with the original images (Figure 5.3.4a) and proves extremely useful as post processing filter. The neighborhood interpolation techniques provides fairly accurate rainfall fields for the ground clutter areas, spatially and quantitatively (Figure 5.3.3b, Figure 5.3.4b), and is extremely fast to compute online.

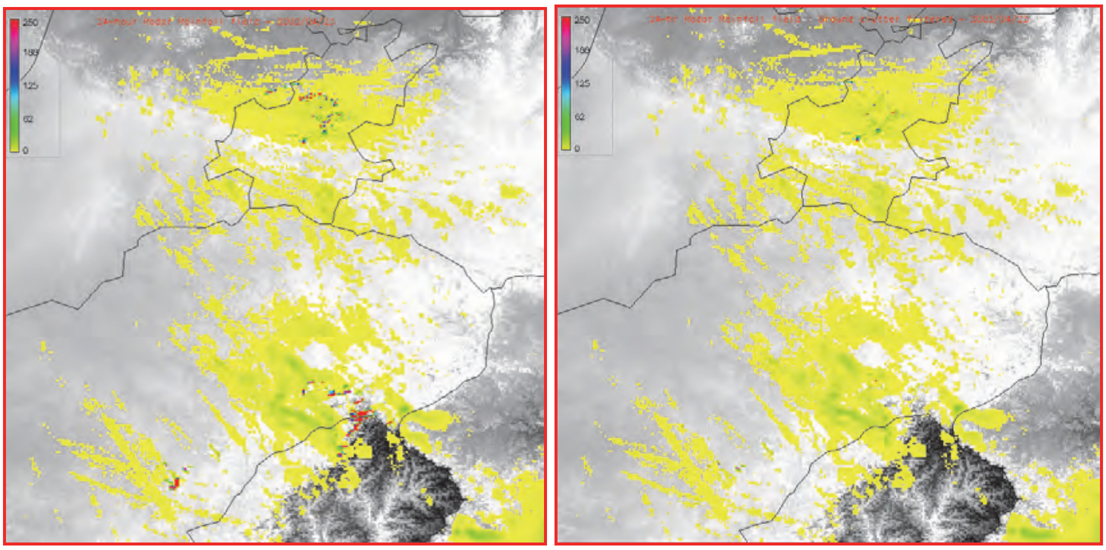

Figure 5.3.4 a) The original radar rainfall field and b) the ground clutter removed from the radar rainfall field.

c) Areal average dilution

This filter is similar to the WAR speckle filter of the MSRR technique. The average radar rainfall of the nearest neighbourhood is used to filter small rainfall areas and to enhance object edges. The average of the 9x9 neighbourhood of a pixel is given by:

$$R_a = \frac{\sum R_{(ij)}}{N} \qquad \textbf{(23a)}$$

$$R_a < T \; \} \; R=0 \qquad \textbf{(23b)}$$

This filter specifically filters the effect of anomalous propagation (AP), where the earth surfaces or ocean areas produce speckles in the radar domain. AP usually occurs during the clear weather days and produce fictitious kriged radar rainfall areas.

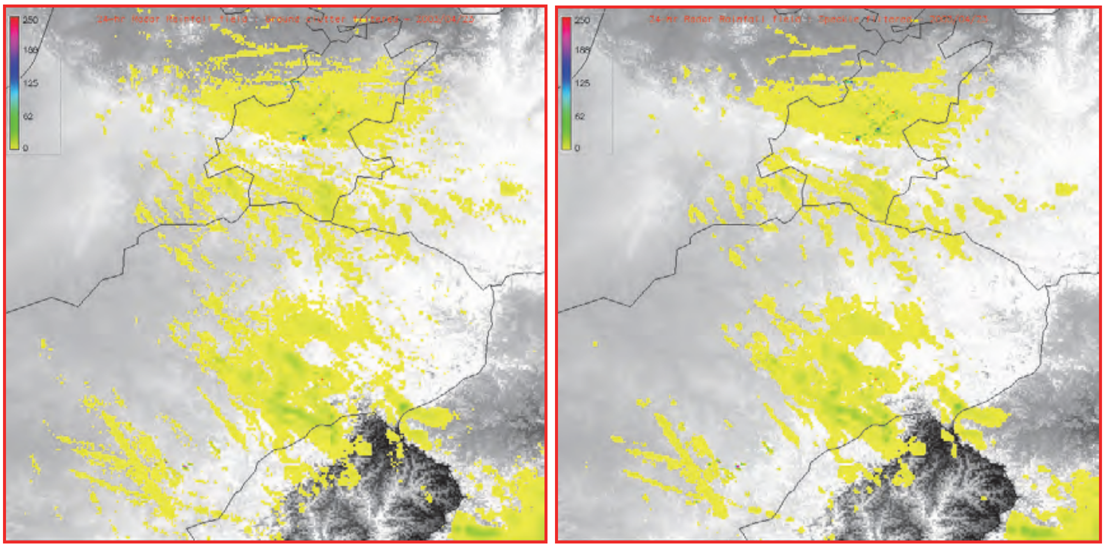

Figure 5.3.5 a) The quality controlled radar rainfall field produced by the clutter filter of 5.3.3a and data infilling of 5.3.3b; b) Areal dilution is applied to the image to clear up the image of small speckles and erroneous data.

d) Image processing

As a post-processing image filter, a median filter is applied to the quality-controlled image to enhance the spatial rainfall fields. This is done to counteract any deterioration of the radar rainfall fields caused by erroneous filtering of the 3 former filters. The median filter is applied to a 5x5 neighbourhood and the central pixel is replaced by the median of the surrounding area. The median usually corresponds to the most dominant feature of the surrounding area.

5.3.3 Radar data extrapolation

This error-filtered image is then used as input for the kriging routine. The aim behind the kriging of the radar field is spreading information beyond the scope of measurement and partly for image processing. As with the rain gauge data, an interpolation accuracy field is created, that is used for merging these two fields.

5.3.4 **Satellite information**

5.3.5 Strengths and weaknesses

This data source was discussed in detail under heading 4.1. The MSRR technique, see heading 4.2.3-4.2.5, is applied for estimating rainfall fields as third leg of the SIMAR data sources. We must look to satellite information to fill the gaps in data from radar and rain gauge rainfall fields, to produce a national rainfall map for Southern Africa. The advantages of utilizing satellites for rainfall estimation include:

- Ability to acquire data for any point on earth, irrespective of country or surface conditions
- Cost-effectiveness, since many countries can share the cost of a single instrument
- One, known calibration of the radiometer on board the satellite, irrespective of point of measurement.

The limitations of estimating rainfall with the MSRR technique include:

- Cloud systems are opaque in IR/VIS channels and at best provide an indirect method of estimating surface rainfall
- Complex nature and variation of cloud top structure under varying dynamical conditions are handled at an average level and produce limitations for non-climatological outlier storms
- The effects of warm, orographic cloud development on rainfall fields are not always correctly quantified
- The simplified approach to cloud structure classification in rain/no-rain systems are fallible and incorrect classifications do occur, especially for widespread tropical moisture and rain systems.

5.3.6 Satellite data processing

The raw satellite IR/WV radiance and VIS albedo data sets are extracted from the global satellite view field, re-projected and calibrated to brightness temperatures for use in the MSRR technique. For a complete description refer to Section 4.4.2.

The satellite rainfall data set is the only source of information, sampled for every area on the national rainfall grid. No interpolation technique is required and rainfall is estimated on the original sampling grid (Section 4.2.4.6).

5.4 Integration of rainfall fields

5.4.1 Merging radar and rain gauge data

The idea of merging these two rainfall fields is to retain the superior sampling resolution of areal rainfall from radar and to remove any quantitative biases by bringing the values closer to that of the ground-truth rain gauges. Merging the two rainfall fields (final step e) is preceded by the following four steps:

a) Extrapolating radar data
b) Interpolating rain gauge point measurements
c) Determining explained variance field for radars
d) Determining explained variance field for rain gauges

a) Extrapolate radar data

The kriging technique is applied to the radar rainfall field R_R to produce R_K. This field is an image-processed version of the original field, in that the ICD and kriging convolution act to blur the original structure of the spatial fields (Figure5.5.1). It has the additional effect of enhancing image quality, especially for areal rainfall. Erroneous high values, from ground clutter, are reduced during this process, but its effect is convolved with the surrounding area during kriging, thereby degrading the qualitative fields. This has both a positive and negative impact on the resultant rainfall field. Other blemishes on the original radar rainfall field, such as anomalous propagation and bright band effects, are also lessened but its effect spread with this technique. It is imperative that the processed 24-hour radar rainfall field is of the highest quality before being processed by this technique. In addition the areas of missing data within the radar domain, such as for offline radars and those areas where ground clutter information was removed, are determined and the missing data interpolated. A radar mask is used in the kriging to limit extrapolation of data to only beyond the radar domain. The extrapolation is limited though, and only 10% of additional data is gained in this process.

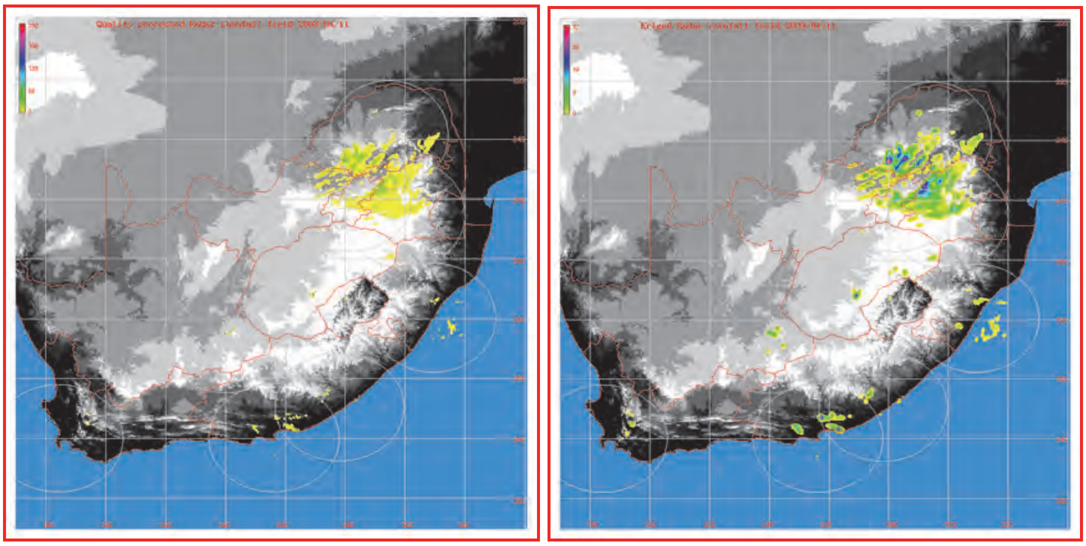

Figure 5.5.1 a) Quality enhanced 24-hour radar rainfall field, with majority of clutter and contamination removed for 2003/04/11; b) The kriged and image processed image using a) as input field.

b) Interpolate rain gauge point measurements

The covariance filter of historical radar information is used in the kriging technique for interpolating rain gauge data in between the gauge positions to produce the surface, G_K. If the gauge density is sufficient and the values accurate as ground truth, the resultant areal rainfall volume and structure more closely resemble that of the radar. When gauges are far apart and the rainfall heavy, interpolation rings are evident in the rainfall fields, which are typical of standard kriging interpolation. In such a case the areal rainfall differs widely from the radar. The rain gauge data forms the foundation of the merging routine, acting as ground truth for the other data sources. By improving the rain gauge density and sampling resolution, the estimates of areal rainfall of the kriged field and of the subsequent merged field will greatly improve.

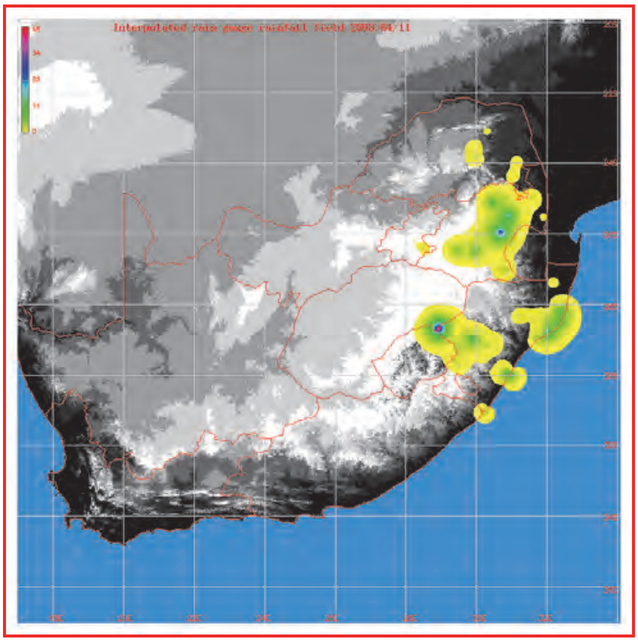

Figure 5.5.2 Interpolated rain gauge data field corresponding to Figure 5.5.1

The poor areal sampling of the interpolated rain gauge field can be seen when comparing with that of the radar (Figure5.5.1). The irregular distribution and density of rain gauges contribute to this poor sampling, although the field is interpolated. In the immediate vicinity of the rain gauges, these rainfall values can be seen as the only respective observation of surface rainfall. The areal sampling of this rainfall field will improve with each rain gauge added, to strategic positions, to this data set.

c) Determine explained variance field for radars

The radar domain mask is used to krige the explained variance field, R_V, that corresponds to the quality of the measured radar data and to the areas of extrapolation. The whole radar domain, corresponding to a 200 km range surrounding every radar, is accepted as being 100% accurate. It is assumed that all missing data areas were infilled accurately. This data accuracy mask assigns a weight to each radar measurement, according to which its value is deteriorated or retained when merged with the rain gauge field.

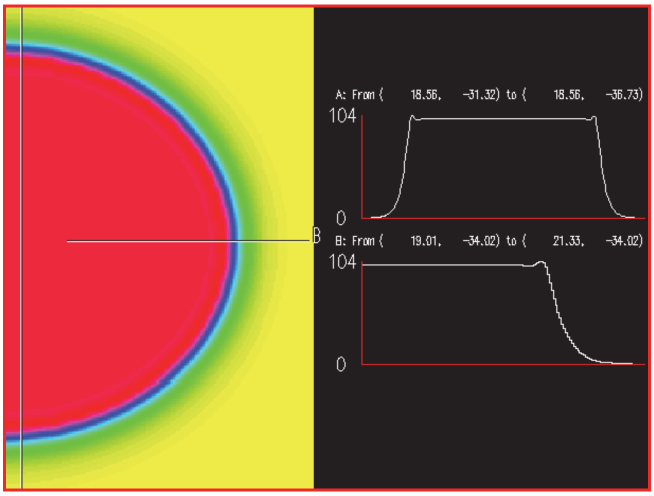

Figure 5.5.3 Example of the shape of the explained variance of individual radar's coverage. The radar coverage extends to 200km and is marked by the strong decrease in information beyond the rim.

d) Determine explained variance field for rain gauges

Each pixel value corresponding to the rain gauge position is accepted as being a 100% accurate reading of ground truth rainfall. Rain gauges are not accurate in measuring areal rainfall and the covariance information of the radar is used to spread information between gauges. This same information relates to the accuracy of the interpolated rainfall surrounding each rain gauge point (Figure 5.5.4) and is used to produce explained variance field, G_K (Figure5.5.5d).

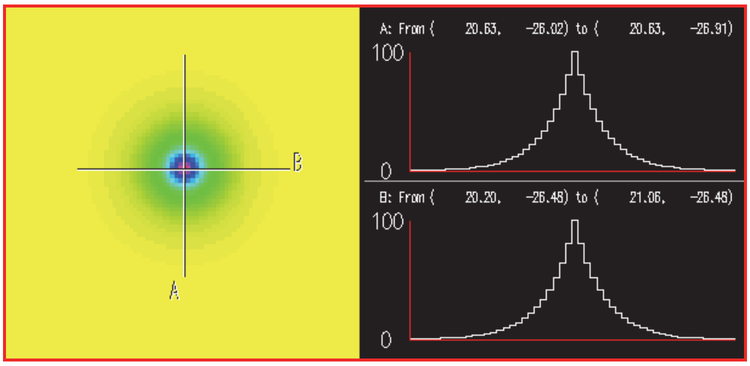

Figure 5.5.4 A cross section of the accuracy of the kriged rain gauge information.

e) Merge the two rainfall fields

These explained variance fields in *c* and *d*, correspond to the domain of information contained in the radar and gauge fields and their accuracy. The explained variance fields are used as weight matrices for merging the two rainfall fields and merging is accomplished by:

$$RG = \left[\frac{R_K R_V + G_K G_V}{R_V + G_V} \right] \qquad \textbf{(24)}$$

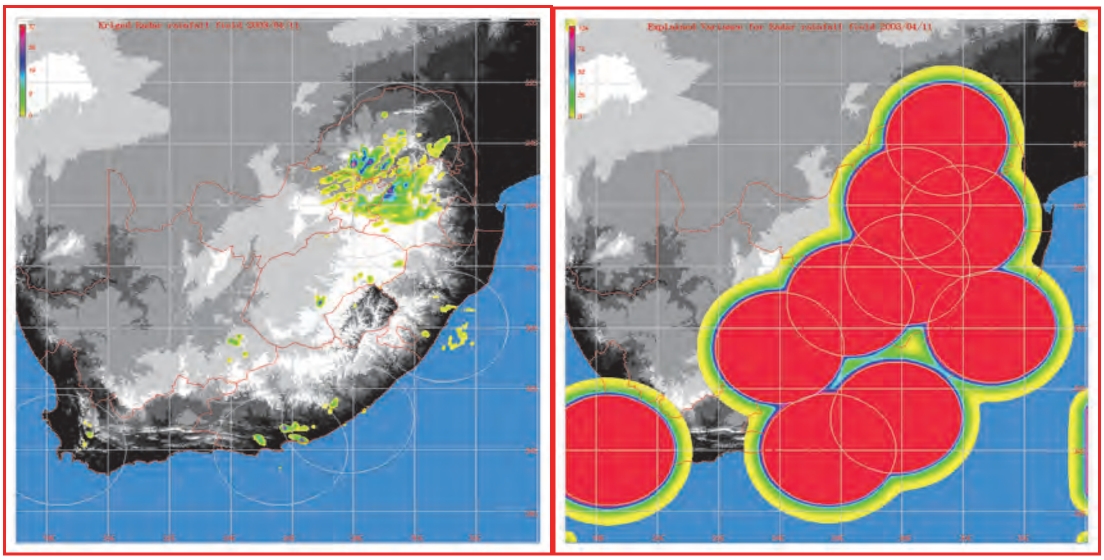

Figure 5.5.5a) Kriged radar rainfall field, R_K; b) Explained variance field for radar domain, R_V.

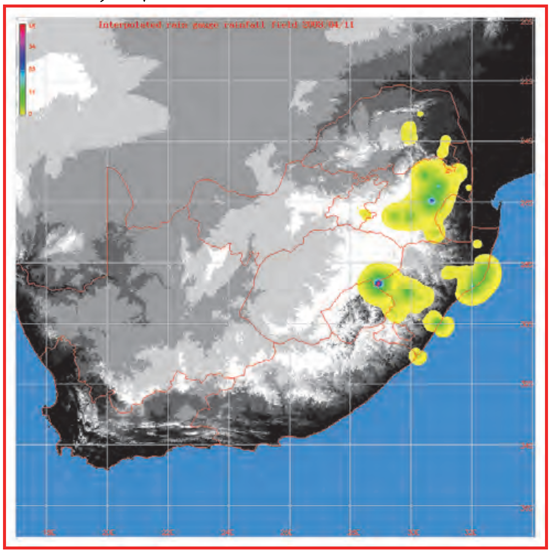

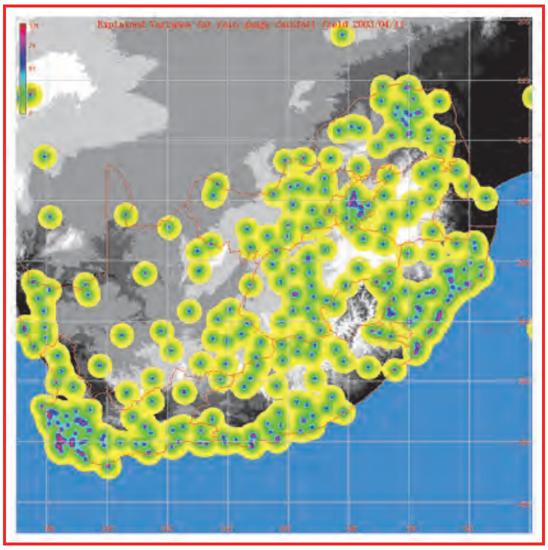

Figure 5.5.5 c) Kriged rain gauge field, G_K; d). Explained variance field of rain gauge domain, G_V.

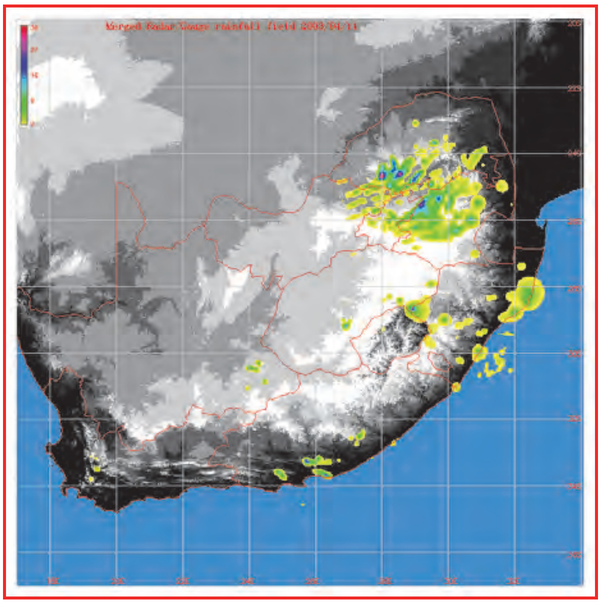

Figure 5.5.6 Produced by merging information in Figure 5.5.5(a-d) using equation [24].

Figure 5.5.6 represents a rainfall field produced by integrating the quantitative values of the rain gauge (ground truth) with the superior spatial information on the distribution of areal rainfall of the radar. The spatial structure of the radar (Figure 5.5.5a) is maintained, but the weight of the rain gauge information reduces the effects of contamination or inconsistencies in the radar rainfall field.

5.4.2 Conditioning satellite data on ground truth

Satellite data is the additional rainfall data source in areas of little or no other information. Owing to the inherent limitations in determining rainfall from the opaque satellite channels, there is a fairly consistent bias in the MSRR satellite rainfall estimates (Section 4.3). Satellite provides invaluable information on the spatial distribution of rainfall in areas where no other means of determining areal rainfall are available. Conditioning the satellite rainfall on the quantitative rainfall values from rain gauges, allows us to remove the bias in rainfall estimates at the rain gauges, and to retain the satellite information between gauges.

Conditioning satellite data on the rain gauge information (final step c) is preceded by the following steps:

a) Interpolating an average satellite rainfall field
b) Interpolating the rain gauge data.

a) Interpolate an average satellite rainfall field

The satellite rainfall pixels are sampled at the positions of the rain gauges, to produce a discrete satellite rainfall field.

$$S_{m,j} = S_{,j} \text{ where } G_j \qquad \textbf{(25)}$$

This data field is interpolated to a regular grid using completely regularized splines (CRS) with tension (Mitasova and Mitas, 1993) to recreate the satellite rainfall grid. CRS and spline interpolation have been widely applied on geographic (Mitasova and Mitas, 1993) and climatological (Hartkamp, et al. 1999) parameters. The problem pertains to solving for discrete values $S_{m0}{}^{j}\ldots\ S_{md}{}^{j}$ for j=0…j=N in a *d* – dimensional space, with function:

$$S_z(S_m) = T(S_m) + \Sigma_{j=0}\, \lambda_j\, R(r_j) \qquad \textbf{(26)}$$

With $T(S_m)$ as a constant trend function for CRS and $R(r_j)$ the radial basis function, given by:

$$R(i,j) = -\left\{ \ln[(\frac{\varphi r_i}{2})^2] + E_1[(\frac{\varphi r_i}{2})^2] + C_E \right\} \qquad \textbf{(27)}$$

Where $r_j^2 = \Sigma^2_{i=0} (S_{mi} - S_{mi}^{\,j})$; E_1 is the exponential integral function (Mitasova and Mitas, 1993); C_E = 0.577215 the Euler distance and φ is the tension parameter, that was determined empirically as 75 (range 10 – 100).

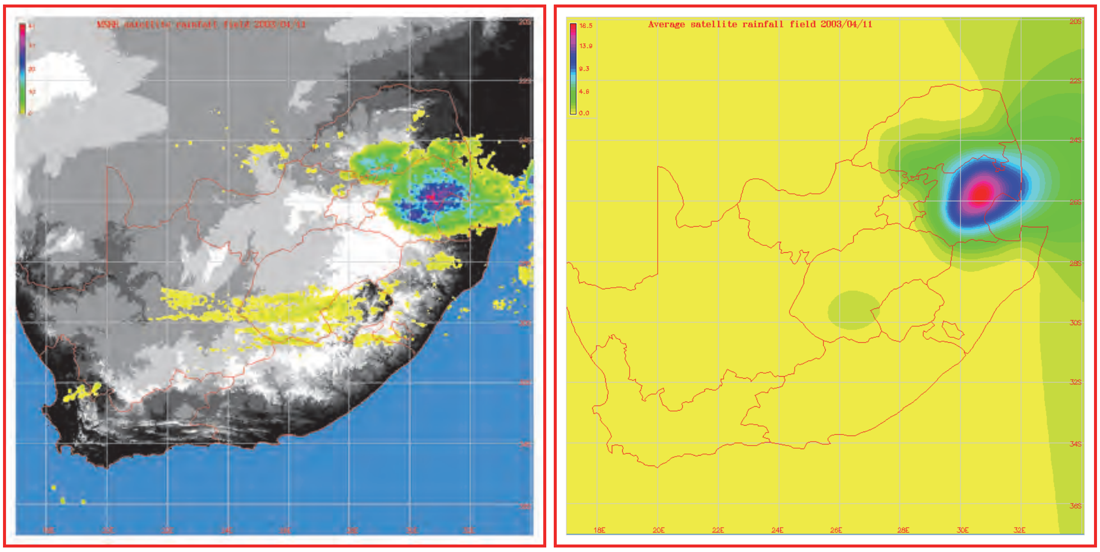

Figure 5.5.7 a) The 24-hour MSRR satellite rainfall field; b) The corresponding average satellite rainfall field.

The spline interpolation cannot resample the original satellite rainfall and at best produce a smoothed and homogeneous version of this rainfall field (Figure 5.5.7). This field is accepted as being the average satellite rainfall field and observed as being the background rainfall relative to the noise, ie the largest rainfall signal in the rainfall field.

b) Interpolate the rain gauge data

The rain gauge point measurements are interpolated to a rainfall surface with the kriging algorithm, heading 5.2.3 and 5.5.1b, using the radar covariance information to spread the rain gauge data to produce G_K (Figure 5.5.5c).

c) Condition the satellite on the rain gauge information

The background information of the satellite rainfall is removed, to produce a field that retains the greatest signal on the spatial distribution of the rainfall, as estimated from satellite. The interpolated ground truth field replaces this data field as information on the background signal of rainfall. This in effect conditions the satellite data on the ground truth, by removing the bias from the satellite data at the rain gauge positions and accepting the interpolated ground truth as average surface.

$$SG = S_R - S_z + G_K \qquad \textbf{(28)}$$

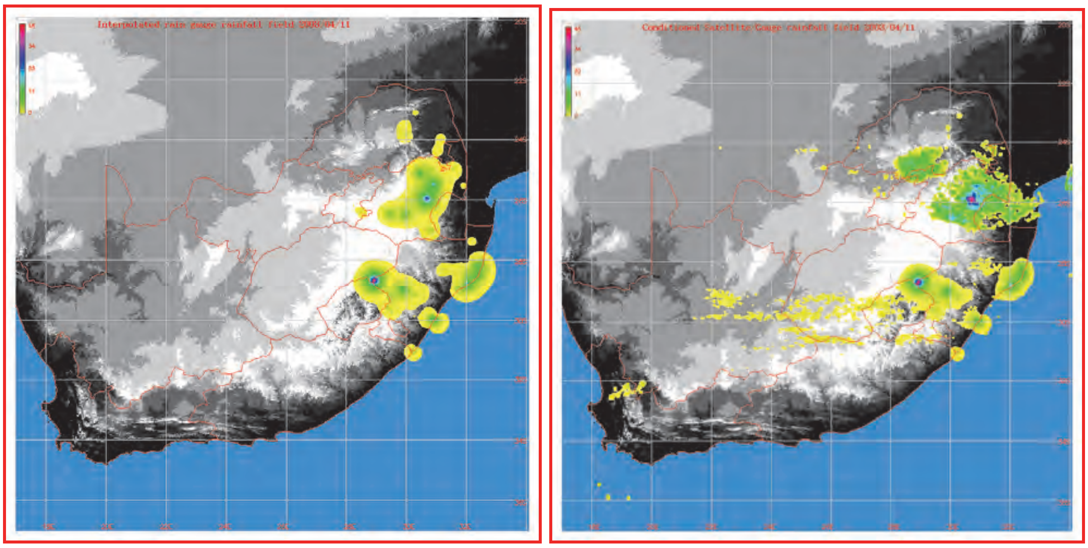

Figure 5.5.8 a) Kriged rain gauge field ; b) Conditional simulation of the satellite rainfall field (Figure 25a) on the interpolated rain gauge information a).

The conditioning of **(28)** produces a rainfall field, SG (Figure 5.5.8), where the rainfall values at the rain gauge positions correspond to ground truth, $SG_{ij}=G_{ij}$. In the areas where there is no ground truth information the fluctuation signal of the satellite rainfall field is retained to estimate the areal rainfall. The major contributor to this rainfall field is the satellite field, by maintaining its spatial distribution of rainfall but removing its biases relative to the gauge field.

5.4.3 Producing the merged rainfall field

The methodology for producing the merged final rainfall field is the optimal combination of the fields produced in Sections 5.5.1 and 5.5.2. This stepwise approach to producing the SIMAR rainfall field is necessitated by the remaining limitations of the satellite rainfall field, since MSG could not be utilised for this projects, and of the radar field, with contamination of ground clutter having a devastating impact on the merged field. Each data source is merged individually with ground truth, so as to remove the greatest component of noise, before accepting these fields as being accurate and reliable representations of the surface rainfall.

Rather than merging these two fields as equals, an individual weight field is composed for each merged data set. For the radar and rain gauge merged field the explained variance masks, G_v and R_v, are integrated with the Boolean "or" statement to produce RG_v (Figure 5.5.9b).

$$RG_v = R_v \mid G_v \qquad \textbf{(29)}$$

This data set resembles the domain of measurement of the radar and rain gauges and is taken to be related to the underlying accuracy of their measurements. This assumes that the individual pixel measurements are as accurate as can be, which is not always the case.

For the conditioned satellite rainfall field, quite a different and novel technique was developed for determining its accuracy. The satellite's perspective covers the whole data domain and although errors in the data set are quite consistent in nature (refer to Section

4.3), the whole data set cannot be handled at the same accuracy level. For this purpose the bias skill score of the satellite rainfall in a neighbourhood surrounding the rain gauges, are used as weight field to accomplish the final merging. This is done by:

- Calculating the bias skill score of satellite rainfall field relative to neighbourhood around rain gauge pixels, S_{BSS}
- Scaling this bias score with the relative field bias of the satellite rainfall values, S_{BIAS}
- Interpolating this skill score values to regular grid, S_{SS}, to be used as weight field for merging the conditionally simulated satellite field with the merged radar-gauge field (Figure 5.5.9d)

The contingency table of a 9x9 neighbourhood surrounding the rain gauge positions is used to calculate the bias skill score and is given by:

	Satellite		
Gauge		Rain	No Rain
	Rain	H	M
	No Rain	FA	CN

Where H is correct hits, M misses, FA false alarms, CN correct nulls.
The kriged rain gauge field is used as ground truth for the 9x9 domain surrounding the rain gauge, since the interpolated values are significant and accurate according to the gauge explained variance field.

$$S_{BS^2(i,j)} = \frac{\lfloor H_{ij} + CN_{ij} \rfloor}{[H_{ij} + M_{ij} + FA_{ij} + CN_{ij}]} \qquad \textbf{(30)}$$

The bias skill score (Haralick, 1979) gives the fraction of correct rain/no-rain classifications made by the satellite. S_{BSS} indicates the bias of the MSRR technique to identify rainfall occurrences correctly. If S_{BSS} = 1 there is no bias in the technique's ability. With S_{BSS} decreasing to zero the techniques ability to classify the rainfall classes correctly, deteriorates.

Again spline interpolation (equation 26) is used to interpolate the discrete $S_{BSS(ij)}$ data set to a gridded surface, to produce a continuous weight surface for the whole data domain of the satellite.

$$S_{S^2}(100 \times S_{BS^2}) = T(100 \times S_{BS^2}) + \sum_{j=o} \lambda_j R(\sum_{i=0}^{2} (S_{BS^2} - S_{BS^2 j})) \qquad \textbf{(31)}$$

The limitation of this technique of determining merging weights is that if the satellite has either a FA or M when compared to a single rain gauge in data sparse areas, such as in neighbouring countries, a low value of skill will be extended to an area, where rainfall may have been correctly classified. This deteriorates the impact of the satellite rainfall on the final merged field. To overcome this limitation, the average skill score of the whole data domain is used as accuracy of the satellite rainfall field in those areas far from radar or rain gauges, where the S_{BSS} may be unreliable. The field skill score, S_{FSS}, is calculated by standardizing this bias skill score matrix:

$$S_{FS^2} = \frac{[\sum_N S_{BS^2_{(ij)}}]}{N} \quad \textbf{(32)}$$

The final merged rainfall field is produce by integrating the satellite-gauge and radar-gauge rainfall fields by using their weight fields RG_V and S_{S^2}

$$R_{MERGED} = \frac{[SG \times S_{S^2} + RG \times RG_V]}{[S_{S^2} + RG_V]} \quad \} \; RG_V > 0 \quad \textbf{(33a)}$$

$$R_{MERGED} = \frac{[SG \times S_{FS^2}]}{100} \quad \} \; RG_V = NULL \quad \textbf{(33b)}$$

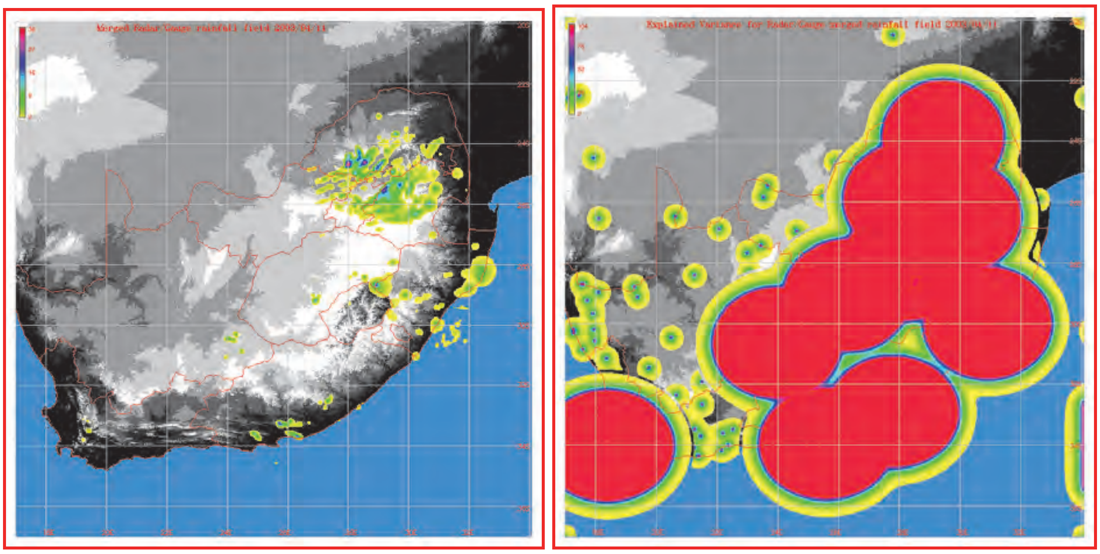

Figure 5.5.9 a) Radar and rain gauge merged rainfall field; b) Explained variance field of a).

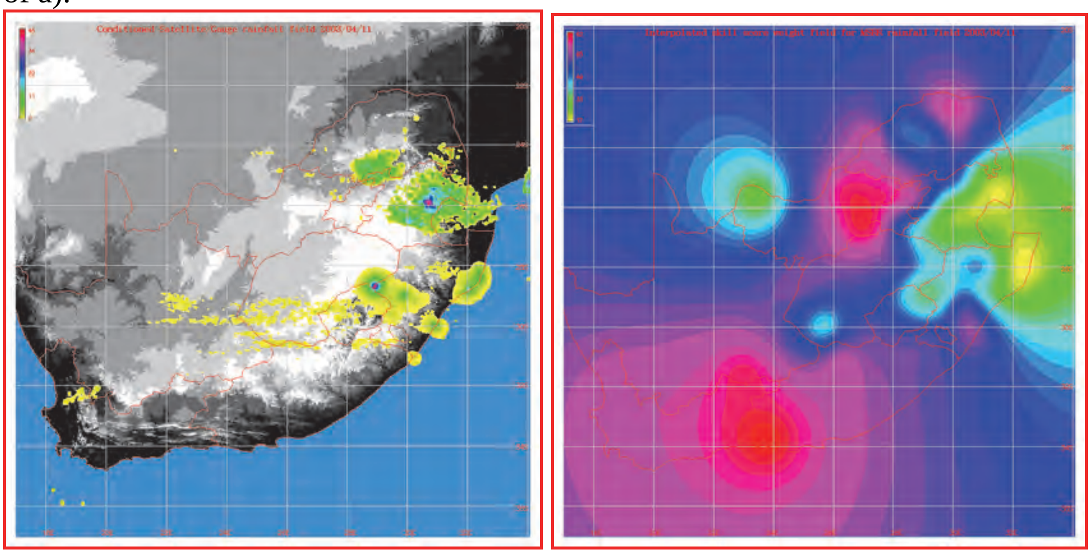

Figure 5.5.9 c) Rain gauge conditioned satellite data; d) Interpolated bias scaled skill score field for satellite rainfall field.

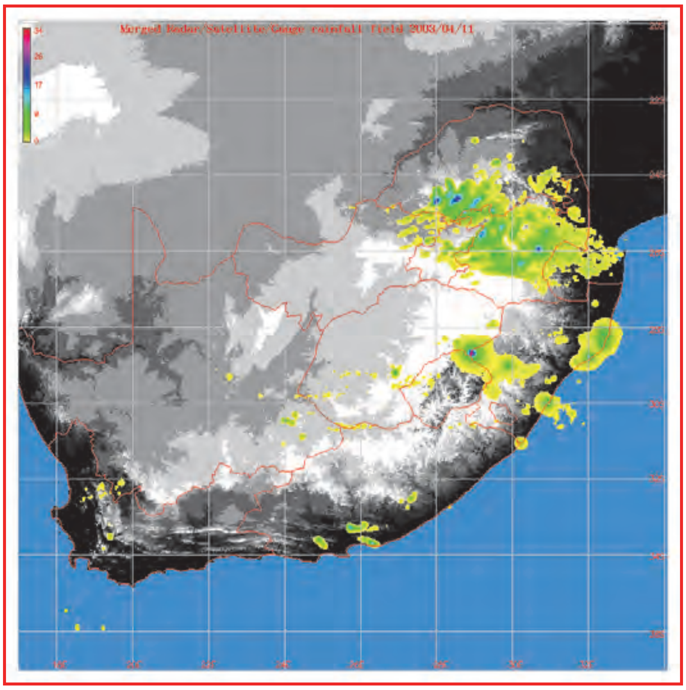

Figure 5.5.10 The SIMAR merged rainfall field produced by integrating Figure 5.5.9 a) – d) using Equation 33.

5.4.4 Validation of merging process

Rain gauge data are the only source of ground truth for validating the intermediate stages of merging, although it inherently forms part of these merged rainfall fields. It is useful to validate the merged rainfall fields relative to their original counterparts.

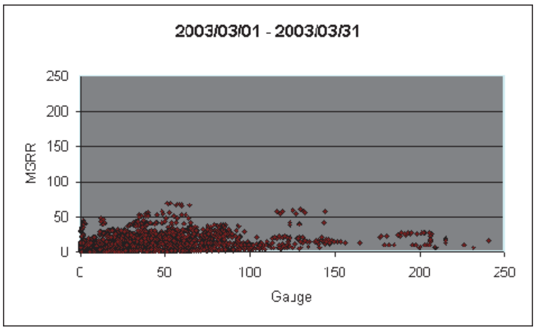

a)

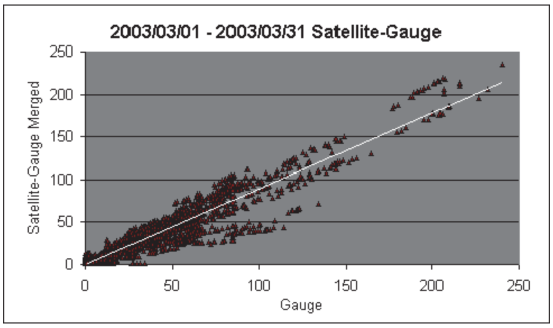

b)

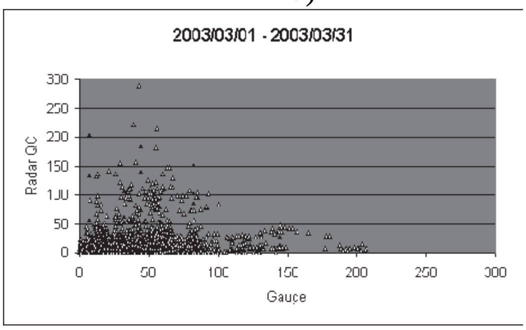

c)

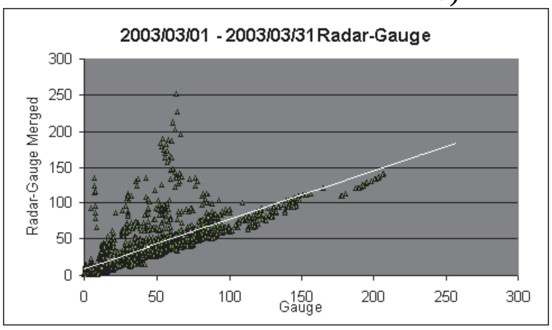

d)

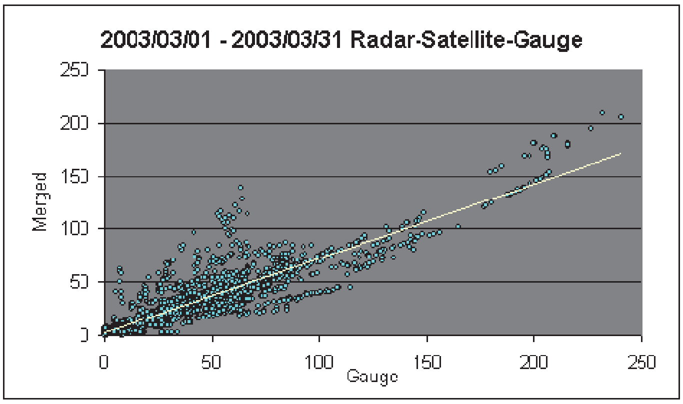

e)

Figure 5.5.11 a) Validation of MSRR rainfall for March 2003; b) MSRR rainfall conditioned on rain gauge data; c) Radar data with quality control schemes applied; d). Kriged radar merged with kriged gauge data; e) Final merged field.

Comparing Figure 5.5.11a and 5.5.11b, the effectiveness of the conditioning technique for removing the bias of the MSRR satellite rainfall field, is evident. There is a vast improvement made in the distribution of values with respect to ground truth, with very little drift observed. This proves to be an extremely efficient method for modelling the satellite rainfall on ground truth.

The kriging explained variance based merging of radar with rain gauge rainfall data, is not as efficient in diminishing bias, as with the conditioning process, but still produces reliable spatial fields. These two techniques differ fundamentally in that the conditioning accept the satellite rainfall field to be flawed in their quantitative representation of rainfall, but acceptable spatially; whilst the kriging-based technique assumed the radar field to be perfect within its domain of measurement. It is assumed that the radar produces perfect rainfall fields up to a range of 200 km, which is not always true (see Section 5.3 for the various limitations). This merging technique proves useful in removing all of the underestimation from the radar rainfall field and manages to cluster the values significantly, as can be seen from the linear fit. Most of the deviation from the best-fit line is caused by remnants of overestimation from ground clutter effects. Improved filtering of ground clutter will drastically improve the quality of this merged data set, since radar provides the highest quality information on the spatial distribution of rainfall.

Merging the rain gauge conditioned satellite (Figure 5.5.9a) and radar/gauge merged fields (Figure 5.5.9c) provides a means of retaining the superior sampling resolution and quality of the radar, but bringing its quantitative values closer to that of the gauge. Using the satellite skill score and kriging explained variance as weight fields in merging these two rainfall fields manages to remove further bias retained from the radar. It produces reliable quantitative fields, but the resultant spatial integration still need some attention since the satellite information tend to deteriorate the sampling resolution of the radar (See Section 5.6, Figure 5.6.2d,f). Also, when extensive overestimation occurs in the satellite technique, it has a devastating effect on merging the rainfall fields (Figure 5.6.1).

5.5 Operational implementation and optimisation

5.5.1 Implementation on Radar data

The technique for the integration of rain gauge and radar rainfall fields, developed by Pegram (2000), was implemented on MDV radar data during winter 2001, to investigate its applications and limitations.

At the foundation of this algorithm we find the Iterative Constrained Deconvolution (ICD) algorithm, borrowed for the science of machine vision, and the Fourier domain kriging convolution. The ICD removes the effect the convolution of the covariance filter would have had on the measured radar field, thus producing the reciprocal data set. This means that the original structure and values of the radar can be retained during the kriging procedure. Fundamental to the ICD routine is the constraint operator, α, which ensures that the data values are reduced sufficiently iteratively to ensure that the ICD routine convergences. The amount of deblurring done to the image relate to its ability to resample the radar information at it original resolution and structure. The more iterations are allowed for in the ICD routine, the closer the resultant kriged field resembles the original data field.

Next, the covariance filter, G(u) is spread in convolution during the kriging interpolation technique. For efficiency this convolution is not done in the spatial domain, but composed in the Fourier domain. This kriging process produces the extrapolated radar rainfall fields. In effect the kriging allows for a Gaussian smoothing of the image, which blurs the original sampling resolution of the radar. The covariance filter is given by:

$$G(u) = \exp[-b(s/L)^a] \qquad \textbf{(34)}$$

Where *a* correspond to *–1* for kringing data and *1* for kriging explained variance, *r* is the radial distance $sqrt(x^2+y^2)$, *L* the correlation length and *b* correspond to *1* for Gaussian and *2* for exponential. *L* relates to the standard deviation, σ, of the standard Gaussian, which is the only parameter affecting the Gaussian distribution. The greater the value of *L*, the coarser the subsequent convolved field will appear, but the greater the distance to which information can be spread. An *L* of 12.3 pixels has been found to be appropriate; this is the distance where correlation within the radar field drops of to 0.1.

A data mask is employed to restrict extrapolation to the region beyond the 200 km radar range. This mask allows the technique to identify which radars are not operational. It allows for interpolation for areas of missing data in conjunction with the extrapolation of the radar domain.

5.5.2 Problems in Paradise

The software was originally tested on 256x256 domains and the technique proved to be extremely efficient. It was when the software was adapted to handle the 1024x1024 national grid, that the efficiency became a problem. The software was tested intensively on instantaneous radar fields and it was found that 100 iterations succeeded in recreating the fine structure of the original radar field. This process took approximately 30 minutes to be completed for a radar field, on a 600 Mhz Pentium III. In real time this process will be required to run in 1-2 minutes to be useful. Decreasing the amount of iterations of the

ICD routine resulted in smoother fields. The effect of smoothing did not increase linearly and at 75 and 50 iterations the loss of data resolution was already too great. For 10 iterations the process took approximately 2-3 minutes, which is more realistic, but smoothing significantly deteriorated the spatial features. The alpha constraint value was determined by trial and error for the ICD routine to convergence.

5.5.3 Improving computational efficiencies

Means of improving the efficiency was investigated and implemented. In order to speed up the time it took for convergence to occur, the first guess field of the ICD routine was scaled by the volume of the covariance filter. This did not have the desired effect. It was found that the first few iterations convergenced quicker, but thereafter the rate of convergence stabilized, being fairly similar to those without scaling. Scaling by fractions of the volume of the filter had the same effect.

Converting the 1024x1024 national grid to a coarser 256x256 grid had a positive effect on the computational efficiency. The ICD routine is run on the coarser grid for a certain amount of iterations. The field produced is converted back to the 1024x1024 grid and is used as first guess field for calculating the reciprocal data on the 1024x1024 grid. Originally it was thought that doing 100 iterations on the coarse grid would allow the results of 10 iterations to be of finer structure and more like the result of 100 iterations on the 1024x1024 grid. This was not the case. The high amount of iterations of the coarse grid led to wavelike features occurring around the rainfall in the final 1024x1024 krige image. This may be due to the periodicity inherent in the Fourier routine. The amount of iterations on the coarse grid had to be lowered to approximately 50 or less, before these fictitious features were removed.

Various combinations of the amount of iterations on the coarser and national grid, and the effects these had, were investigated. Testing indicated that 25 iterations on the coarse grid and 25 on the national grid produced acceptable results. The resultant image was similar in structure to the image produced by 50 iterations on the national grid. The 50 iterations took approximately 15 minutes to be completed, while 25 coarse and 25 national iterations took only 6 minutes. This technique improved the computational efficiency by decreasing the amount of iterations needed on the national grid, that took approximately 11 seconds per iteration, and also by improving the rate of convergence of the ICD routine on the national grid, especially for the first 5 - 10 iterations. 25 iterations on the coarse grid and 10 on the national grid took approximately 2 min 30 sec to be completed.

5.5.4 Applying Kriging to 24-hour rainfall fields

The kriging routine was developed on the assumption that the radar rainfall fields were isotropic in nature. This meant that the technique could be applied to instantaneous radar images, without violating this assumption. In such a real-time context this technique could not be applied since it is too cumbersome to solve the equations effectively (sufficient iterations of the ICD), so as to produce a reliable rainfall field. On hourly-accumulated fields the covariance structure is elongated and violates isotropy. It was found, though, that after subsequent accumulations of the hourly-accumulated fields, the resultant rainfall field approached isotropy. The application of this technique on 24-hour accumulated data sets, consisting of 288 5-minute volume scans, was investigated and it was found that the kriged 24-hour radar rainfall field managed to reproduce the original spatial field effectively, so as to warrant its use on this time scale. This is an approximation and there are times, though, when isolated convective storms leave elongated rainfall tracks behind which are not isotropic. Even then the rainfall fields seemed accurate representations of the original fields, quantitatively and qualitatively (Figure 5.5.1).

This technique was implemented on radar and rain gauge data sets during winter 2002, with the aim to produce a national merged radar and rain gauge rainfall field. 24-hour radar rainfall and rain gauge data differ widely in that radar is a continuous surface, within the data coverage, and rain gauges are mere point measurements. The ICD routine to react differently to these two data sets and unique parameters had to be determined for this technique to converge on the rain gauge point data field.

Parameters	Radar	Rain gauge
α	0.0018	0.06
Correlation Length	12.3	9.225
Iterations_{256}	50	50
Iterations_{1024}	125	125

With these parameters, individual extrapolated/interpolated radar and interpolated rain gauge surface are produced and in conjunction with their individual kriged explained variance fields are used to produce the merged 24-hour radar and rain gauge rainfall field (5.5.1). Each individual field takes approximately 10 minutes to compute, meaning that a merged field is available in 40 minutes using a PIII machine.

5.5.5 Data dissemination

The various data fields are processed within a GIS and produces static images of these products. These products include 24-hourly rainfall fields (Figure 31a-f)of: 1). Satellite; 2) interpolated rain gauge; 3). Radar; 4). radar and gauge merged; 5). conditioned satellite; and 6). Integrated satellite, radar and rain gauge (see figure 30 for examples). The METSYS web site, http://metsys.weathersa.co.za, is used as interface of displaying the data to possible data users and the general public. These data sets are hosted under the heading of SIMAR and are available without charge and should be available to anyone interested in such data sets. This form of publishing the data, limits its accessibility only to those fortunate enough to have Internet access. No interface exists of publishing these data sets in a rural environment. An example of the web interface is given in Figure 5.6.1.

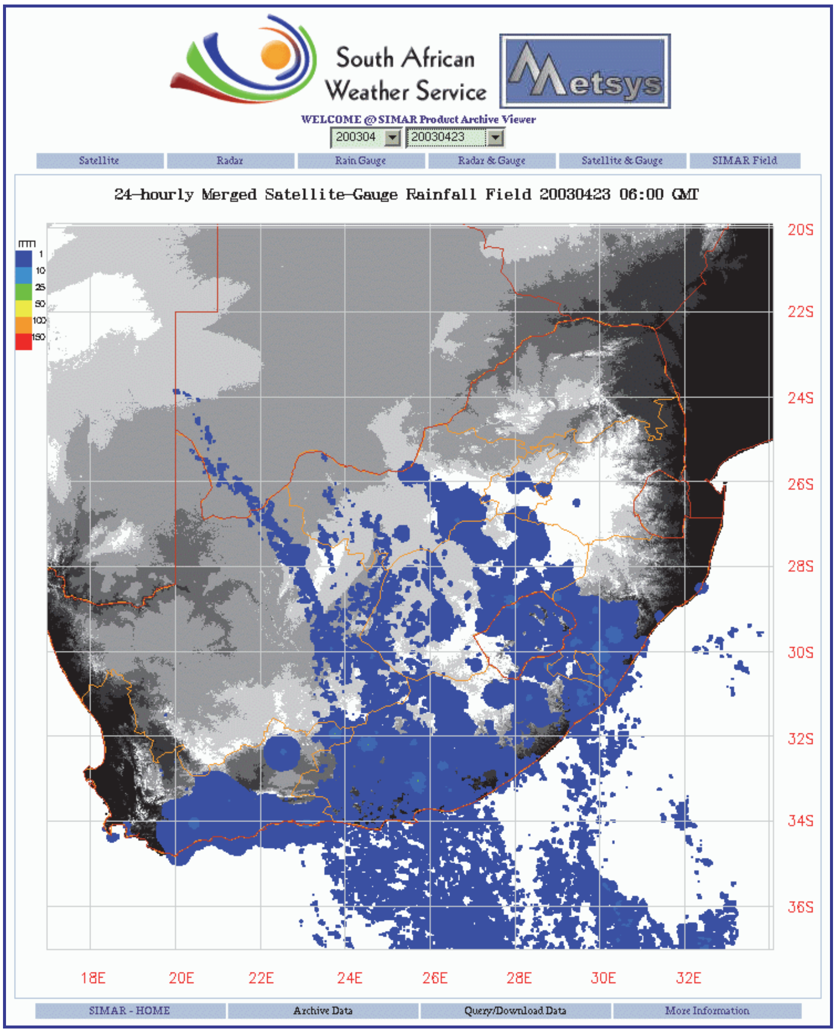

Figure 5.6.1 The SIMAR web interface

The SIMAR products (Figure 5.6.2a-f), as with all METSYS radar products, are non-interactive and merely static imprints of the data set. A latitude/longitude grid, topographical data and provincial boundaries are included on the image for ease of navigation. The first possible rainfall data set, available at 08:30SAST from the local forecast data server, is utilised as building block for these products. Since rainfall is measured each day at 08:00 SAST, this allows the data sets to be available in real time. This is essential for these data sets to be applied for hydrological monitoring. Updating the web, at this stage, is dynamic and depends on the availability of the rain gauge data set and the amount of reported stations. This data set may not always be on time and the product generation is delayed until sufficient data is available for producing a reliable first guess merged rainfall field. A comprehensive rain gauge data set is extracted from the SAWS Climate data base at 11:00 and 14:00 SAST, which triggers an update of all the products on the web. If data flow is reliable, the products are available as follow:

	Radar	**Interpolated Gauge**	**Satellite**	**Radar/ Gauge**	**Satellite/ Gauge**	**Merged**
Partial data set	08:35	08:45	09:00	09:15	09:25	09:30
Comprehensive	11:35	11:45	12:00	12:15	12:25	12:30

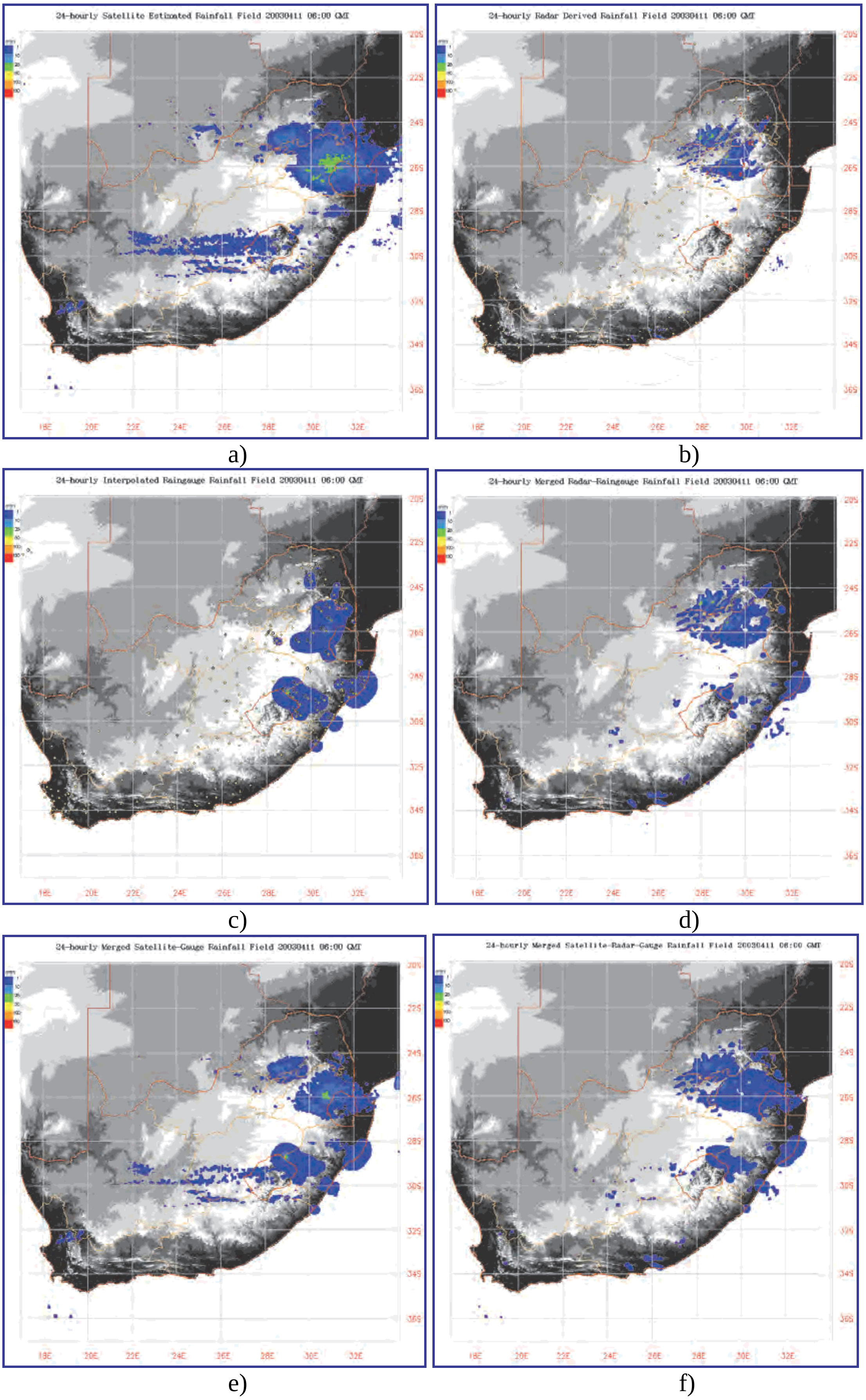

Figure 5.6.2 Example of SIMAR products: a) Satellite; b) Radar; c) Gauge; d) Radar-gauge; e) Satellite-gauge; f) Merged.

REFERENCES

1. ADLER RF and NEGRI AJ (1988) A satellite infrared technique to estimate tropical convective and stratiform rainfall. *Jnl. appl Met.* **27** 30-38
2. ADLER, RF; NEGRI AJ; KEEHN PR and HAKKARINEN IM (1993) Estimation of monthly rainfall over Japan and surrounding waters from a combination of low-orbit microwave and geostationary IR data. *J. Appl. Meteorol.* **32** 335-356
3. ARKIN PA (1979) The relationship between fractional coverage of high cloud and rainfall accumulations during GATE over the B-scale array. *Mon. Weath. Rev.* **107** 1382-1387
4. ARKIN PA and MEISNER BN (1987) The relationship between large-scale convective rainfall and cold cloud over the Western Hemisphere during 1982-1984. *Mon. Weath. Rev.* **115** 51-74
5. ARKIN PA and MEISNER BN (1987) The relationship between large-scale convection rainfall and cold clouds over the Western Hemisphere during 1982 - 1984. *Mon. Weath. Rev.* **115** 51-74
6. BADER MJ, FORBES GS, GRANT JR, LILLEY RBE and WATERS AJ (1995) Images in Weather Forecasting. *Cambridge University Press, Cambridge, Great Brittian*
7. BATTEN L (1973) Radar Observations of the Atmosphere. *University of Chicago Press* 324pp
8. BELLON A and AUSTIN GL (1986) On the relative accuracy of satellite and rain gauge rainfall measurements over middle latitudes during daylight hours. *J. Clim. Appl. Met.* **25** 1712-1724
9. BRANDES EA and WILSON JW (1987) Measuring Storm Rainfall by Radar and Rain Gauge. *Instruments and Techniques for Thunderstorm Observation and Analysis edited by E. Kessler* 171 – 186
10. CHAN JCW, DEFRIES RS, ZHAN X, HUANG C and TOWNSHEND RG (2000) Texture features for land cover change detection at 250m resolution - an application for machine learning feature subset selection.
11. CRESSWELL MP (1998) *University of Liverpool web site,* *http://www.liv.ac.uk/~mark/meteosat/*
12. CSISZAR I, MAJOR G, KERENYI J and DIOSZEGHY M (1997) Precipitation Estimation with Satellites and Radar. *Adv. Space Res.* **19** (3) 461-467
13. DAHLSTRÖM B (1973) Investigation of errors in rainfall observations: a continued study. *Rep. 34 Department of Meteorology University of Uppsala Sweden*
14. DIXON M.J. and G Wiener, 1993:TITAN: Thunderstorm identification, tracking, analysis and nowcasting. *J. Atmos. Ocean. Tech,* **10(6)**, 785-797
15. DOVIAK R and ZRNIK D (1984) Dopler Radar and Weather Observations. *Academic Press* 458pp
16. DOYLE (1997) Vision: AI Qual Summary http://www.cs.dartmouth.edu/~brd/Teaching/AI/Lectures/Summaries/vision.html

17. DULYYAKARN P, RANGSANSERI Y and THITIMAJSHIMA P (2000) Comparison of two texture features for multispectral analysis. *GISdevelopment.net, AARS, ACRS2000, Image Processing*

18. EBERT EE and LE MARSHALL J (1995) An evaluation of infrared satellite rainfall estimation techniques over Australia. *Aust. Met. Mag.* **44** 177-190

19. ENGELMANN U, SCHROTER A, GUNNEL U, and MEIZNER HP. Basic Image Processing Service (BIPS) User Manual Version 0.59, Department of Medical and Biological Informatics, http://mbi.dkfz-heidelberg.de/helios/doc/manuals/ip/bips/bips.book.html, accessed November 2001

20. EUMETSAT (1988) The European Organization for Meteorological Satellites, EUMETSAT brochure.

21. EUMETSAT (1999) *EUMETSAT web site, http://www.eumetsat.de/en/* **accessed:** 2000

22. EVANS IS (1979) An integrated system of terrain analysis and slope mapping. *Final report on grant DA-ERO-591-73-G0040*, University of Durham, England.

23. FU R, DEL GENIO D and ROSSOW WB (1990) Behavior of deep convective clouds in the tropical Pacific from ISCCP radiances. *J. Climate* **3** 1129-1152

24. GOODMAN B, MENZEL WP, CUTRIM EC and MARTIN DW (1193) A non-linear algorithm for estimating 3-hourly rain rates over Amazonia from GOES/VISSR observations. *Remote Sensing Reviews* **10** 169-177

25. GOODMAN B, MENZEL WP, CUTRIM EC and MARTIN DW (1993) A non-linear algorithm for estimating 3-hourly rain rates over Amazonia from GOES/VISSR observations. *Remote Sensing*

26. GRIMES DIF (1999) *Artemis web-site, Department of Meteorology, University of Reading, HYPERLINK http://www.met.reading.ac.uk/~swsgrime/artemis/) http://www.met.reading.ac.uk/~swsgrime/artemis/* **accessed:** 2000

27. GRODY NC (1991) Classification of snow cover and precipitation using SSM/I. *J. geophys. Res.* **96** 7423-7435

28. HARALICK RM (1979) Statistical and structural approaches to texture. *Proceedings IEEE* **67** (5) 786-803

29. HARTKAMP AD, DE BEURS K, STEIN A and WHITE JW (1999) Interpolation techniques for Climate variables. *NRG-GIS Series 99-01Mexico, D.F.: CIMMYT*

30. HENDON HH and WOODBERRY K (1993) The diurnal cycle of tropical convection. *J. Geophys. Res* **98** 16623-16637

31. INOUE T (1987) A cloud type classification with NOAA 7 split-window measurements. *J. Geophys. Res.* **92** 3991-4000

32. JAIN R, KASTURI R and SCHUNCK BG (1985) Machine vision. Mc Graw-Hill International Editions, 234-239

33. KALESCHKE L and BOCHERT A Classification of ERS-SAR images for sea ice identification by texture analysis with neural networks. *Institute of Environmental Physics, University of Bremen, Germany*

34. KIDD C (1999) Rainfall Estimation Using Infrared and Passive Microwave Sources. *Proceedings of The 1999 EUMETSAT Meteorological Satellite Data Users' Conference* 207-213

35. KING PWS, HOGG WD and ARKIN PA (1995) The role of visible data in improving satellitee rain rate estimates *J. Appl. Meteorol.* **34** 1608-1621

36. KURINO T (1996) A rainfall estimation with GMS-5 infrared split-window and water vapour measurements. *Technical Note* **33**

37. KURINO T (1997) A satellite infrared technique for estimating “deep/shallow” precipitation. *Adv. Space Res.* **19** (3) 511-514

38. LEVIZZANI V (2001a) Intense rainfall monitoring from geostationary satellites

39. LEVIZZANI V (2001b) Satellite rainfall estimates: a look back and a perspective

40. LOVEJOY S and AUSTIN GL (1979) The delineation of rain areas from visible and IR satellite data for 17. GATE and mid-latitudes. *Atmos. Ocean* **17** 77-92

41. MARSHALL JS, HITCSHFELD W and GUNN KLS (1955) Advances in Weatehr Radar. *Adv. Geophys.* **2** 1-56

42. MARTIN DW, GOODMAN B, SCHMIT TJ AND CUTRIM EC (1990) Estimates of daily rainfall over the Amazon Basin. *J. Geo. Res.* **95** (D10) 17043-17050

43. McCAIN B, COSC453 Lecture Notes, http://www.cs.otago.ac.nz/cosc453/4532001NFIS.pdf, 2001, accessed January 2002.

44. MITASOVA H and MITAS L (1993) Interpolation by Regularized spline with Tension: I. Theory and Implementation *Mathematical Geology* **25** 641-655

45. MORSE BS (2000) Lecture Notes, Data structures for image analysis, Brigham Young University

46. NEGRI AJ and ADLER RF (1993) An intercomparison of three satellite infrared rainfall techniques over Japan and surrounding waters. *J. Appl. Meteorol.* **32** 357-373

47. NEGRI AJ, ADLER RF and WETZEL PJ (1984) Rain estimation from satellites: An examination of the Griffith-Woodly technique. *Jnl. Clim. Appl. Met.* **23** 102-116

48. PANOFSKY HA and BRIER GW (1968) Some application of statistics in Meteorology. The University of Pennsylvania, University Park, PA, 224

49. PEGRAM GGS (2001) Kriging and Variance Field Estimation using the Fast Fourier Transform : The Large Data Mapping Problem

50. PETTY GW and KATSATOS KB (1990) Precipitation observed over the South China Sea by the Nimbus-7 Scanning Multi-channel Microwave Radiometer during Winter MONEX. *Jnl. Appl. Met.* **29** 273-287

51. PEUCKER T K and DOUGLAS D H (1974). Detection of surface specific points by local parallel processing of discrete terrain elevation data. *Computer Graphics and Image Processing 4, pp.375-387.*

52. PICAN N, TRUCCO E, ROSS M, LANE DM, PETILLOT Y and TENA RUIZ (1998) Texture analysis for seabed classification: Co-occurrence matrices vs. self-organizing maps. *Ocean 1998 Conference*

53. PORCU F, BORGA M and PRODI F (1999) Rainfall estimation by combining radar and infrared satellite data for now casting purposes. *Meteorol. Appl.* **6** 289-300

54. PORCU F, BORGA M and PRODI F (1999) Rainfall estimation by combining radar and infrared satellite data for now casting purposes. *Meteorol. Appl.* **6** 289-300

55. PRABHAKARA C, DALU G, SUHASINI R, NUCCIARONE JJ and LIBERTI GL (1992) Rainfall over oceans: Remote sensing from satellite microwave radiometers. *Meteorology and Atmospheric Physics* **47** 179-199

56. PULLEN S and BUTTERWORTH P (2001) Assimilation of satellite-derived estimates of tropical convective rainfall. *Forecasting Research Technical Report No.360*, The Met Office, Bracknell, UK

57. ROSENFELD A and KAK AC (1982) *Digital picture processing.* Academic Press, New York, Second edition

58. ROSENFIELD D and GUTMAN G (1994) Retrieving microphysical properties near the tops of potential rain clouds by multispectral analysis of AVHRR data. *Atmos. Res.* **34** 259-283

59. ROZUMALSKI RA (2000) A Quantitative Assessment of the NESDIS Auto-Estimator. *Weather and Forecasting* **15** (4) 397-415

60. SAUVAGEOUT H (1992) Radar Meteorology. *Artech House* 366pp

61. SCHERER WD and HUDLOW MD (1971) A technique for assessing probable distributions of tropical precipitation echo lengths for X-band radar from Nimbus 3 HRIR data. *BOMEX Bull.* **10** 63-68

62. SCOFIELD RA (1987) The NESDIS operational convective precipitation technique. *Mon. Wea. Rev.* **115** 1773-1792

63. SEVIRI Science Plan (2000) *EUMETSAT Doc. No. EUM/MSG/PLN/193 Revision 3, http://www.eumetsat.de/en/* **accessed:** 2000

64. SUGIER J., J. PARENT DU CHATELET, P. ROQUAIN and A. SMITH. 2002. Proceedings of ERAD 2002:17-24. Delft University of Technology. The Netherlands

65. SMITS PC and ANNONI A (1999) Updating land-cover maps by using texture information from very high-resolution space-borne imagery. *IEEE Trans on Geoscience and Remote Sensing* **37** 1244-1254

66. SONKA M, HLAVAC V and BOYLE R (1993) Image Processing, Analysis, and Machine Vision. Chapman and Hall Inc

67. SPENCER RW, GOODMAN HM and HOOD RE (1989) Precipitation retrieval over land and ocean with the SSM/I: Identification and characteristics of the scattering signal. *Journal of Atmospheric and Oceanic Technology* **6** 254-273

68. SUTTER LL, MichiganTech School of Technology http://www.tech.mtu.edu/~llsutter/menus/process.html, accessed October 2001

69. SZEJWACH G (1982) Determination of semi-transparent cirrus cloud temperature from infrared radiances: Application to METEOSAT. *Jnl. Appl.Met.* **21** 384-393

70. TERBLANCHE, D.E. 1996. A simple digital signal processing method to simulate linear and quadratic responses from a radar's logarithmic receiver. *J. Atmos Ocean. Technol.***10**, 785-797

71. TERBLANCHE D E., P.J.M VISSER, M.P. MITTERMAIER and N.J. KROESE, 2000. VIPOS: Vaal Dam catchment integrated precipitation observation system. WRC Report NO 954/1/01.

72. TERBLANCHE DE, PEGRAM G.G.S and MITTERMAIER M.P. (2001) The development of weather radar as a research and operational tool for hydrology in South Africa. *J. Hydrol* . **241**, 3-25.

73. TJEMKES S, ARRIAGE A, GOVAERTS Y, KÖNIG M, LUTZ H-J and HOLMLUND K (1999) Preparing for a new generation: The Meteosat Second Generation Meteorological Product Extraction Facility. *Proceedings of The 1999 EUMETSAT Meteorological Satellite Data Users' Conference* 639-643

74. TJEMKES SA, VAN DE DERG L and SCHMETZ J (1997) Warm water vapour pixels over high clouds as observed by Meteosat. *Beitr. Phys. Atmosph.* **70** 15-21

75. TSONIS AA and ISAAC GA (1985) On a new approach for instantaneous rain area delineation in the midlatitudes using GOES data. *J. Climate. Appl. Meteorol.* **24** 1208-1218

76. TYAN SG (1981) *Median filtering, deterministic properties. In TS Huang, editor, Two dimensional digital processing*, volume 2

77. VAN HEERDEN J and STEYN P.L, Weather radar measurement of rainfall for hydrological and other purposes. WRC Report No 961/1/99.

78. VELDEN C GOES Water Vapour Images Interpretation. University of Wisconsin

79. VICENTE GA, SOFIELD RA and MENZEL WP (1998) The operational GOES infra-red Rainfall Estimation Technique**.** *Bulletin of American Meteorological Society*

80. WOOD J (1996) The Geomorphological characterization of digital elevation models. *Ph.D. Thesis*

81. YAROSLAVSKII LP (1987) *Digital signal processing in optics and hylography* (in Russian). Radio isvjaz, Moscow